

**MATERIALS FOR ADAPTIVE STRUCTURAL
ACOUSTIC CONTROL**

Period February 1, 1995 to January 31, 1996

Annual Report

VOLUME IV

OFFICE OF NAVAL RESEARCH
Contract No.: N00014-92-J-1510

APPROVED FOR PUBLIC RELEASE — DISTRIBUTION UNLIMITED

Reproduction in whole or in part is permitted
for any purpose of the United States Government

L. Eric Cross

19960703 066

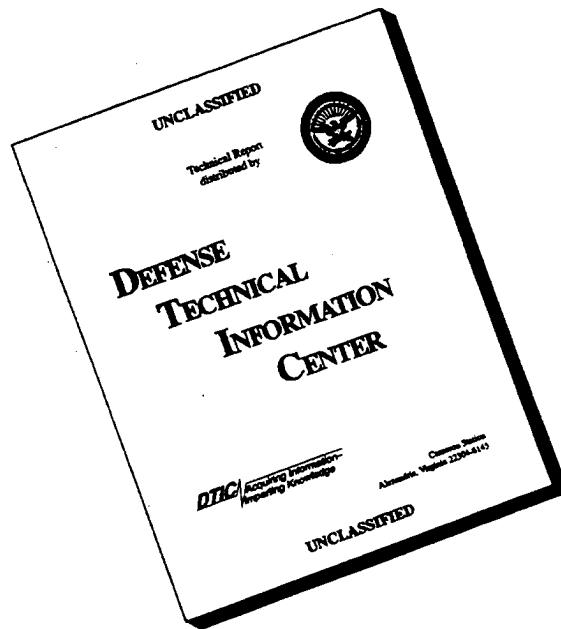
PENNSTATE



THE MATERIALS RESEARCH LABORATORY
UNIVERSITY PARK, PA

DTIC QUALITY INSPECTED 1

DISCLAIMER NOTICE

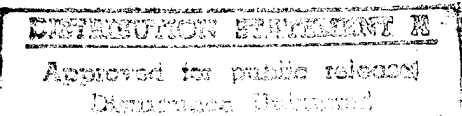


THIS DOCUMENT IS BEST QUALITY AVAILABLE. THE COPY FURNISHED TO DTIC CONTAINED A SIGNIFICANT NUMBER OF PAGES WHICH DO NOT REPRODUCE LEGIBLY.

REPORT DOCUMENTATION PAGE

Form Approved
OMB No. 0704-0188

Public reporting burden for this collection of information is estimated to average 1 hour per response, including the time for reviewing instructions, searching existing data sources, gathering and maintaining the data needed, and completing and reviewing the collection of information. Send comments regarding this burden estimate or any other aspect of this collection of information, including suggestions for reducing this burden, to Washington Headquarters Services, Directorate for Information Operations and Reports, 1215 Jefferson Davis Highway, Suite 1204, Arlington, VA 22202-4302, and to the Office of Management and Budget, Paperwork Reduction Project (0704-0188), Washington, DC 20503.

1. AGENCY USE ONLY (Leave blank)		2. REPORT DATE 3/13/96	3. REPORT TYPE AND DATES COVERED ANNUAL REPORT 02/01/95 TO 01/31/96		
4. TITLE AND SUBTITLE MATERIALS FOR ADAPTIVE STRUCTURAL ACOUSTIC CONTROL			5. FUNDING NUMBERS		
6. AUTHOR(S) L. ERIC CROSS					
7. PERFORMING ORGANIZATION NAME(S) AND ADDRESS(ES) MATERIALS RESEARCH LABORATORY THE PENNSYLVANIA STATE UNIVERSITY UNIVERSITY PARK, PA 16802			8. PERFORMING ORGANIZATION REPORT NUMBER		
9. SPONSORING/MONITORING AGENCY NAME(S) AND ADDRESS(ES) OFFICE OF NAVAL RESEARCH GERALD T. SMITH CODE 1513:NRJ OFFICE OF NAVAL RESEARCH RES. 800 NORTH QUINCY STREET 536 SOUTH CLARK STREET, RM 286 ARLINGTON, VA 22217-5660 CHICAGO, ILLINOIS 60606-1588			10. SPONSORING/MONITORING AGENCY REPORT NUMBER REP.		
11. SUPPLEMENTARY NOTES					
12a. DISTRIBUTION/AVAILABILITY STATEMENT			12b. DISTRIBUTION CODE		
					
13. ABSTRACT (Maximum 200 words)					
SEE FOLLOWING THREE PAGES					
14. SUBJECT TERMS			15. NUMBER OF PAGES		
			16. PRICE CODE		
17. SECURITY CLASSIFICATION OF REPORT		18. SECURITY CLASSIFICATION OF THIS PAGE	19. SECURITY CLASSIFICATION OF ABSTRACT	20. LIMITATION OF ABSTRACT	

GENERAL INSTRUCTIONS FOR COMPLETING SF 298

The Report Documentation Page (RDP) is used in announcing and cataloging reports. It is important that this information be consistent with the rest of the report, particularly the cover and title page. Instructions for filling in each block of the form follow. It is important to *stay within the lines* to meet optical scanning requirements.

Block 1. Agency Use Only (Leave blank).

Block 2. Report Date. Full publication date including day, month, and year, if available (e.g. 1 Jan 88). Must cite at least the year.

Block 3. Type of Report and Dates Covered. State whether report is interim, final, etc. If applicable, enter inclusive report dates (e.g. 10 Jun 87 - 30 Jun 88).

Block 4. Title and Subtitle. A title is taken from the part of the report that provides the most meaningful and complete information. When a report is prepared in more than one volume, repeat the primary title, add volume number, and include subtitle for the specific volume. On classified documents enter the title classification in parentheses.

Block 5. Funding Numbers. To include contract and grant numbers; may include program element number(s), project number(s), task number(s), and work unit number(s). Use the following labels:

C - Contract	PR - Project
G - Grant	TA - Task
PE - Program Element	WU - Work Unit Accession No.

Block 6. Author(s). Name(s) of person(s) responsible for writing the report, performing the research, or credited with the content of the report. If editor or compiler, this should follow the name(s).

Block 7. Performing Organization Name(s) and Address(es). Self-explanatory.

Block 8. Performing Organization Report Number. Enter the unique alphanumeric report number(s) assigned by the organization performing the report.

Block 9. Sponsoring/Monitoring Agency Name(s) and Address(es). Self-explanatory.

Block 10. Sponsoring/Monitoring Agency Report Number. (If known)

Block 11. Supplementary Notes. Enter information not included elsewhere such as: Prepared in cooperation with...; Trans. of...; To be published in... When a report is revised, include a statement whether the new report supersedes or supplements the older report.

Block 12a. Distribution/Availability Statement. Denotes public availability or limitations. Cite any availability to the public. Enter additional limitations or special markings in all capitals (e.g. NOFORN, REL, ITAR).

DOD - See DoDD 5230.24, "Distribution Statements on Technical Documents."

DOE - See authorities.

NASA - See Handbook NHB 2200.2.

NTIS - Leave blank.

Block 12b. Distribution Code.

DOD - Leave blank.

DOE - Enter DOE distribution categories from the Standard Distribution for Unclassified Scientific and Technical Reports.

NASA - Leave blank.

NTIS - Leave blank.

Block 13. Abstract. Include a brief (*Maximum 200 words*) factual summary of the most significant information contained in the report.

Block 14. Subject Terms. Keywords or phrases identifying major subjects in the report.

Block 15. Number of Pages. Enter the total number of pages.

Block 16. Price Code. Enter appropriate price code (*NTIS only*).

Blocks 17. - 19. Security Classifications. Self-explanatory. Enter U.S. Security Classification in accordance with U.S. Security Regulations (i.e., UNCLASSIFIED). If form contains classified information, stamp classification on the top and bottom of the page.

Block 20. Limitation of Abstract. This block must be completed to assign a limitation to the abstract. Enter either UL (unlimited) or SAR (same as report). An entry in this block is necessary if the abstract is to be limited. If blank, the abstract is assumed to be unlimited.

ABSTRACT

This report documents work carried forward over the fourth year of a five year ONR sponsored University Research Initiative (URI) entitled "Materials for Adaptive Structural Acoustic Control." The program has continued to underpin the development of new electro-ceramic, single crystal and composite materials combinations for both the sensing and actuation functions in adaptive structures.

For the lead based perovskite structure relaxor ferroelectric electrostrictors, new experimental and theoretical studies have underscored the critical role of nano-scale heterogeneity on either A or B sites of the ABO_3 in promoting dispersive dielectric response and the very strong opposing role of elastic stress and electrostrictive coupling in suppressing polarization fluctuations. Most important for practical application is the regimen where, under high electric field nano-polar regions begin to amalgamate into ferroelectric macro-domains with very mobile walls lead to unusually large extrinsic piezoelectric coefficients.

The program has explored a range of new relaxor:ferroelectric solid solutions which exhibit morphotropic phase boundaries between rhombohedral and tetragonal ferroelectric phases. Some of these compositions are much more tractable than PZT to grow in single crystal form. A major surprise is the very strong enhancement of the piezoelectric d_{33} and d_{31} in the crystal over that in the corresponding ceramic, and the massive anisotropy for different orientations and directions of poling. Optical studies suggest that the unusual effects reside largely in the extrinsic (domain controlled) response and we speculate about the mobility of walls in metastable phases, however further studies are required.

Antiferroelectric:ferroelectric phase switching studies in a wide range of compositions in the lead lanthanum zirconate stannate titanate system show that the first abrupt switchover to the rhombohedral ferroelectric phase only produces volume strain $\sim 0.2\%$ as checked both by dilatometry and by X-ray. There is a large enhancement under higher field to $\sim 0.6\%$ volume strain although the polarization does not change markedly. From thin film and single crystals studies there is mounting evidence of higher field ferroelectric:ferroelectric phase change, but again additional work is needed.

Size effect studies in perovskite ferroelectrics are continuing on this program and on the NSF/MRG in MRL. Scaling of the 90° stripe domains in thinned TEM samples of tetragonal composition begin to show departure from the accepted $1/2$ power law at sub micron sizes. The structure of domains under the three dimensional constraints of grains inside the ceramic is still however almost completely unknown. Computer modeling appear to show promise and codes are being explored which permit the mutual interactions to be varied and the corresponding two dimensional structures visualized.

In composite sensors, the focus has continued upon the flextensional configurations with the new inexpensive cymbal shaped amplifier proving superior in every respect to the original "moonie." The flat section on the cymbal end cap permits very easy stacking of elements and work is now in progress to develop large area panels for low frequency testing at the Penn State ARL.

Work has continued on the thin sheet 2:2 piezoceramic polymer composites, where the transverse poling and low density lead to a desirable combination of low electrical and low acoustic impedance. An alternative fabrication procedure using extruded PZT honeycomb appears most attractive.

Two problems of major importance in actuation have been topics for study. First what are the "intrinsic" material limitations for high strain electrically driven actuation in polarization controlled systems, and secondly what are the practical limitations in multilayer actuators as they are currently fabricated and how may they be alleviated. Work on the first topic is now largely completed, showing that strains $\sim 0.4\%$ could be switched more than 10^9 cycles in suitable PLZT compositions. Such reliability however requires near theoretical density, homogeneity, grain size control, critical attention to electrodes and electric field uniformity, none of which are adequately controlled in current actuator systems.

For practical actuators fabricated by inexpensive tape casting and co-firing techniques electrode termination is a major problem. In the simple MLC like designs, cracks initiate at field concentrations associated with the tip of the buried conductor layer. A new floating electrode design has been found to reduce this problem. For cracking near the end surfaces, poling of the termination layers reduces their stiffness and markedly improves performance. In the conventional structures it is also found that the floating electrode may be used directly as an acoustic emission pickup, giving early warning of cracking problems.

Under resonant driving conditions, the problems in actuators are markedly different. Heat build up and temperature run-away are significant problems traceable to dielectric loss, and new hard compositions and anti-resonant driving methods have been explored to reduce these problems.

In integration work on the high activity 0-3 composites is nearing completion. A new type of zig-zag actuator is being explored for the capability to combine both longitudinal and transverse actuation. Under a new ONR sponsored program with Virginia Polytechnic Institute and University new double amplifiers combining bimorph and flextensional concepts are being examined.

Processing studies permit the fabrication of the wide range of compositions and forms required in these material researches. Rate controlled sintering is proving to be highly advantageous, particularly for reducing delamination in integrated structures. Electrophoretic and

dielectrophoretic forming are showing promise in green assembly of thick film components where high green density is critical.

Thin film papers have been selected from the very broad range of work in MRL because of their relevance to transduction in piezoelectric and in phase switching systems.

**MATERIALS FOR ADAPTIVE STRUCTURAL
ACOUSTIC CONTROL**

Period February 1, 1995 to January 31, 1996

Annual Report

VOLUME IV

OFFICE OF NAVAL RESEARCH

Contract No.: N00014-92-J-1510

APPROVED FOR PUBLIC RELEASE — DISTRIBUTION UNLIMITED

Reproduction in whole or in part is permitted
for any purpose of the United States Government

L. Eric Cross

PENNSSTATE



THE MATERIALS RESEARCH LABORATORY
UNIVERSITY PARK, PA

TABLE OF CONTENTS

ABSTRACT	8
INTRODUCTION	10
1.0 GENERAL SUMMARY PAPERS	11
2.0 MATERIALS STUDIES	12
3.0 COMPOSITE SENSORS	12
4.0 ACTUATORS STUDIES	13
5.0 INTEGRATION ISSUES	14
6.0 PROCESSING STUDIES	14
7.0 THIN FILM FERROELECTRICS	15
8.0 GRADUATE STUDENTS IN THE PROGRAM	16
9.0 HONORS AND AWARDS	16
10.0 APPRENTICE PROGRAM	16
11.0 PAPERS PUBLISHED IN REFEREED JOURNALS	17
12.0 INVITED PAPERS PRESENTATIONS AT NATIONAL AND INTERNATIONAL MEETINGS	21
13.0 INVITED PAPERS PRESENTED AT UNIVERSITY, INDUSTRY AND GOVERNMENT LABORATORIES	23
14.0 CONTRIBUTED PAPERS AT NATIONAL AND INTERNATIONAL MEETINGS	24
15.0 BOOKS (AND SECTIONS THEREOF)	27

APPENDICES

VOLUME I

General Summary Papers

1. Cross, L.E., "Ferroelectric Materials for Electromechanical Transducer Applications," *Jpn. J. Appl. Phys.* **34**, 2525-2532 (1995).
2. Fernandez, J.F., A. Dogan, Q.M. Zhang, J.F. Tressler, and R.E. Newnham, "Hollow Piezoelectric Composites," submitted to *Sensors and Actuators: A. Physical* (1995).
3. Uchino, K., "Recent Developments in Ceramic Actuators—Comparison among USA, Japan and Europe," Workshop on Microsystem Technologies in the USA and Canada, Dusseldorf (1995).
4. Trolier-McKinstry, S., J. Chen, K. Vedam, and R.E. Newnham, "In Situ Annealing Studies of Sol-Gel Ferroelectric Thin Films by Spectroscopic Ellipsometry," *J. Am. Ceram. Soc.* **78** [7], 1907-1913 (1995).
5. Nair, N., A. Bhalla, and R. Roy, "Inorganic Lead Compounds in Electroceramics and Glasses," *Am. Cer. Soc. Bull.* **75** [1], 77-82 (1996).
6. Gentile, A. and F.W. Ainger, "Single Crystals," Chapter 9, Materials Science and Technology, A Comprehensive Treatment, **17A** Processing of Ceramics, Part 1 (R.J. Brook, editor), VCH Verlagsgesellschaft mbH, Weinheim, Fed. Repl. of Germany (1996).

Materials Studies

7. Choi, S.W., J.M. Jung, and A.S. Bhalla, "Dielectric, Pyroelectric and Piezoelectric Properties of Calcium-Modified Lead Magnesium Tantalate-Lead Titanate Ceramics."
8. Kim, Y.J., S.W. Choi, and A.S. Bhalla, "Dielectric, Pyroelectric Properties, and Morphotropic Phase Boundary in La-Doped $(1-x)\text{Pb}(\text{Mg}_{1/3}\text{Ta}_{2/3})-x\text{PbTiO}_3$ Solid Solution Ceramics", *Ferroelectrics* **173**, 87-96 (1995).
9. Alberta, E. and A.S. Bhalla, "A Processing and Electrical Property Investigation of the Solid Solution: $(x)\text{Pb}(\text{In}_{1/2}\text{Nb}_{1/2})\text{O}_3-(1-x)\text{Pb}(\text{Sc}_{1/2}\text{Ta}_{1/2})\text{O}_3$," submitted to *Ferroelectrics* (1995).
10. Zhang, Q.M., H. You, M.L. Mulvihill, and S.J. Jang, "An X-ray Diffraction Study of Superlattice Ordering in Lead Magnesium Niobate," *Solid State Comm.* **97** [8], 693-698 (1996).
11. Zhang, Q.M., J. Zhao, and L.E. Cross, "Aging of the Dielectric and Piezoelectric Properties of Relaxor Ferroelectric Lead Magnesium Niobate-Lead Titanate in the Electric Field Biased State," *J. Appl. Phys.* **79** (6), 1-7 (1996).

VOLUME II

Materials Studies (continued)

12. Zhang, Q.M., J. Zhao, T.R. Shrout, and L.E. Cross, "The Effect of Ferroelastic Coupling in Controlling the Abnormal Aging Behavior in Lead Magnesium Niobate-Lead Titanate Relaxor Ferroelectrics," submitted *J. Mat. Res.*
13. Mulvihill, M.L., L.E. Cross, and K. Uchino, "Low-Temperature Observation of Relaxor Ferroelectric Domains in Lead Zinc Niobate," *J. Am. Ceram Soc.* **78** (12) 3345-3351 (1995).
14. Mulvihill, M.L., L.E. Cross, and K. Uchino, "Dynamic Motion of the Domain Configuration in Relaxor Ferroelectric Single Crystals as a Function of Temperature and Electric Field," 8th Euro. Mtg. Ferroelectricity, Nijmegen (1995).
15. Mulvihill, M.L., K. Uchino, Z. Li, and Wenwu Cao, "In-Situ Observation of the Domain Configurations During the Phase Transitions in Barium Titanate," accepted *Phil. Mag. B* (1995).
16. Oh, K.Y., K. Uchino, and L.E. Cross, "Electric Properties and Domain Structures in Ba(Ti,Sn)O₃ Ceramics."
17. Cao, W., "Elastic and Electric Constraints in the Formation of Ferroelectric Domains," *Ferroelectrics*, **172**, 31-37 (1995).
18. Cao, W. and C.A. Randall, "The Grain Size and Domain Size Relations in Bulk Ceramic Ferroelectric Materials," accepted *J. Phys. Chem. Solids* (1995).
19. Cao, W., "Defect Stabilized Periodic Amplitude Modulations in Ferroelectrics," accepted *Phase Transitions* (1995).
20. Sopko, J., A. Bhalla, and L.E. Cross, "An Improved Quantitative Method for Determining Dynamic Current Response of Ppyroelectric Materials," *Ferroelectrics*, **173**, 139-152 (1995)

VOLUME III

Composite Sensors

21. Tressler, J.F., A. Dogan, J.F. Fernandez, J.T. Fielding, Jr., K. Uchino, and R.E. Newnham, "Capped Ceramic Hydrophones," submitted to Proc. IEEE Int'l Ultrasonics Symp., Seattle (1995).
22. Koc, B., A. Dogan, J.F. Fernandez, R.E. Newnham, and K. Uchino, "Accelerometer Application of the Modified Moonie (Cymbal) Transducer," submitted *Jpn. J. Appl. Phys.* (1995).
23. Zhao, J., Q.M. Zhang, and W. Cao, "Effects of Face Plates and Edge Strips on Hydrostatic Piezoelectric Response of 1-3 Composites," *Ferroelectrics* **173**, 243-256 (1995).
24. Wu, S.J., W. Qi, and W. Cao, "Numerical Study of Ultrasonic Beam Pattern of a 1-3 Piezocomposite Transducer," accepted *Proc. IEEE Trans. Ultrasonics, Ferroelectrics and Frequency Control.* (1995).

Composite Sensors (continued)—Volume III

25. Wang, H., Q.M. Zhang, and L.E. Cross, "Tailoring Material Properties by Structure Design--Radially Poled Piezoelectric Cylindrical Tube," *Ferroelectrics Lett.* (in press).
26. Zhang, Q.M. and X. Geng, "Electric Field Forced Vibration of a Periodic Piezocomposite Plate with Laminated Structure and Reflection and Transmission of a Plane Wave at the Fluid-Composite Interface," submitted to *IEEE Transactions on Ultrasonics, Ferroelectrics, and Frequency Control* (1995).
27. Geng, X., and Q.M. Zhang, "Dynamic Behavior of Periodic Piezoceramic-Polymer Composite Plates," *Appl. Phys. Lett.* **67** (21) (1995).
28. Zhang, Q.M., "Transverse Piezoelectric Mode Piezoceramic Polymer Composites with High Hydrostatic Piezoelectric Responses," *Proc. Int. Conf. on Electronic Components and Materials Sensors and Actuators*, Xi'an, China, 159-162 (1995)
29. Zhang, Q.M., H. Wang, J. Zhao, J.T. Fielding, Jr., R.E. Newnham, and L.E. Cross, "A High Sensitivity Hydrostatic Piezoelectric Transducer Based on Transverse Piezoelectric Mode Honeycomb Ceramic Composites," *IEEE Transactions on Ultrasonics, Ferroelectrics and Frequency Control* **43** (1), 26-42 (1996).
30. Zhang, Q.M., J. Chen, H. Wang, J. Zhao, L.E. Cross, and M.C. Trottier, "A New Transverse Piezoelectric Mode 2-2 Piezocomposite for Underwater Transducer Applications," *IEEE Transactions on Ultrasonics, Ferroelectrics, and Frequency Control* **42** (4), 774-780 (1995).
31. Cao, W., Q.M. Zhang, J.Z. Zhao, and L.E. Cross, "Effects of Face Plates on Surface Displacement Profile in 2-2 Piezoelectric Composites," *IEEE Transactions on Ultrasonics, Ferroelectrics, and Frequency Control* **42** (1), 37-41 (1995).
32. Cao, W. and W. Qi, "Plane Wave Propagation in Finite 2-2 Composites," *J. Appl. Phys.* **78** (7), 4627-4632 (1995).
33. Qi, W. and W. Cao, "Finite Element Analysis and Experimental Studies on the Thickness Resonance of Piezocomposite Transducers," accepted *Ultrasonic Imaging* (1995).
34. Cao, W. and W. Qi, "Multisource Excitations in a Stratified Biphase Structure," *J. Appl. Phys.* **78** (7), 4640-4646 (1995).

VOLUME IV

Actuator Studies

35. Uchino, K., "Materials Update: Advances in ceramic actuator materials," *Materials Lett.* **22**, 1-4 (1995).
36. Uchino, K., "Novel Ceramic Actuator Materials."
37. Aburatani, H., K. Uchino, and A.F. Yoshiaki, "Destruction Mechanism and Destruction Detection Technique for Multilayer Ceramic Actuators," *Proc. of the 9th Annual International Symposium on the Applications of Ferroelectrics*, 750-752 (1995).

Actuator Studies (continued)—Volume IV

38. Uchino, K. "Manufacturing Technology of Multilayered Transducers," *Proc. Amer. Ceram. Soc.*, Manufacture of Ceramic Components, 81-93 (1995).
39. Uchino, K. "Piezoelectric Actuators/Ultrasonic Motors--Their Development and Markets," *Proc. 9th ISAF*, 319-324 (1995).
40. Dogan, A., J.F. Fernandez, K. Uchino, and R.E. Newnham, "New Piezoelectric Composite Actuator Designs for Displacement Amplification," in press *Proc. Euroceram 95* (1995).
41. Onitsuka, O., A. Dogan, J.F. Tressler, Q.Su, S. Yoshikawa, and R.E. Newnham, "Metal-Ceramic Composite Transducer, The 'Moonie' ," *J. Intelligent Materials Systems and Structures* **6**, 447-455 (1995).
42. Fernandez, J.F., A. Dogan, J.T. Fielding, K. Uchino, and R.E. Newnham, "Tailoring High Displacement Performance of Ceramic-Metal Piezocomposite Actuators 'Cymbals'," submitted to *IEEE Transactions on Ultrasonics, Ferroelectrics, and Frequency Control* (1995).
43. Hirose, S., S. Takahashi, K. Uchino, M. Aoyagi, and Y. Tomikawa, "Measuring Methods for High-Power Characteristics of Piezoelectric Materials," *Mat. Res. Soc. Symp. Proc.* **360**, 15-20 (1995).
44. Takahashi, S., S. Hirose, K. Uchino, and K.Y. Oh, "Electro-Mechanical Characteristics of Lead-Zirconate-Titanate Ceramics Under Vibration-Level Change," *Proc. 9th ISAF*, 377-382 (1995).
45. Takahashi, Sadayuki, Yasuhiro Sasaki, Seiji Hirose, and Kenji Uchino, "Electro-Mechanical Properties of $\text{PbZrO}_3\text{-PbTiO}_3\text{-Pb}(\text{Mn}_{1/3}\text{Sb}_{2/3})\text{O}_3$ Ceramics Under Vibration-Level Change," *Mat. Res. Soc. Symp. Proc.* **360**, 305-310 (1995).

VOLUME V

46. Zheng, Jiehui, Sadayuki Takahashi, Shoko Yoshikawa, Kenji Uchino, and J.W.C. de Vries, "Heat Generation in Multilayer Piezoelectric Actuators," submitted to *J. Am. Ceram. Soc.* (1995).
47. Uchino, Kenji, "Review: Photostriction and its Applications," in press *J. Innovations in Mater. Res.* (1995).
48. Chu, Sheng-Yuan, and Kenji Uchino, "Photo-Acoustic Devices Using $(\text{Pb,L a})(\text{Zr,Ti})\text{O}_3$ Ceramics," *Proc. 9th ISAF*, 743-745 (1995).

Integration Issues

49. Matsko, M.G., Q.C. Xu, and R.E. Newnham, "Zig-Zag Piezoelectric Actuators: Geometrical Control of Displacement and Resonance," *J. Intell. Mat. Syst. and Struct.* **6** (6), 783-786 (1995).
50. Xu, Baomin, Qiming Zhang, V.D. Kugel, and L.E. Cross, "Piezoelectric Air Transducer for Active Noise Control," submitted *Proc. SPIE* (1996).

Integration Issues (continued)—Volume V

51. Kumar, S., A.S. Bhalla, and L.E. Cross, "Underwater Acoustic Absorption by Collocated Smart Materials," accepted *Ferroelectric Letters* (1995).
52. Elissalde, Catherine and Leslie Eric Cross, "Dynamic Characteristics of Rainbow Ceramics," *J. Am. Ceram. Soc.* **78** [8], 2233-2236 (1995).

Processing Studies

53. Bowen, Christopher P., Thomas R. Shrout, Robert E. Newnham, and Clive A. Randall, "Tunable Electric Field Processing of Composite Materials," *J. of Intelligent Material Systems and Structures* **6** (2), 159-168 (1995).
54. Zhang, Q.M., J. Zhao, T. Shrout, N. Kim, and L.E. Cross, "Characteristics of the Electromechanical Response and Polarization of Electric Field Biased Ferroelectrics," *J. Appl. Phys.* **77** (5), 2549-2555 (1995).
55. Zhao, J., Q.M. Zhang, N. Kim, and T. Shrout, "Electromechanical Properties of Relaxor Ferroelectric Lead Magnesium Niobate-Lead Titanate Ceramics," *Jpn. J. Appl. Phys.* **34**, 5658-5663 (1995).
56. Zipparo, M.J., K.K. Shung, and T.R. Shrout, "Piezoelectric Properties of Fine Grain PZT Materials," *Proc. IEEE Int'l Ultrasonics Symposium* (1995).
57. Yoshikawa, Shoko, Ulagaraj Selvaraj, Paul Moses, John Witham, Richard Meyer, and Thomas Shrout, "Pb(Zr,Ti)O₃[PZT] Fibers—Fabrication and Measurement Methods," *J. Intell. Mat. Syst. and Struct.* **6** (2), 152-158 (1995).
58. Hackenberger, W.S., T.R. Shrout, A. Nakano, and R.F. Speyer, "Rate Controlled Sintering of Low Temperature Cofired Ceramic Multilayers Used for Electronic Packaging."
59. Randall, C.A., N. Kim, W. Cao, and T.R. Shrout, "Domain-Grain Size Relation in Morphotropic Phase Boundary, Pb(Zr_{0.52}Ti_{0.48})O₃," 7th US:Japan Mtg. on Dielectric and Piezoelectric Ceramics, Tsukuba, 145-149 (1995).
60. Cann, David P., Clive A. Randall, and Thomas R. Shrout, "Investigation of the Dielectric Properties of Bismuth Pyrochlores," accepted *Solid State Communication* (1995).

VOLUME VI

61. Mulvihill, Maureen L., Seung Eek Park, George Risch, Zhuang Li, Kenji Uchino, and Thomas R. Shrout, "The Role of Processing Variables in the Flux Growth of PZN-PT Relaxor Ferroelectric Single Crystals."

Thin Films Ferroelectrics

62. Chen, H.D., K.R. Udayakumar, L.E. Cross, J.J. Bernstein, and L.C. Niles, "Dielectric, Ferroelectric, and Piezoelectric Properties of Lead Zirconate Titanate Thick Films on Silicon Substrates," *J. Appl. Phys.* **77** (7), 3349-3353 (1995).

Thin Films Ferroelectrics (continued)—Volume VI

63. Udayakumar, K.R., P.J. Schuele, J. Chen, S.B. Krupanidhi, and L.E. Cross, "Thickness-Dependent Electrical Characteristics of Lead Zirconate Titanate Thin Films," *J. Appl. Phys.* **77** (8), 3981-3986 (1995).
64. Chen, H.D., K.R. Udayakumar, C.J. Gaskey, and L.E. Cross, "Electrical Properties' Maxima in Thin Films of the Lead Zirconate-Lead Titanate Solid Solution System," *Appl. Phys. Lett.* **67** (23), 3411-3413 (1995).
65. Gaskey, C.J., K.R. Udayakumar, H.D. Chen, and L.E. Cross, "'Square' Hysteresis Loops in Phase-Switching Nb-Doped Lead Zirconate Stannate Titanate Thin Films," *J. Mater. Res.* **10** (11), 2764-2769 (1995).
66. Yamakawa, K., S. Trolier-McKinstry, J.P. Dougherty, and S. Krupanidhi, "Reactive Magnetron Co-Sputtered Antiferroelectric Lead Zirconate Thin Films," *Appl. Phys. Lett.* **67** (14), 2014-2016 (1995).
67. Ravichandran, D., K. Yamakawa, A.S. Bhalla, and R. Roy, "Alkoxide Derived $\text{SrBi}_2\text{Ta}_2\text{O}_9$ Phase Pure Powder and Thin Films."
68. Thakoor, Sarita, A.P. Thakoor, and L. Eric Cross, "Optical Non-Invasive Evaluation of Ferroelectric Films/Memory Capacitors," *Mat. Res. Soc. Symp. Proc.* **360**, 157-167 (1995).

ACTUATOR STUDIES

APPENDIX 35

Materials Update

Advances in ceramic actuator materials

Kenji Uchino

*International Center for Actuators and Transducers, Materials Research Laboratory, The Pennsylvania State University,
University Park, PA 16802, USA*

Piezoelectric and electrostrictive actuators, capable of moving something electromechanically, are forming a new field between electronic and structural ceramics. The application fields are classified into three categories: positioners, motors and vibration suppressors. The manufacturing precision of optical instruments such as lasers and cameras, and the positioning accuracy for fabricating semiconductor chips are of the order of 0.1 μm , which must be adjusted using solid-state actuators. Regarding conventional electromagnetic motors, tiny motors smaller than 1 cm^3 , are often required in equipment for office use or for factory automation and are rather difficult to produce with sufficient energy efficiency. Ultrasonic motors whose efficiency is insensitive to size are superior in the minimotor area. Vibration suppression in space structures and vehicles using piezoelectric actuators is also a promising technology. New solid-state displacement transducers controlled by temperature (shape memory alloy) or magnetic field (magnetostrictive alloy) have been proposed, but are generally inferior to the piezoelectric/electrostrictive actuators because of technological trends aimed at reduced driving power and at miniaturization.

Ceramic actuator materials are classified into three categories; piezoelectric, electrostrictive and phase-change materials. Modified lead zirconate titanate [PZT, $\text{Pb}(\text{Zr}, \text{Ti})\text{O}_3$] ceramics are currently the leading materials for piezoelectric applications. The compound PLZT [$(\text{Pb}, \text{La})(\text{Zr}, \text{Ti})\text{O}_3$] 7/62/38 is one such composition. The strain curve is shown on the left in Fig. 1a. When the applied field is small, the

induced strain is nearly proportional to the field ($x=dE$). As the field becomes larger, however, the strain curve deviates from this linear trend and significant hysteresis is exhibited due to polarization reorientation. This sometimes limits the usage of this material in actuator applications that require non-hysteretic response. An interesting new family of actuators has been fabricated from barium stannate titanate [$\text{Ba}(\text{Sn}, \text{Ti})\text{O}_3$] solid solution. The useful property of $\text{Ba}(\text{Sn}_{0.15}\text{Ti}_{0.85})\text{O}_3$ is a very unusual strain curve, in which the domain reorientation occurs only at low fields and there is then a long linear range at higher fields (Fig. 1a, right-hand side).

On the other hand, electrostriction in PMN [$\text{Pb}(\text{Mg}_{1/3}\text{Nb}_{2/3})\text{O}_3$] based ceramics, though a second-order phenomenon of electromechanical coupling ($x=ME^2$), is extraordinarily large (more than 0.1%). An attractive feature of these materials is the near absence of hysteresis (Fig. 1b). The superiority of PMN to PZT was demonstrated in a scanning tunneling microscope (STM). The PMN actuator could provide extremely small distortion of the image even when the probe was scanned in the opposite direction.

With regard to the phase-change related strains, polarization induction by switching from an antiferroelectric to a ferroelectric state, has been proposed. Fig. 1c shows the field-induced strain curves taken for the lead zirconate stannate based system [$\text{Pb}_{0.99}\text{Nb}_{0.02}((\text{Zr}_x\text{Sn}_{1-x})_{1-y}\text{Ti}_y)_{0.98}\text{O}_3$]. The longitudinally induced strain reaches up to 0.4%, which is much larger than that expected in normal piezoelectrics or electrostrictors. A rectangular-shaped hysteresis

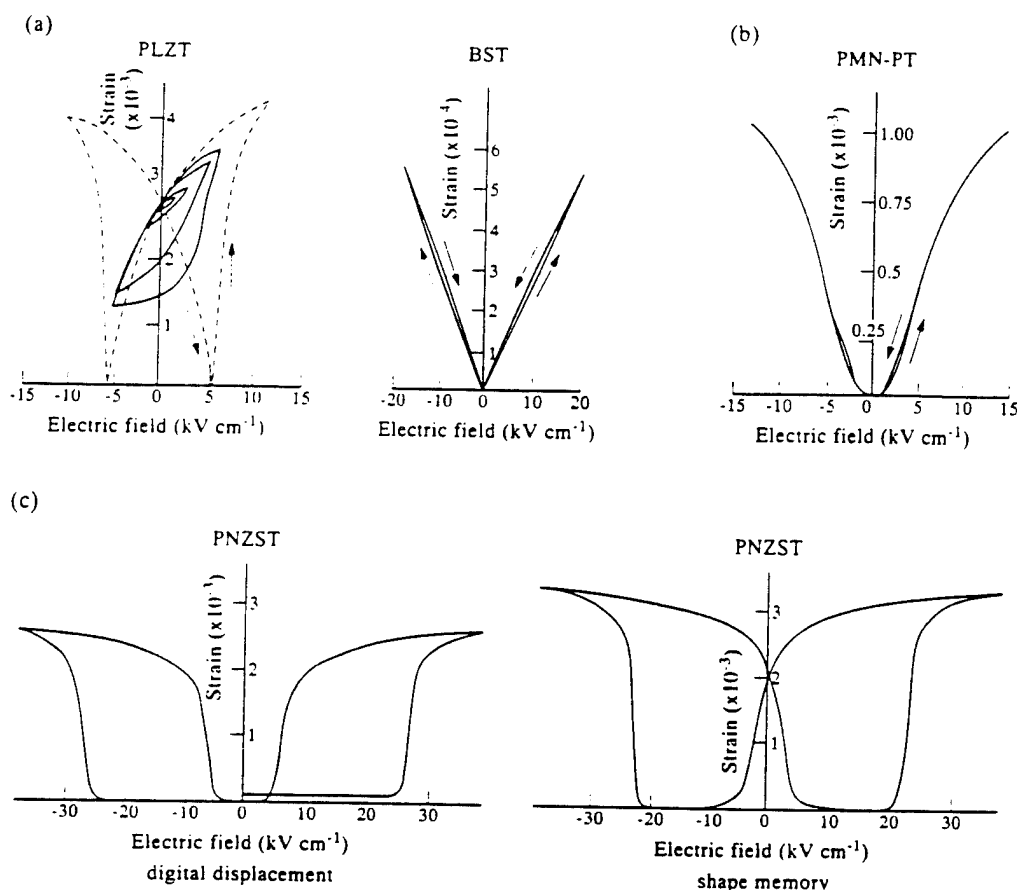


Fig. 1. Electric field-induced strains in ceramics: (a) piezoelectric $(\text{Pb,Lu})(\text{Zr,Ti})\text{O}_3$ and $\text{Ba}(\text{Sn,Ti})\text{O}_3$; (b) electrostrictor $\text{Pb}(\text{Mg}_{1/3}\text{Nb}_{2/3}\text{Ti})\text{O}_3$; (c) phase-change material $\text{Pb}(\text{Zr,Sn,Ti})\text{O}_3$.

esis in Fig. 1c, left-hand side, is referred to as a "digital displacement transducer" because of the two on/off strain states. Moreover, this field-induced transition exhibit shape memory effect in appropriate compositions (Fig. 1c, right-hand side). Once the ferroelectric phase has been induced, the material will "memorize" its ferroelectric state even under zero-field conditions, although it can be erased with the application of a small reverse bias field. This shape memory ceramic is used in energy saving actuators such as latching relays. Compared with the conventional electromagnetic relays, the new relay is much simpler and more compact in structure with almost the same response time.

Two of the most popular actuator designs are multilayers and bimorphs (Fig. 2). The multilayer, in which roughly 100 thin piezoelectric/electrostrictive ceramic sheets are stacked together, has the advantages of: low driving voltage (50 V), quick response (10 μs), high generative force (1 kN) and high electromechanical coupling. But the displacement in the

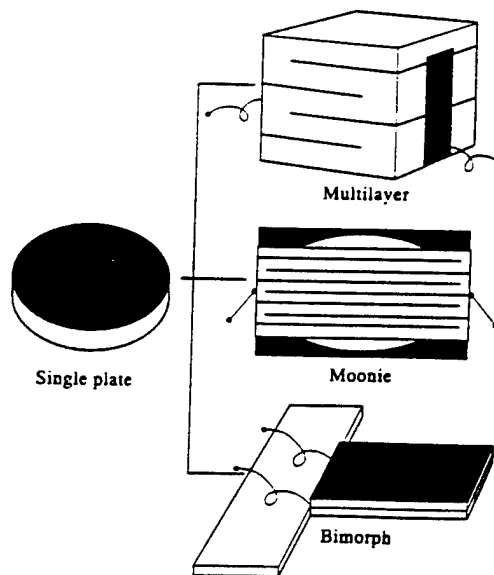


Fig. 2. Typical designs for ceramic actuators: multilayer, moonie and bimorph.

range of 10 μm is not sufficient for some applications. This contrasts with the bimorph consisting of multiple piezoelectric and elastic plates bonded together to generate a large bending displacement of several hundred microns, but the response (1 ms) and the generative force (1 N) are low.

A composite actuator structure called the "moonie" has been developed to provide characteristics intermediate between the multilayer and bimorph actuators; this transducer exhibits a displacement an order of magnitude larger than the multilayer, and a much larger generative force with a quicker response than the bimorph. The device consists of a thin multilayer piezoelectric element and two metal plates with narrow moon-shaped cavities bonded together as shown in Fig. 2. A moonie with a size of $5 \times 5 \times 2.5$ mm can generate a 20 μm displacement under 60 V, which is eight times as large as the generative displacement of the multilayer having the same size. This new compact actuator has been applied to make a miniaturized laser beam scanner.

A monomorph device has been developed to replace to conventional bimorphs, with simpler structure and manufacturing process. The principle is a superimposed effect of piezoelectricity with semiconductivity. The contact between a semiconductor and a metal electrode (Schottky barrier) causes non-uniform distribution of the electric field, even in a compositionally uniform ceramic. Suppose that the ceramic possesses also piezoelectricity, only one side of a ceramic plate tends to contract, leading to a bending deformation in total.

A monomorph plate with 20 mm in length and 0.4 mm in thickness can generate 200 μm tip displacement, in equal magnitude of that of the conventional bimorphs. The "rainbow" actuator is a modification of the abovementioned semiconductive piezoelectric monomorphs, where half of the piezoelectric plate is reduced so as to make a thick semiconductive electrode to cause a bend.

Piezoelectric/electrostrictive actuators may be classified into two categories based on the type of driving voltage applied to the device and the nature of the strain induced by the voltage: (a) rigid displacement devices for which the strain is induced unidirectionally along an applied dc field; and (b) resonating displacement devices for which the alternating strain is excited by an ac field at the mechani-

cal resonance frequency (ultrasonic motors). The first can be further divided into two types: servo displacement transducers (positioners) controlled by a feedback system through a position-detection signal, and pulse-drive motors operated in a simple on/off switching mode, exemplified by dot-matrix printers. An actuator, referred to as a flight actuator, has been proposed which strikes a steel ball by means of a pulse-drive unit made from a multilayer piezodevice similar to that found in a pinball machine.

The materials requirements for these classes of devices are somewhat different, and certain compounds will be better suited to particular applications. The ultrasonic motor requires a very hard type piezoelectric with a high mechanical quality factor Q , leading to the suppression of heat generation. The servo-displacement transducer suffers the most from strain hysteresis and, therefore, a PMN electrostrictor is used for this purpose. The pulse-drive motor requires a low permittivity material aiming at a quick response rather than a small hysteresis so that soft PZT piezoelectrics are preferred to the high-permittivity PMN for this application.

Eighteen years have passed since the intensive development of piezoelectric actuators began, and piezoelectric shutters and automatic focusing mechanisms in cameras, dot-matrix printers and part-feeders have been commercialized and mass-produced by tens of thousands of pieces per month. Taking account of the annual sales estimation in 2000 for ceramic actuator units (\$500 million), camera-related devices (\$300 million) and ultrasonic motors (\$150 million), the market-share of piezoelectric actuators would reach up to \$1 billion in the future.

It is evident that the application field of ceramic actuators is remarkably wide. There still remain, however, problems in durability and reliability that need to be overcome before these devices can become general-purpose commercialized products. The final goal is, of course, to develop much tougher actuator ceramics mechanically and electrically. However, the reliability can be improved significantly if the destruction symptom of the actuator is monitored. An intelligent actuator system composed of two feedback mechanisms has been proposed: position feedback which can compensate the position drift and the hysteresis, and breakdown detection feedback which can stop the actuator system safely without

causing any serious damage to the equipment. Acoustic emission measurement of a piezo-actuator under a cyclic electric field, which exhibits a maximum when the crack propagates extensively, is a good predictor for the lifetime.

Finally, a future promising actuator material is introduced: photostrictive actuators developed recently exhibit an intelligent function incorporating sensing of illumination, and self-production of drive/control voltage together with final actuation. In certain ferroelectrics, a constant electromotive force is generated with exposure to light, and a photostrictive strain results from the coupling of this bulk photovoltaic effect with inverse piezoelectricity. A bimorph unit has been made from PLZT 3/52/48 ceramic doped with slight addition of tungsten. The remnant polarization of one PLZT layer is parallel to

the plate and in the direction opposite to that of the other plate. When violet light is radiated onto one side of the PLZT bimorph, a photovoltage of 1 kV/mm is generated, causing a bending motion. The tip displacement of a 20 mm bimorph was 150 μm with a response time of 1s. A photo-driven micro walking device, a relay and a photoacoustic device ("photo-phone") have been designed to begin moving by light illumination without any electrical circuitry.

Further reading

- [1] K. Uchino, *Piezoelectric/electrostrictive actuators* (Morikita Publishing, Tokyo, 1986).
- [2] K. Uchino, *Bull. Am. Ceram. Soc.* 65 (1986) 647.
- [3] K. Uchino, *J. Rob. Mech.*, 1 (1989) 124.
- [4] K. Uchino, *Mater. Res. Soc. Bull.* 18 (1993) 42.

APPENDIX 36

NOVEL CERAMIC ACTUATOR MATERIALS

Kenji Uchino

International Center for Actuators and Transducers
Materials Research Laboratory, The Pennsylvania State University
University Park, PA 16802-4801

Abstract

Novel functions of materials are sometimes realized by superimposing two different effects. Newly discovered materials, shape memory ceramics, monomorphs and photostrictors, are using sophisticatedly coupled effects of piezoelectricity with another different phenomenon. The shape memory function arises from a phase transition, while the monomorph and the photostriction are associated with a semiconductor contact effect and a bulk photovoltaic effect, respectively. These "very smart" multifunctional actuator materials will be utilized for future promising devices. This paper reviews principles and fundamental and applicational developments of these three materials.

INTRODUCTION

Recent developments in micro-electromechanical systems (MEMS), particularly in solid state actuators, have been remarkable.^{1,2)} Application fields are classified into three categories: positioners, motors and vibration suppressors. The manufacturing precision of optical instruments such as lasers and cameras, and the positioning accuracy for fabricating semiconductor chips, which must be adjusted using solid-state actuators, is of the order of 0.1 μm . Regarding conventional electromagnetic motors, tiny motors smaller than 1 cm^3 are often required in office or factory automation equipment and are rather difficult to produce with sufficient energy efficiency. Ultrasonic motors whose efficiency is insensitive to size are superior in the mini-motor area. Vibration suppression in space structures and military vehicles using piezoelectric actuators is also a promising technology.

Among the smart solid-state actuators, capable of moving something mechanically, controlled by temperature (shape memory alloy), magnetic field (magnetostrictive alloy) and electric field (piezoelectric/electrostrictive ceramic), the former two are generally inferior to the piezoelectric actuators because of technological trends aimed at reduced driving power and miniaturization.

This paper concerns newly discovered ceramic actuator materials using sophisticatedly coupled effects of piezoelectricity with another different phenomenon: shape memory

ceramics, monomorphs and photostrictors. Novel functions of materials are sometimes realized by superimposing two different effects. The shape memory function arises from a phase transition, while the monomorph and the photostriction are associated with a semiconductor contact effect and bulk photovoltaic effect, respectively. These "very smart" multifunctional actuator materials will be utilized for future promising devices. This paper reviews principles and fundamental and applicational developments of these three materials.

SHAPE MEMORY CERAMICS

Concerning the phase-change-related strains, polarization induction by switching from a macroscopically nonpolar into a polar state, as in switching from an antiferroelectric to a ferroelectric state, has been proposed. Different from a shape memory alloy, the strain control is made electrically in the antiferroelectric ceramic, leading to much faster response and lower drive power than in the alloy. After the first report by Berlincourt et al.,³⁾ lead zirconate based ceramics were investigated intensively on the field induced strain characteristics by the authors, and a shape memory effect was discovered.⁴⁻⁶⁾

Figure 1 shows the field-induced strain curves taken for the lead zirconate stannate-based system $[Pb_{0.99}Nb_{0.02}((Zr_xSn_{1-x})_{1-y}Ti_y)_{0.98}O_3]$. The longitudinally induced strain reaches up to 0.4%, which is much larger than that expected in normal piezoelectrics or electrostrictors. A rectangular-shape hysteresis in Fig.1 left, referred to as a "digital displacement transducer" because of the two on/off strain states, is interesting. Moreover, this field-induced transition exhibits a shape memory effect in appropriate compositions (Fig.1 right). Once the ferroelectric phase has been induced, the material will "memorize" its ferroelectric state even under a zero-field condition, although it can be erased with the application of a small reverse bias field. The shape memory effect was also verified in the domain observation with an optical CCD microscope (Fig.2).⁷⁾ While no domain was observed at the initial state, clear domains appeared with an electric field due to the phase transition and remained even when the electric field was removed. Recent researches by other groups were focused on sample fabrication processes and composition search for obtaining larger induced strains.^{8,9)}

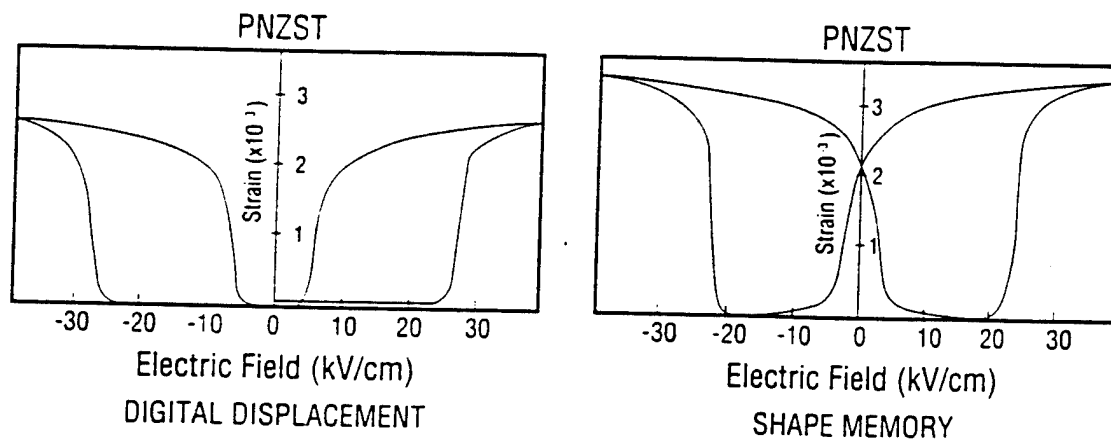


Figure 1 Electric field-induced strains in phase-change materials $Pb(Zr,Sn,Ti)O_3$.

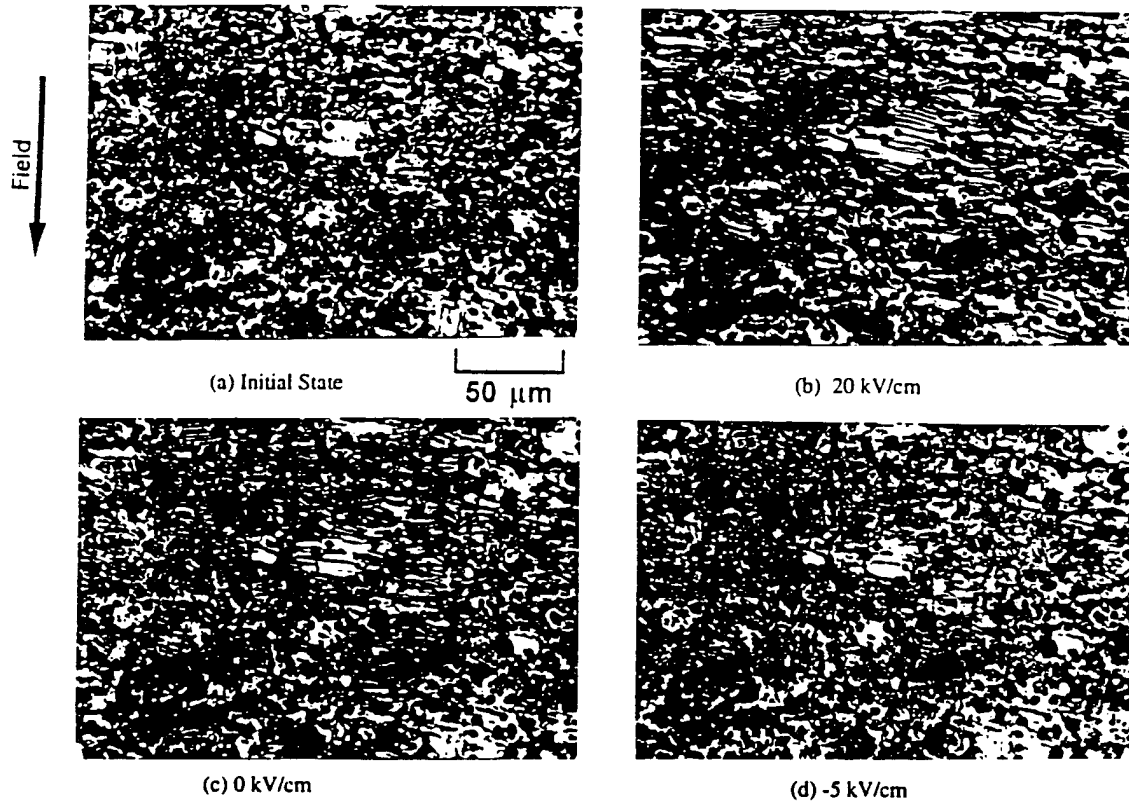


Figure 2 Variation of the domain structure in a shape memory material $\text{Pb}(\text{Zr},\text{Sn},\text{Ti})\text{O}_3$ with an electric field.

This shape memory ceramic was used in energy saving actuators. A latching relay in Fig.3 was composed of a shape memory ceramic unimorph and a mechanical snap action switch, which was driven by a pulse voltage of 4ms.¹⁰⁾ Compared with the conventional electromagnetic relays, the new relay was much simple and compact in structure with almost the same response time.

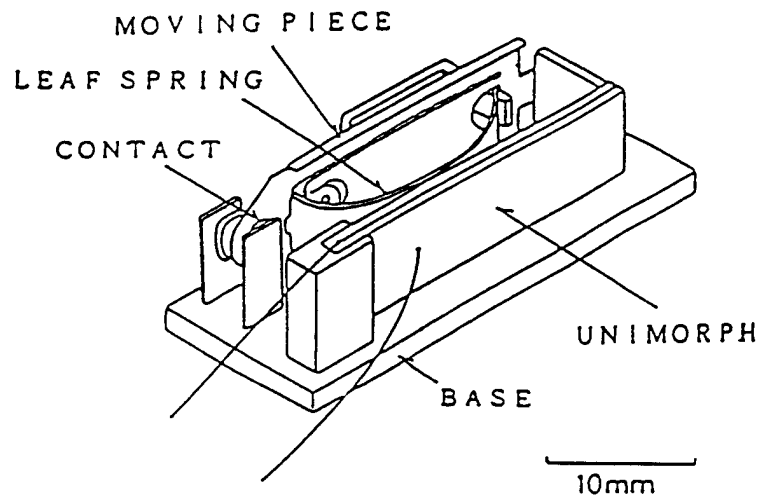


Figure 3 Latching relay using a shape memory ceramic unimorph.

MONOMORPH ACTUATORS

A conventional bimorph-type actuator consists of two piezoelectric plates bonded together and electroded so that their piezoelectric expansion/contraction directions are opposing one another. This actuator will execute a large bending motion of several $100\mu\text{m}$ with the application of an electric field. The most serious problem associated with this type of actuator concerns the bonding of the ceramic plates and the elastic shim. Poor adhesion between these individual elements results in the rapid deterioration of the device after repeated use and displacement drift (creep). The monomorph actuator made from only one ceramic plate, which can achieve the bending displacement, will be a promising design in its simple construction. While avoiding the bonding problems of the bimorph structure, it also allows for significant cost reduction and production efficiency in manufacturing.

The operating principle is based on the coupling of a semiconductor contact phenomenon with the piezoelectric/electrostrictive effect.¹¹⁾ When metal electrodes are applied to both surfaces of a semiconductor plate and a voltage is applied as shown in Fig.4(a), electric field is concentrated on one side (Schottky barrier), thereby generating a non-uniform field within the plate. By making the piezoelectric slightly semiconductive in this manner, contraction along the surface occurs through the piezoelectric effect only on the side at which the electric field is concentrated. The non-uniform field distribution generated in the ceramic causes an overall bending of the entire plate. Figure 4(b) is a modified structure, where a very thin insulative layer improves the breakdown voltage.¹²⁾

Research is underway focused on barium titanate-based and lead zirconate titanate-based piezoelectric ceramics to which additives have been doped to produce semiconductive properties. The PZT ceramics were made semiconductive by preparing solid solutions with a semiconductive perovskite compound $(\text{K}_{1/2}\text{Bi}_{1/2})\text{ZrO}_3$. When 300V was applied to a ceramic plate with 20 mm in length and 0.4 mm in thickness, fixed at one end, the tip deflection as much as $200\mu\text{m}$ could be obtained, equal in magnitude to that of bimorphs (Fig.5).¹³⁾

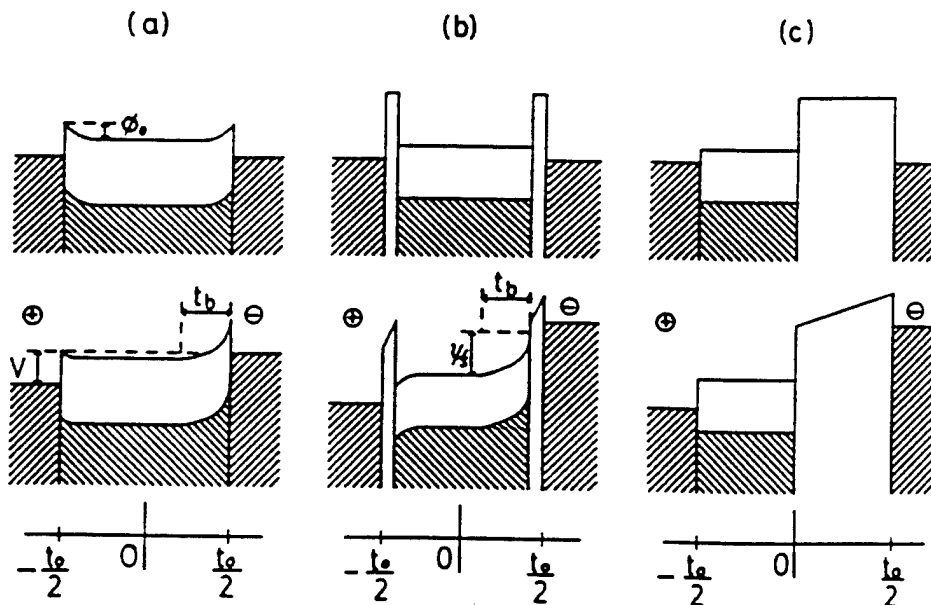


Figure 4 Energy band models for the monomorph actuator: (a) Schottky type, (b) Metal-Insulator-Semiconductor structure with very thin insulative layers, (c) MIS structure with a very thick insulative layer.

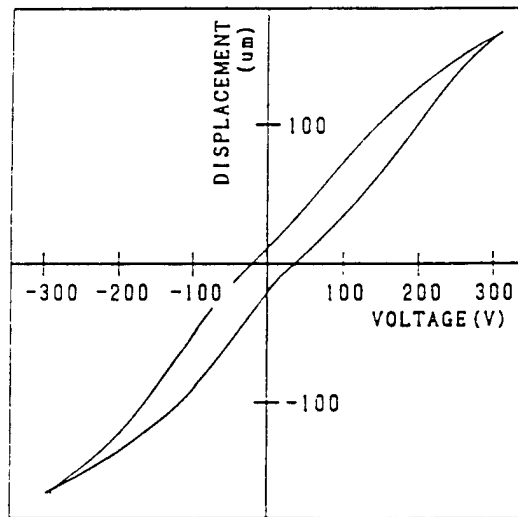


Figure 5 Drive voltage versus tip displacement of a monomorph plate. The sample was made of $0.7\text{Pb}(\text{Zr}_{0.9}\text{Ti}_{0.1})\text{O}_3-0.3(\text{K}_{1/2}\text{Bi}_{1/2})\text{ZrO}_3$ (20mm x 10mm x 0.4mm in size).

The "rainbow" actuator by Aura Ceramics¹⁴⁾ is a modification of the above-mentioned semiconductive piezoelectric monomorphs, where half of the piezoelectric plate is reduced so as to make a thick semiconductive electrode to cause a bend. Figure 4(c) shows the electron energy band structure of the "rainbow".¹²⁾

The monomorph was applied to a simple speaker. Figure 6 shows the sound pressure level versus frequency relation.¹⁵⁾ Though its acoustic characteristics were not satisfactory in comparison with the conventional piezoelectric unimorph types, the monomorph speaker has advantages in mass-production and cost. (b)

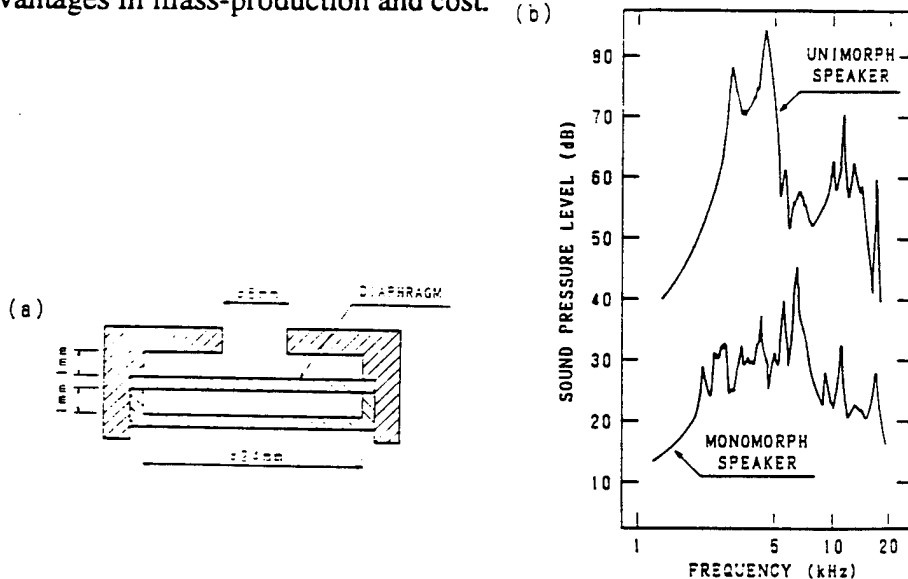


Figure 6 Frequency dependence of the sound pressure level measured at 10 cm in front of the monomorph or unimorph speaker.

PHOTOSTRICTIVE ACTUATORS

The photostrictive effect is a phenomenon in which strain is induced in the sample when it is illuminated. This effect is focused especially in the field of micromechanism. On decreasing the size of miniaturized robots/actuators, the weight of the electric lead wire connecting the power supply becomes significant, and remote control will be definitely required for sub-millimeter devices. A photo-driven actuator is a very promising candidate for micro-robots.¹⁶⁾

In certain ferroelectrics, a constant electromotive force is generated with exposure of light, and a photostrictive strain results from the coupling of this bulk photovoltaic effect to inverse piezoelectricity. A bimorph unit has been made from PLZT 3/52/48 ceramic doped with slight addition of niobium or tungsten.^{17,18)} The remnant polarization of one PLZT layer is parallel to the plate and in the direction opposite to that of the other plate. Figure 7 shows the structure of a photo-driven bimorph in contrast to a voltage-driven one. Notice large illumination area, small capacitance and d_{33} usage, leading to large bending with quick response. When a violet light is irradiated to one side of the PLZT bimorph, a photovoltaic voltage of 1 kV/mm is generated, causing a bending motion. Figure 8 shows the displacement response observed at the tip of a 20 mm bimorph 0.4 mm in thickness. 150 μm was obtained within a couple of seconds.

A photo-driven micro walking device, designed to begin moving by light illumination, has been developed.¹⁹⁾ As shown in Fig.9, it is simple in structure, having neither lead wires nor electric circuitry, with two bimorph legs fixed to a plastic board. When the legs are irradiated alternately with light, the device moves like an inchworm with a speed of 100 $\mu\text{m}/\text{min}$.

Very recently photo-mechanical resonance of a PLZT ceramic bimorph has been successfully induced using chopped near-ultraviolet irradiation, having neither electric lead wires nor electric circuits.²⁰⁾ A dual beam method was used to irradiate the two sides of the bimorph alternately. The tip displacement of the sample is plotted as a function of chopper frequency in Fig.10. The resonance frequency was about 75 Hz with the mechanical quality factor Q of about 30. The achievement of photo-induced mechanical resonance suggests the promise of photostrictors as vibration actuators such as "ultrasonic motors."

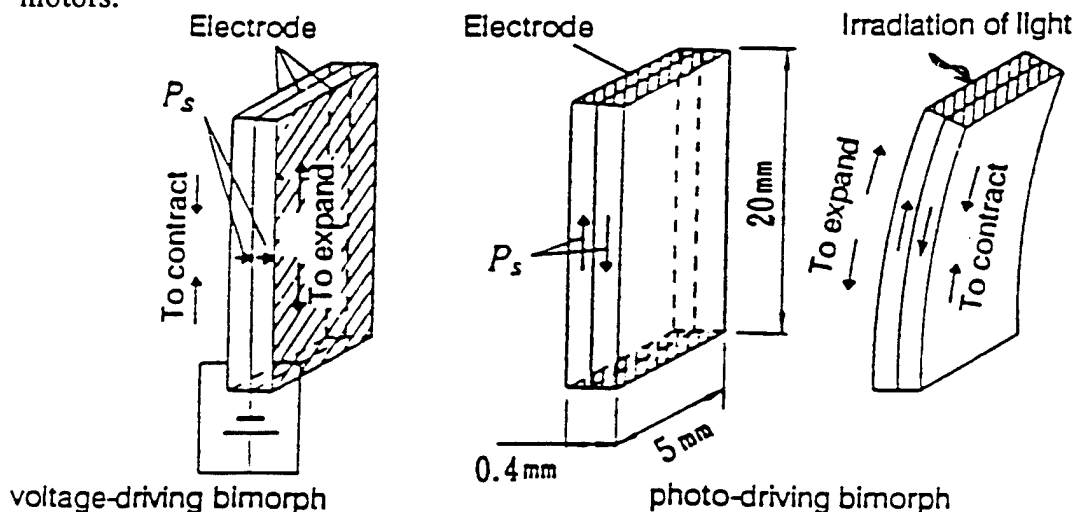


Figure 7 Structures of voltage- and photo-driven bimorphs and their driving principles.

15.000000
 6 / 0

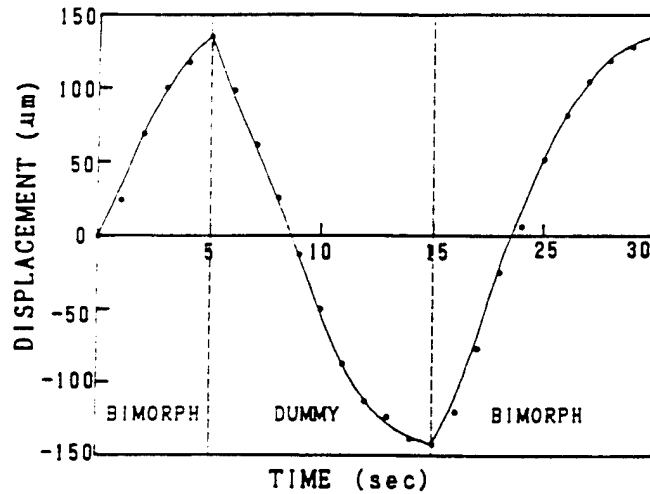


Figure 8 Tip deflection of the bimorph device made of WO_3 0.5 at.% doped PLZT under a dual beam control (illumination intensity: 10 mW/cm^2).

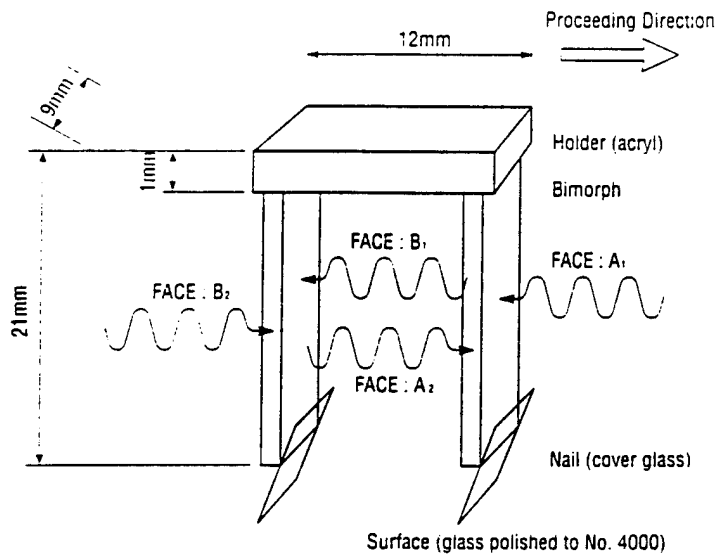


Figure 9 Structure of the photo-driven micro walking machine.

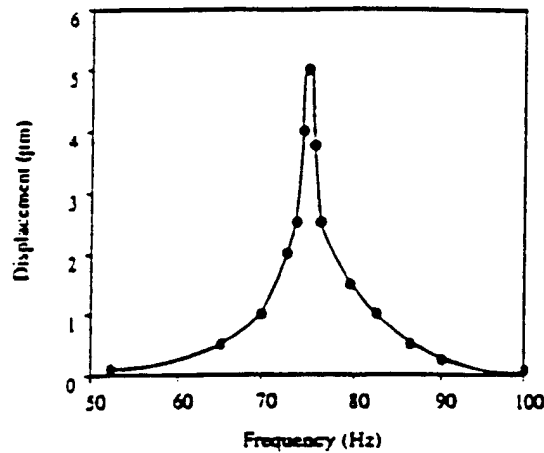


Figure 10 Photo-induced mechanical resonance behavior of the PLZT bimorph.

Acknowledgement

This work was partly supported by US Army Research Office and Office of Naval Research through Contracts No. DAAL 03-92-G-0244 and No. N00014-91-J-4145.

REFERENCES

- 1) K.Uchino, "Ceramic Actuators: Principles and Applications," *Mater. Res. Soc. Bull.* **18** (1993) 42-48.
- 2) K.Uchino, "New Piezoelectric Devices for Smart Actuator/Sensor Systems," *Proc. Electroceramics IV, Aachen, Sept. 5-7 (1994)* 179-191.
- 3) D.Berlincourt, H.H.A.Krueger and B.Jaffe, *J. Phys. & Chem. Solids* **25** (1964) 659.
- 4) K.Uchino and S.Nomura, "Electrostriction in PZT-Family Antiferroelectrics," *Ferroelectrics* **50** (1983) 191.
- 5) K.Uchino, "Shape Memory Effect Associated with the Forced Phase Transition in Antiferroelectrics," *Proc. MRS Int'l. Mtg. on Adv. Mater.* **9** (1989) 489.
- 6) K.Y.Oh, A.Furuta and K.Uchino, "Shape Memory Unimorph Actuators Using Lead Zirconate-Based Antiferroelectrics," *J. Ceram. Soc. Jpn.* **98** (1990) 905.
- 7) K.Y.Oh, K.Uchino and L.E.Cross, "Optical Study of Domains in Antiferroelectric Ceramics," *J. Adv. Performance Mater.* [in press].
- 8) W.Y.Pan, Q.Zhang, A.Bhalla and L.E.Cross, *J. Amer. Ceram. Soc.* **72** (1989) 571.
- 9) Z.Xu, D.Viehland and D.A.Payne, *J. Appl. Phys.* **74** (1993) 3406.
- 10) A.Furuta, K.Y.Oh and K.Uchino, "Shape Memory Ceramics and Their Application to Latching Relays," *Sensors and Mater.* **3** (1992) 205.
- 11) K.Uchino, M.Yoshizaki, K.Kasai, H.Yamamura, N.Sakai and H.Asakura, *Jpn. J. Appl. Phys.* **26** (1987) 1046.
- 12) K.Uchino, M.Yoshizaki and A.Nagao, *Jpn. J. Appl. Phys.* **26**, Suppl.26-2 (1987) 201.
- 13) K.Uchino, M.Yoshizaki and A.Nagao, "Monomorph Characteristics in Pb(Zr,Ti)O₃ Based Ceramics," *Ferroelectrics* **95** (1989) 161-164.
- 14) Aura Ceramics, Inc., USA, Catalogue "Rainbow".
- 15) K.Uchino and S.Suzuki, "Speakers Utilizing Semiconductive Piezoelectric Monomorph Devices," *J. Ceram. Soc. Jpn.* **100** (1992) 1221-1224.
- 16) S.Y.Chu and K.Uchino, "Photostrictive Effect in PLZT-Based Ceramics and Its Applications," *Ferroelectrics* [in press].
- 17) K.Uchino, M.Aizawa and S.Nomura, *Ferroelectrics* **64** (1985) 199-208.
- 18) M.Tanimura and K.Uchino, *Sensors and Mater.* **1** (1988) 47-56.
- 19) K.Uchino, "Micro Walking Machines Using Piezoelectric Actuators," *J. Rob. Mech.* **1** (1989) 124-127.
- 20) S.Y.Chu, Z.Ye and K.Uchino, *J. Adv. Performance Mater.* **1** (1994) 129-143.

APPENDIX 37

Destruction Mechanism and Destruction Detection Technique for Multilayer Ceramic Actuators

Hideaki Aburatani and Kenji Uchino
The Pennsylvania State University, IMRL
University Park, PA 16802

Atushi Furuta and Yoshiaki Fuda
Tokin Corporation, 6-7-1 Koriyama Taihakoku
Sendai-city Miyagi-Pref. 982, Japan

Abstract -- The destruction process of piezoelectric actuators under bipolar driving was studied using Acoustic Emission (AE) monitoring and induced-displacement measurement. The effect of floating electrode over the internal electrode's end was also investigated. Floating electrodes can suppress the field concentration and cracking in the actuator.

I. INTRODUCTION

Piezoelectric multilayer ceramic actuators have been widely used as key components of electromechanical devices, because of their large displacement, low driving voltage, quick response, large generative force and high electromechanical transduction capability[1],[2]. This type of actuator can be fabricated by a tape casting method with an interdigital electrode configuration that used in the conventional multilayer ceramic capacitor industry. The interdigital electrode (Fig. 1(a)) structure is appropriate for large-volume production, but the field concentration is an inevitable problem, which creates stress concentration and cracking in the actuators[3],[4]. Figure 1(b) and Fig. 1(c) show the plate-through and the interdigital with slits type electrode configurations which can provide uniform distribution of electric field and release the stress concentration respectively. The latter two designs, however, require much sophisticated technology, leading to high production cost. Note that in piezoelectric ceramic materials, the field concentration is equivalent to the stress concentration.

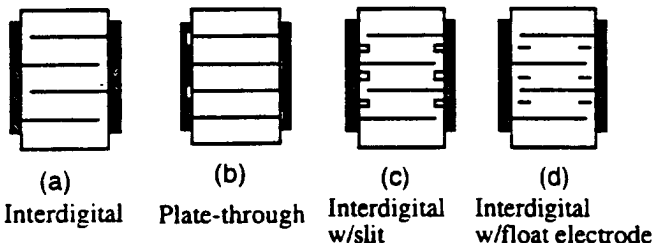


Figure 1 Various of internal electrode configuration.

This paper deals with the destruction mechanism the interdigital electrode type actuator first and a couple of detection techniques are introduced [5]. Finally, a new internal electrode design with float electrodes (Fig.1 (d)), which can release the electric field concentration, will be proposed.

II. EXPERIMENTAL

Piezoelectric $Pb((Ni_{1/3}Nb_{2/3})_xZr,Ti)O_3$ (PNN-PZT) ceramic was selected for this study, because this material is presently widely commercialized in co-fired multilayer actuators. The samples, prepared by a tape casting method, have two internal electrodes which is simulating the interdigital electrode configuration with an electrode gap of 200 μ m. Figure 2 shows the structure of samples. The floating electrodes were placed right over the end of internal electrodes and in the center of the layer.

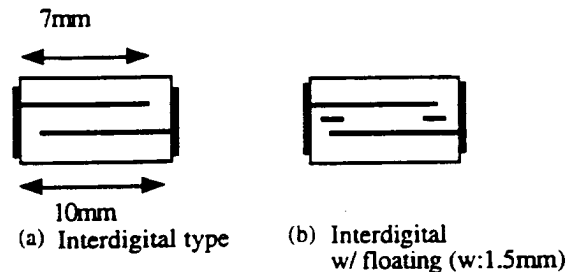


Figure 2 Structure of the samples. Layer thickness :200 μ m.

Figure 3 shows the measuring system consisting of a linear variable differential transducer (LVDT) (Millitron, Model 1301) and an acoustic emission sensor (NF Corporation, AE- 905USF116). A large electric field was applied (KEPCO BOP 1000M) in order to accelerate the actuator collapse. The samples were bipolar-driven at 1 Hz by a triangular electric field of ± 2.0 kV/mm. To detect Acoustic Emission (AE), an AE sensor was placed under the actuator. The acoustic emission signal was amplified by 50dB, and a high pass filter (100kHz) was used to discriminate noise. Induced displacement were also monitored during the driving. Induced displacement measurement was held at the center of the samples.

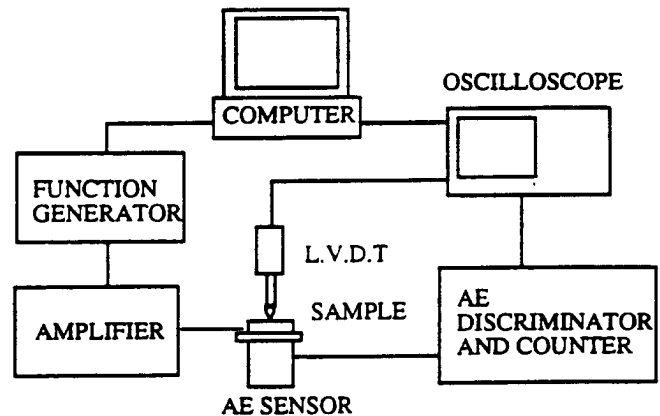


Figure 3 Measurement system.

III. RESULTS AND DISCUSSIONS

A. Crack and delamination

Figure 4 shows typical crack patterns in the samples. The crack is usually initiated at the edge of the internal electrode and propagates obliquely outward to another electrode (Fig. 4(a)). At the same time, delamination is generated between the electrode and ceramic interface (Fig. 4(b)). Occasionally, a crack which propagates vertically between a pair of internal electrodes is observed. This crack is probably due to an internal defect located near the electrode (Fig. 4 (b)) [6].

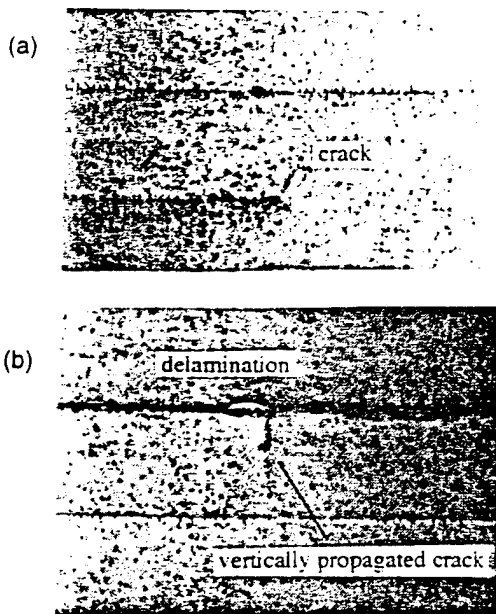


Figure 4 (a) Crack at the end of internal electrode.
(b) Delamination and vertically-propagated crack.

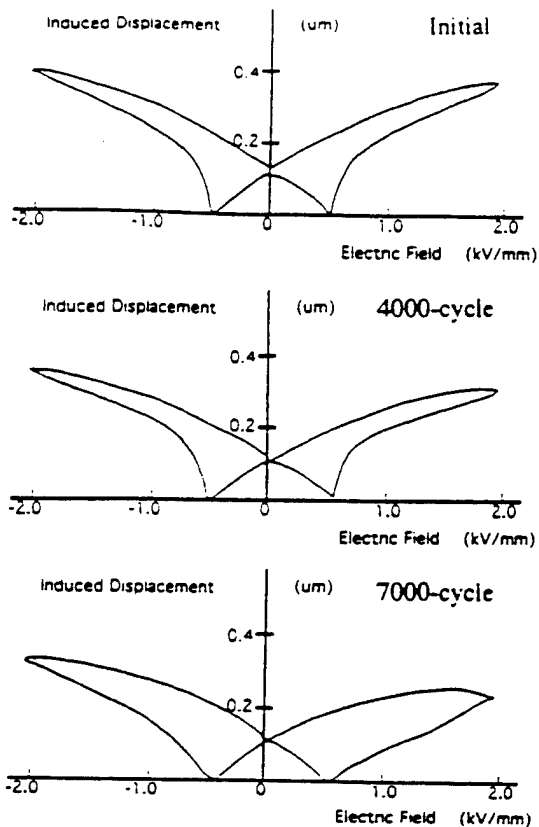


Figure 6 Induced displacement change in the interdigital type.

B. Acoustic Emission

Figure 5 shows AE from the actuator plotted as a function of drive cycle. At the first stage, rather many AE were counted intermittently, which is caused by the poling process, and can be interpreted as the initiation of micro-crack. After this process, AE count is stabilized, owing to the alleviation of stress by micro-cracking. Continuous AE started after several thousands cycle, and the number of AE was remarkably increased. This AE indicates fast crack-growth and delamination in the actuator.

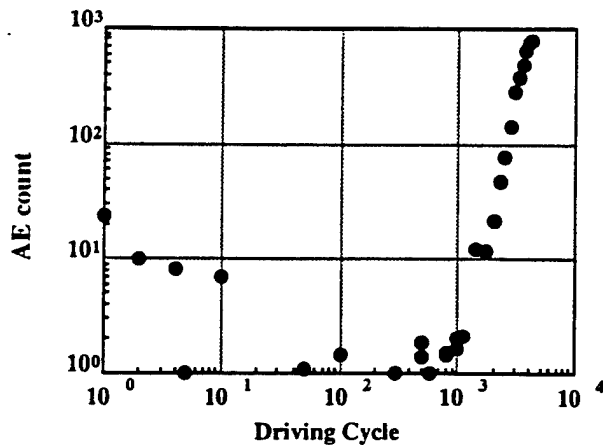


Figure 5 AE count as a function of drive cycle.

C. Change in induced displacement

Figure 6 shows the induced displacement change of the model actuator. Obvious change was observed after 7000-cycle. The magnitude of induced displacement hysteresis-loop increased, and sharpness at the coercive field was lost. These results indicate crack and delamination in an actuator, but it is difficult to distinguish these failure from thermal and aging effect.

D. Effect of field suppression using float electrodes

Figure 7 shows comparison of AE generation among the interdigital type and interdigital & floating electrode type actuators. It is clarified that the interdigital & float electrode type endure longer than the conventional interdigital type. This result implies that the floating electrode suppress the cracking at the end of internal electrode.

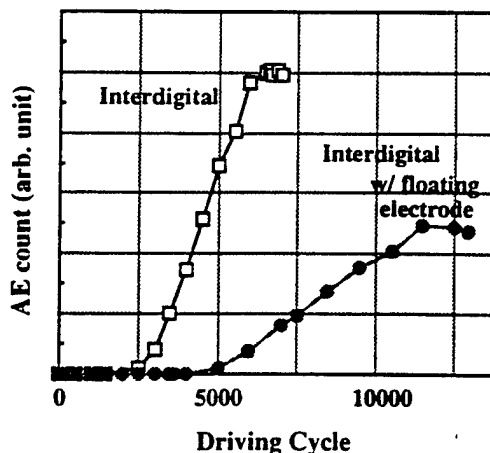


Figure 7 AE count in the interdigital and interdigital & floating electrode type actuators as a function of driving cycle.

IV. SUMMARY

The destruction process of the actuator was studied. Acoustic Emission related to the poling was observed. From induced-displacement measurement, indirect information about destruction was obtained. It is confirmed that AE monitoring can be an excellent actuator's failure predictor.

The effect of suppressing electrical field concentration was studied. It was clarified that suppressing electrical field by floating electrodes over the end of internal electrodes gives longer life time to the actuators.

V. ACKNOWLEDGMENT

This work was supported by the Office of Naval Research through Contract No. N00014-92-J-1510.

REFERENCES

- [1] K. Uchino, *Piezoelectric/Electrostrictive Actuators*. Tokyo, Morikita, Japan, 1986
- [2] K. Uchino. MRS bull. 18. 42 (1993)
- [3] S. Takahashi, A. Ochiai, M. Yonezawa, T. Yano, T. Hamatsuki and I. Fukui. "Internal Electrode Piezoelectric Ceramic Actuator," *Ferroelectrics*, vol.50, pp.181-190 (1983).
- [4] A. Furuta and K. Uchino. "Dynamic Observation of Crack Propagation in Piezoelectric Multilayer Actuators." *J. Am. Ceram. Soc.* vol.76 No. 6, pp.1615-1617 (1993).
- [5] Hideaki Aburatani, Shuichi Harada, Kenji Uchino, Atushi Furuta and Yoshiaki Fuda. "Destruction Mechanism in Ceramic Multilayer Actuators," *Jpn. J. Appl. Phys.*, vol 33, part 1, No. 5B, pp. 3091-3094 (1994)
- [6] Z. Suo, "Models for breakdown-resistance dielectric and Ferroelectric ceramics," *J. Mech. Phys. Solids*, vol41, No. 7 pp1155-1176 (1993)

APPENDIX 38

MANUFACTURING TECHNOLOGY OF MULTILAYERED TRANSDUCERS

Kenji Uchino
International Center for Actuators and Transducers
Materials Research Laboratory, The Pennsylvania State University
University Park, PA 16802

ABSTRACT

Multilayer structures have been investigated intensively in the application fields of ferroelectric ceramics; dielectrics, piezoelectrics and electrooptics. General problems for manufacturing actual devices are discussed and possible solutions are introduced in this paper, focusing on particle and grain size effects on properties, electrode materials and designs, and reliability issues of hybrid structures. Key words to the future trend will be "finer" and "hybridization."

INTRODUCTION

In the recent application fields of ferroelectric ceramics, multilayered structures have been investigated intensively, aiming at miniaturization and hybridization of the devices. Figure 1 exemplifies multilayer, multimorph and multi-moonie structures. This paper reviews the applications of these devices first, then the preparation processes, and finally current problems are pointed out and possible solutions are introduced.

Key words to the future trend will be "finer" and "hybridization." Layers thinner than 10 μm , which is currently used in multilayer capacitors, will also be introduced in the actuator devices instead of the present 100 μm sheets. Non-uniform configurations or hetero-structures of the materials, layer thickness or the electrode pattern will be adopted for practical devices.

APPLICATIONS OF MULTILAYERED CERAMICS

Multilayered structures are widely utilized in the application fields of dielectrics, piezoelectrics and electrooptics.

Multilayered Dielectrics

Electrostatic capacitance of a multilayer capacitor is given by the following formula:

$$C = n\epsilon_0\epsilon_r S/(L/n), \quad (1)$$

where ϵ_r is the relative permittivity of the material, n the number of layers, S area, and L is the total thickness of the capacitor. Note that the capacitance increases drastically in proportion to the square of the number of layers, when the total size is fixed. The conventional capacitor of 10 μF with 30 μm layer thickness used to have 70 mm^3 in

To the extent authorized under the laws of the United States of America, all copyright interests in this publication are the property of The American Ceramic Society. Any duplication, reproduction, or republication of this publication or any part thereof, without the express written consent of The American Ceramic Society or fee paid to the Copyright Clearance Center, is prohibited.

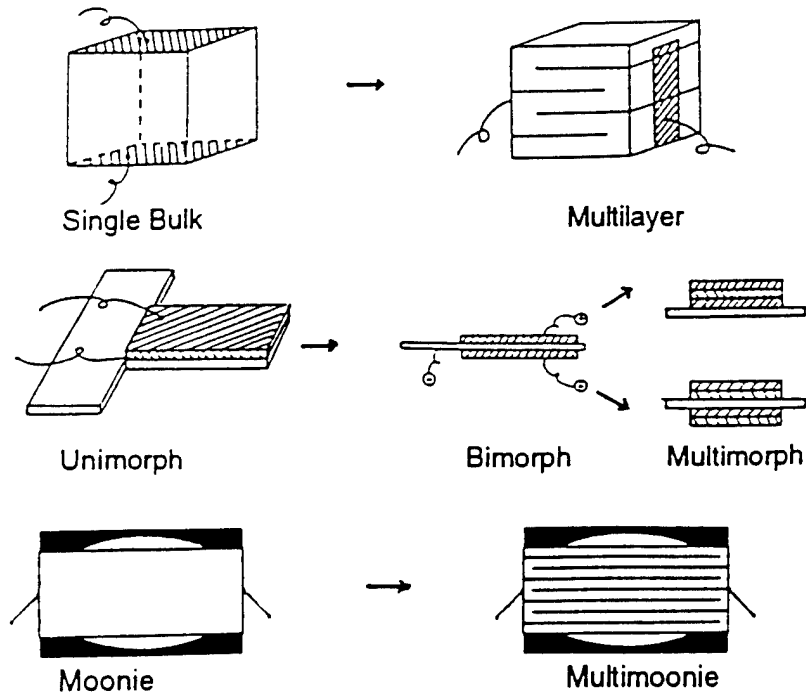


Fig. 1 Examples of multilayer, multimorph and multi-moonie structures.

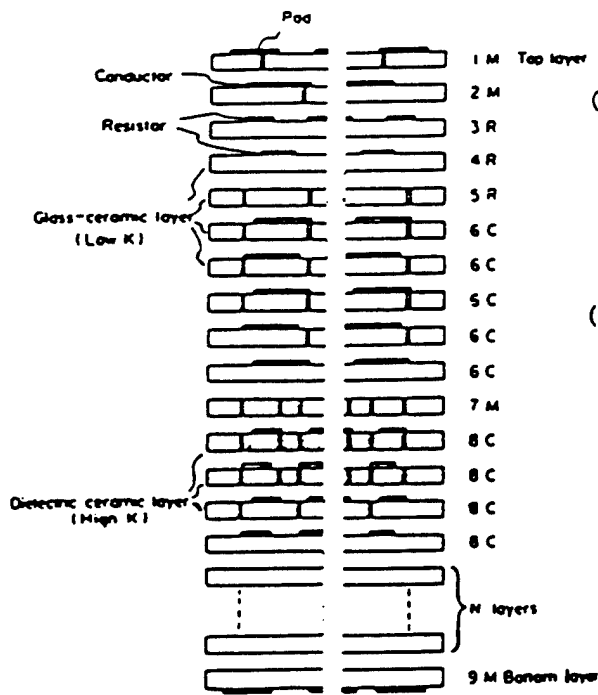


Fig. 2 Section view of a monolithic multicomponent ceramic.

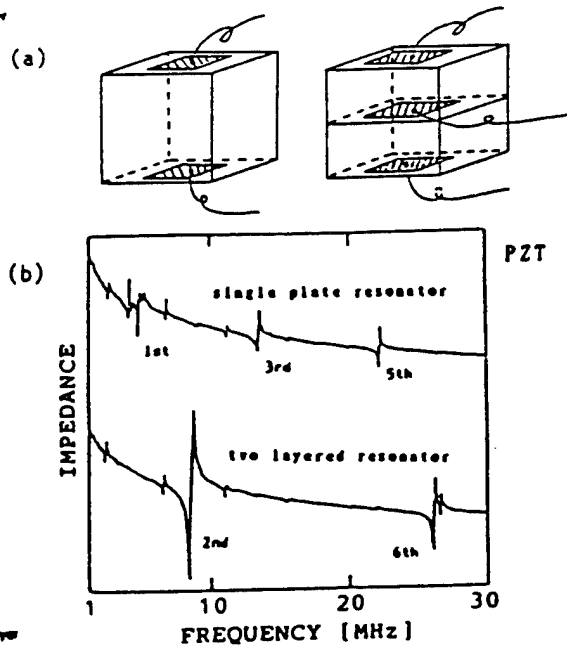


Fig. 3 (a) Single- and two-layer piezo-resonators. (b) Impedance curves.

volume size. With decreasing the layer thickness down to 10 μm , the device volume could be reduced into 7.7 mm^3 .¹⁾

Multilayered substrates are also very promising for making a hybrid structure of an electrical circuit. Figure 2 shows a sectional view of a monolithic multicomponents-ceramic for a voltage controlled crystal oscillator,²⁾ where resistors and capacitors are included in the substrate.

Piezoelectric Multilayers

A two-layered piezoelectric resonator has been proposed for a higher-order mode oscillator.³⁾ Figure 3(a) illustrates single- and two-layered structures and Fig. 3(b) shows impedance curves for these two resonators as a function of frequency. It is notable that the second-order harmonic mode is significant in the two-layered structure compared with the fundamental mode.

Multilayer piezoceramics have been applied to actuators. First example is found in an ultrasonic linear motor.⁴⁾ The merits of the usage of a multilayer structure are low drive voltage and a large (input electrical energy /volume) ratio. The motor consists of a metal fork and a piezoelectric element (Fig. 4(a)) and the motion of the fork legs is illustrated in Fig. 4(b). The maximum speed of 30 cm/s and the maximum load (thrust) of 10 N were realized for the input energy of 0.7 W with an efficiency of 16 %.

Second example is a dot matrix printer.⁵⁾ The displacement of 16 μm in a 20 mm-long piezo-actuator is magnified by 30 times with a hinge lever mechanism as shown in Fig. 5(a), and 24 head elements are arranged to make a printer head for Chinese characters (Fig. 5(b)). The printing speed of 100 characters /sec is 3 times quicker than the conventional electromagnetic printer.

Thirdly, a deformable mirror is introduced,⁶⁾ which is useful for the phase matching of the light wave in image detectors such as an astronomic telescope. The device consists of three plates of lead magnesium niobate based (PMN) electrostrictive ceramics bonded together with a glass mirror. Each ceramic plate possesses a different electrode pattern to generate focus or coma aberration on the mirror surface (See Fig. 6(a) and (b)).

A laser beam scanner is the most recent application of a multi-moonie actuator.⁷⁾ The moonie consists of a thin multilayer ceramic element and two metal plates with a narrow moon-shaped cavity bonded together, and can amplify the small displacement induced in a piezoelectric ceramic. The moonie with a size of 5mm x 5mm x 2.5mm can generate a 18 μm displacement under 60 V, which is an order of magnitude larger than the generative displacement of the multilayer with the same size. This compact actuator has been applied to make a miniaturized laser beam scanner for laser printers (Fig. 7).

Multilayer Electrooptic Devices

In order to reduce the half-wavelength voltage (i. e. drive voltage), the multilayer structure is also used in electrooptic devices. Figure 8 shows a PLZT (lead lanthanum zirconate titanate) light valve with internal electrodes. Much smaller voltage (80V) is sufficient to drive the valve in comparison with the usual shutter (300V).

A recent application is found in a 2-dimensional display for projection type TV's.⁸⁾ Several tens of PLZT sheets are stacked alternately with plate-through and separate electrodes,

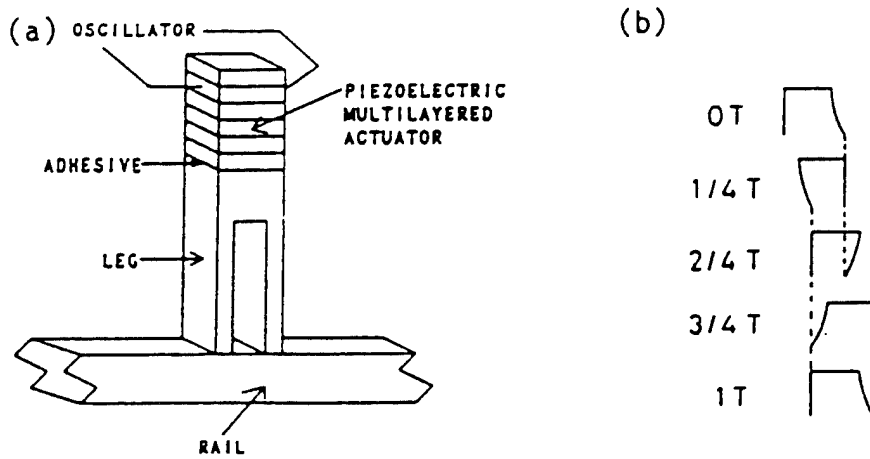


Fig.4 (a) Structure of an ultrasonic linear motor. (b) Motion of the fork legs.

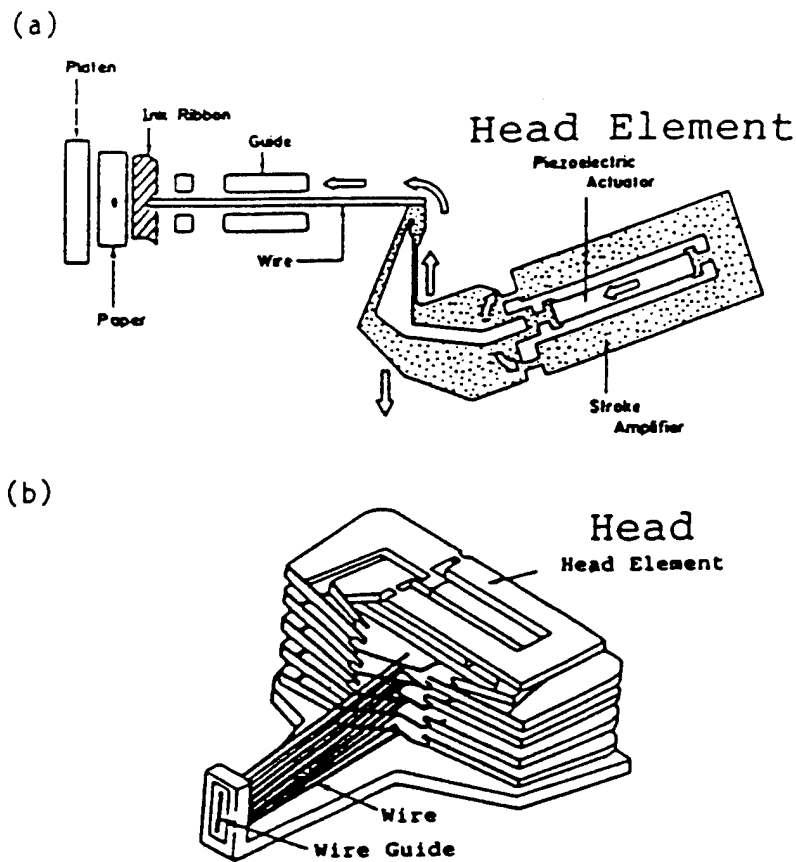
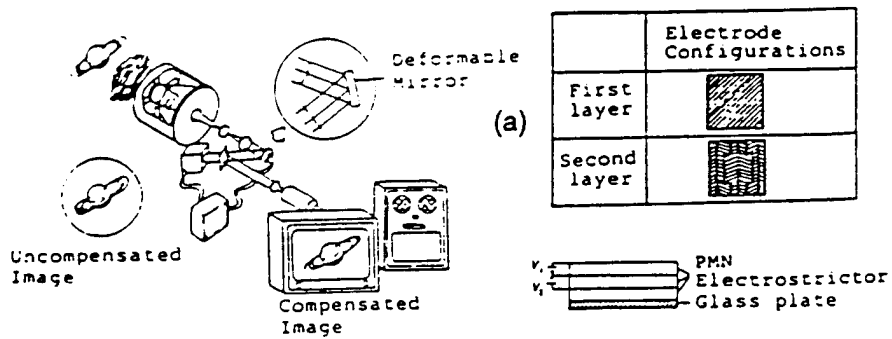


Fig. 5 (a) Printer head element consisting of a multilayer piezoceramic. (b) Dot matrix printer head.



(b)

Aberration	Desired Interference pattern	Generated Interference pattern
Focus $x^2 + y^2$		
Coma $x^3 + xy^2$		
Focus + Coma $C_R(x^2 + y^2)$ $-C_C(x^3 + xy^2)$		

Fig.6 (a) Structure of a multi-morph deformable mirror. (b) Actual control of wavefront.

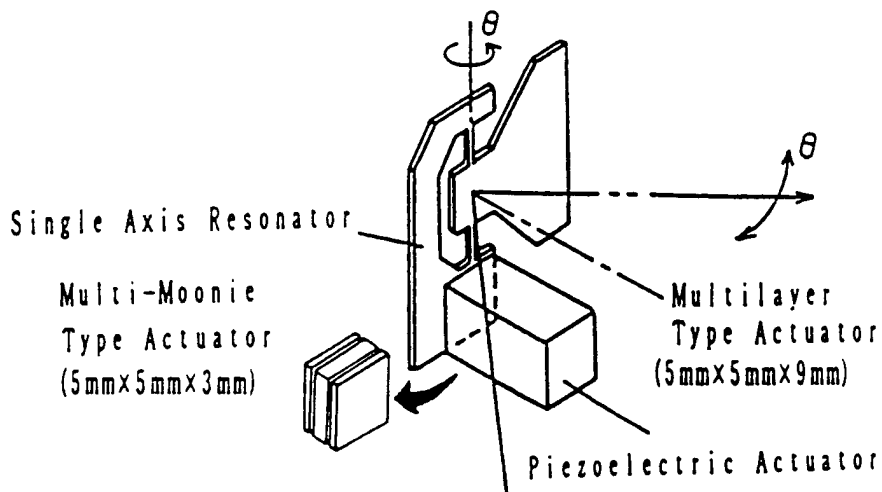


Fig.7 Laser beam scanner utilizing a piezoelectric multi-moonie actuator.

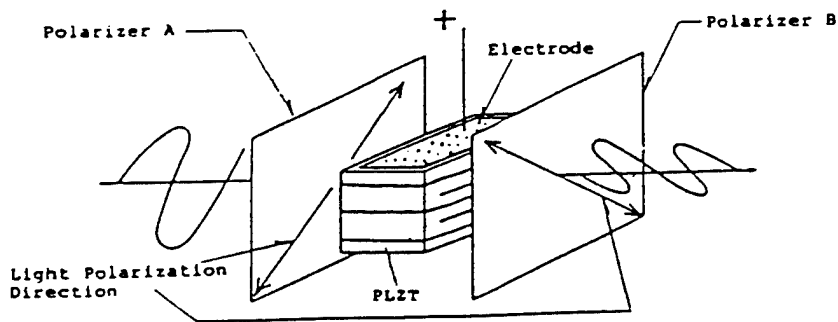


Fig.8 PLZT light valve.

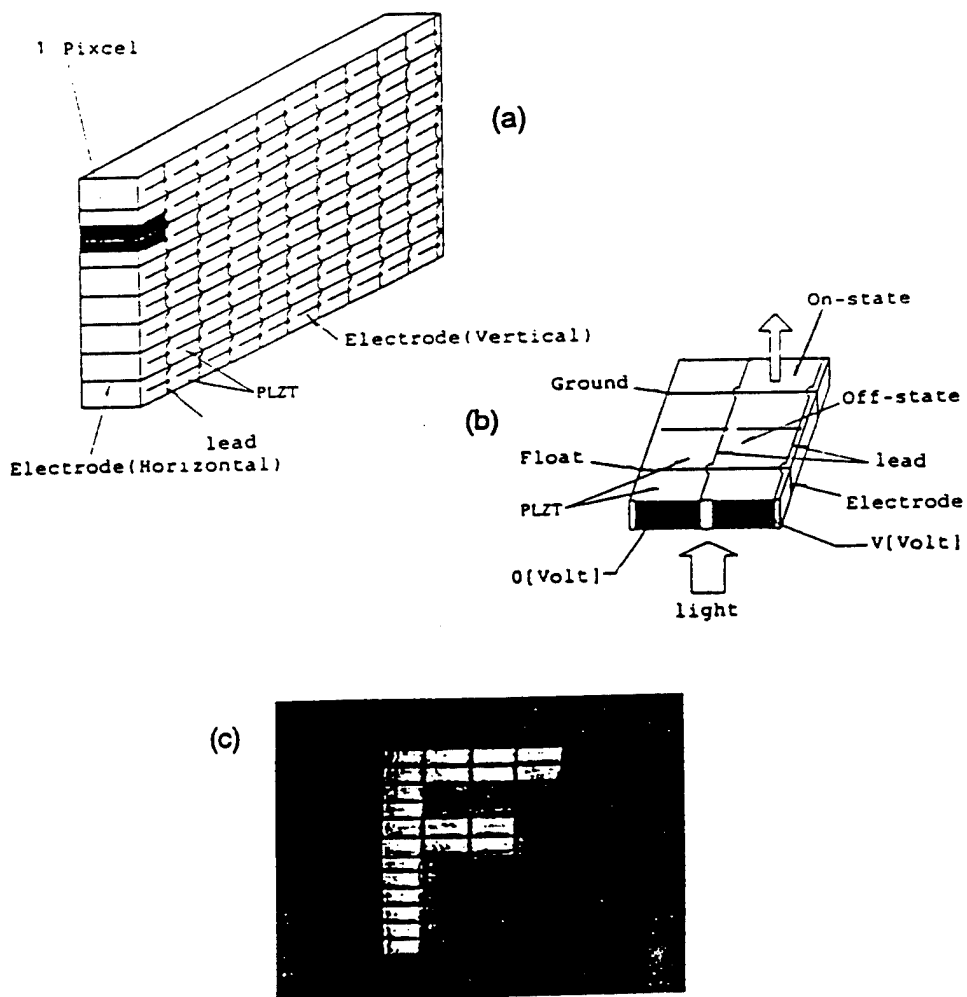


Fig.9 (a) Design of a 2-dimensional display. (b) Operation principle of a pixel. (c) An example image on the screen.

as shown in Fig. 9(a). Plate-through and separate electrodes are used for horizontal and vertical addressing, respectively. A pixel consists of a pair of PLZT sections beside a plate-through electrode (Fig. 9(b)). Figure 9(c) shows a character "F" projected on a screen.

PREPARATION PROCESS OF MULTILAYERED STRUCTURES

Two preparation processes are possible for multilayered ceramic devices: one is a cut-and-bond method and the other is a tape-casting method. Figures 10(a) and 10(b) show the flow-charts of the both methods. The tape-casting method requires expensive fabrication facilities and sophisticated techniques, but is suitable for mass-production more than 10 K pieces per month.

PROBLEMS OF MULTILAYERED CERAMIC DEVICES

There are several problems in multilayered ceramic devices to be overcome. Three of them are particularly mentioned here (particle/grain size effect, internal electrode, reliability), and possible solutions will be discussed.

Ultra-Fine Particle/Grain

With reducing the thickness of a layer, recent tendency to fabricating fine ceramic particles or fine grain samples has prompted to reduce the size down to nano-meter range. However, we must notice that the sample with fine particles below a certain critical size will not exhibit ferroelectricity-related properties (piezoelectricity, primary electrooptic effect, pyroelectricity etc.)

Let us review here the particle size dependence of ferroelectricity in BaTiO_3 .⁹⁾ Figure 11 shows the lattice parameter change with temperature measured for several particle size BaTiO_3 powders. With decreasing particle size, the tetragonality at room temperature decreases gradually with a drastic drop to 1.0 (i. e. cubic) at $0.12 \mu\text{m}$. The tetragonality decreases also with temperature and exhibits an abrupt change at $c/a = 1.0025$ into the cubic state; this implies that the phase transition must be of the first order. A decrease of the particle size leads to a decrease of the Curie temperature. The permittivity versus temperature curves are shown in Fig. 12 for several grain size samples.⁹⁾ Both the permittivity and the peak temperature decrease with decreasing grain size.

Figure 13 plots the hydrostatic pressure P required for depressing T_C down to room temperature and the critical particle size $2R_{\text{crit}}$ as a function of Curie/Neel temperature of the perovskite materials ($(\text{Ba},\text{Sr})\text{TiO}_3$, $(\text{Ba},\text{Pb})\text{TiO}_3$ and PbZrO_3).¹⁰⁾ The plot provides two important empirical rules that the critical hydrostatic pressure P_{crit} is almost proportional to the Curie temperature T_C , and that the critical particle size $2R_{\text{crit}}$ is inversely proportional to the Curie or Neel temperature T_C/T_N . This leads to an interesting equation;

$$P_{\text{crit}} = 2 \gamma / R_{\text{crit}} \quad (\gamma = \text{constant}), \quad (2)$$

which suggests a phenomenological semi-macroscopic model related to the "effective" surface tension of a fine particle. Almost constant value of 55 N/m is obtained for the γ of any perovskite ferroelectrics, which is two-orders of magnitude as large as the γ of non-polar oxides such as MgO .

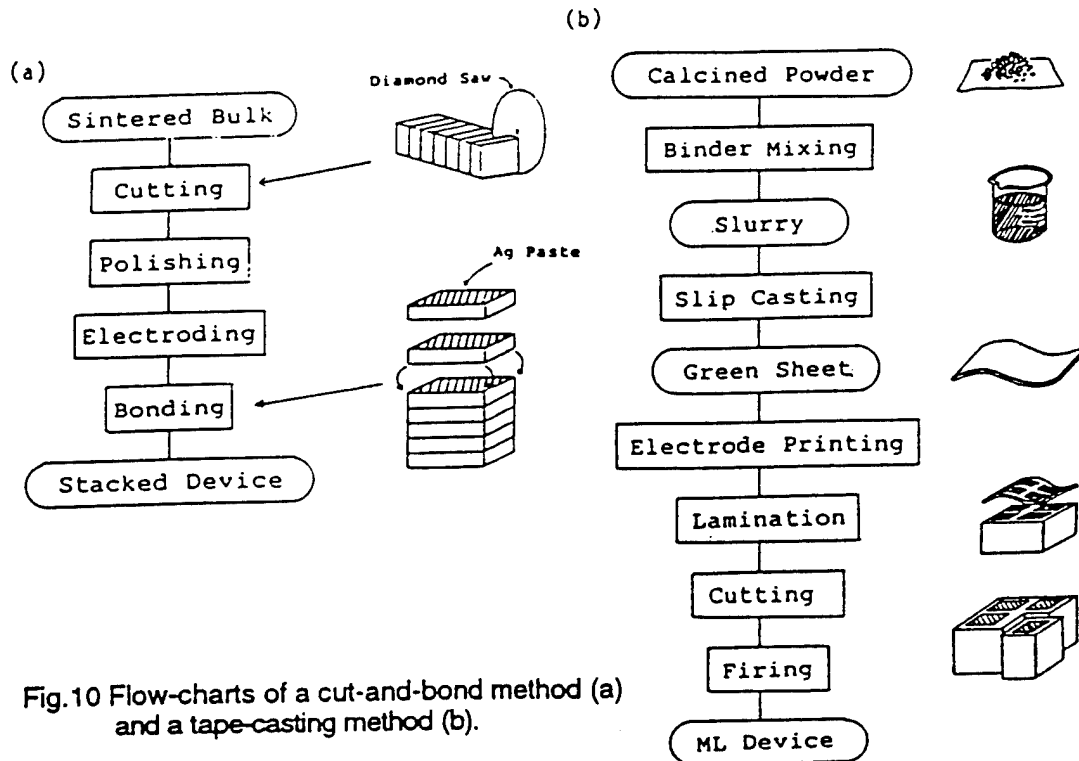


Fig.10 Flow-charts of a cut-and-bond method (a) and a tape-casting method (b).

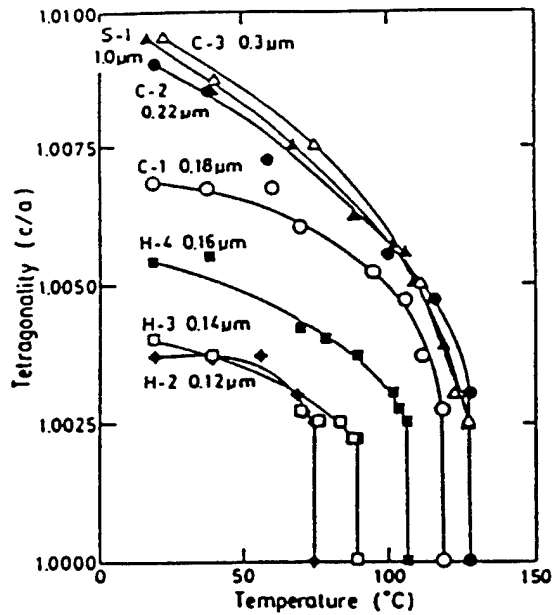


Fig.11 Lattice parameter change with temperature measured for several particle size BaTiO₃ powders.

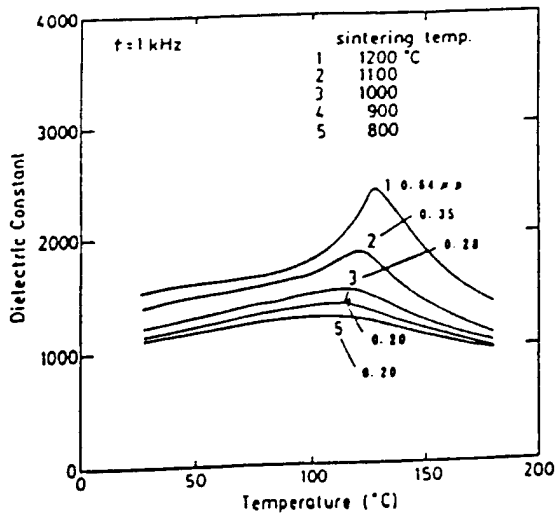


Fig.12 Permittivity vs. temperature curves for several grain size samples.

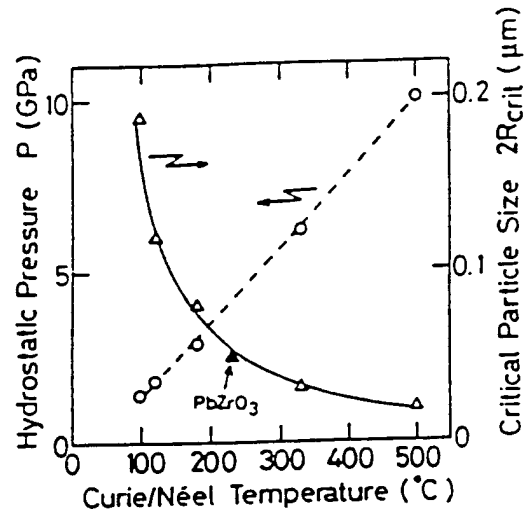


Fig.13 Curie/Neel temperature dependence of critical hydrostatic pressure P_{crit} and critical particle size $2R_{crit}$ in ferro- and antiferroelectric materials.

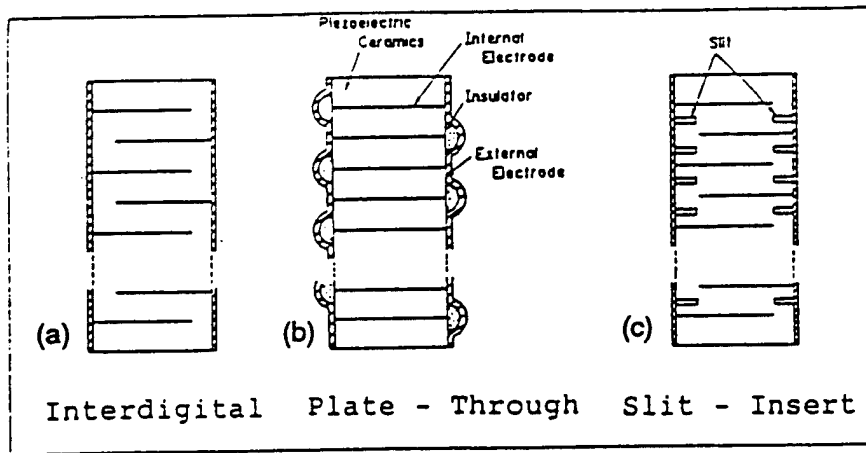


Fig.14 Electrode designs of multilayer piezoelectric actuators.

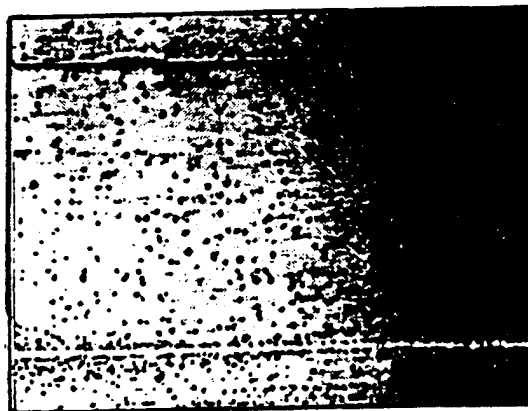


Fig.15 Crack propagation pattern in the multilayer piezoelectric component.

In conclusion, we need to be very careful to use submicron (or less than the critical grain size) grain samples for practical ferroelectric applications.

Mechanically-Weak Electrode

Concerning electrode materials, migration of Ag into ceramics under an application of high voltage sometimes causes troubles. Electrode alloys such as Ag-Pd can solve this problem. On the other hand, expensive cost of rare-metals (Ag, Au, Pt) gives difficulties for mass-production. Possibility of Cu or Ni for electrodes is now under investigation with the development of new dielectric materials which require low sintering temperature not to oxidize the electrode materials.

Mechanical weakness on the junction between the ceramic and the electrode metal often provides delamination problems. One solution is to reduce the internal stress generated during driving. Figure 14 shows typical designs of multilayer piezo-actuators. Type (a) called an "interdigital" configuration generates significantly large tensile stress just outside the internal electrode edge during an electrical drive, so as to expand microcracks gradually. A typical crack pattern is shown in Fig. 15.¹¹⁾ Type (b) is called a "plate-through" design, where no stress is induced, but the fabrication process of the insulative covers on the edge is rather laborious.¹²⁾ In Type (c), a slit-insert design, the induced stress is relaxed by the narrow slits.

Another solution against the delamination is the usage of stiff electrode materials. Ceramic powder (identical with the actuator material) is sometimes mixed into the metal electrode paste. We introduce here a PTCR (positive temperature coefficient of resistivity) BaTiO₃ based ceramics for electrode materials.¹³⁾ Figure 16 shows the resistivity change of BaTiO₃ ceramics with La₂O₃ doping concentration. Multilayered actuators with non-doped resistive BaTiO₃ sheets and 0.2 atm% doped semiconductive sheets have been fabricated using the tape-casting process. It is notable that the sintering temperature is almost the same for both electrode and piezoelectric materials and the La diffusion is negligibly small on the boundaries because the two sheet materials have just slightly different compositions. Mechanical strength has been tested by a 3-points bend method, and the resulting Weibull plot is shown in Fig. 17. The relation between non-destructive probability and load is plotted for ceramic electrode samples in comparison with Pd-electroded samples. Mechanical strength is improved by 3-4 times when the ceramics electrode is used. To realize PZT-based semiconductive ceramics will be a future focus of development.

Reliability of Hybrid Structures

The more the multilayered device becomes hybridized and complicated, the more the reproducibility and the reliability of the device must be taken into account. An "intelligent" actuator system has been proposed containing both a position drift compensation mechanism and a safety feedback function, as illustrated in Fig. 18.¹⁴⁾ Detection of the destruction symptom of the multilayer ceramic actuator is very important, particularly when the actuator is utilized in a precision cutting machine not to cause any serious damages onto the work, or when quality classification of the actuators is required.

There are three possible predictors for the actuator failure; induced-displacement monitoring, acoustic emission (AE) counting and surface voltage measurement. In order to monitor the potential change, an additional surface electrode was coated on the

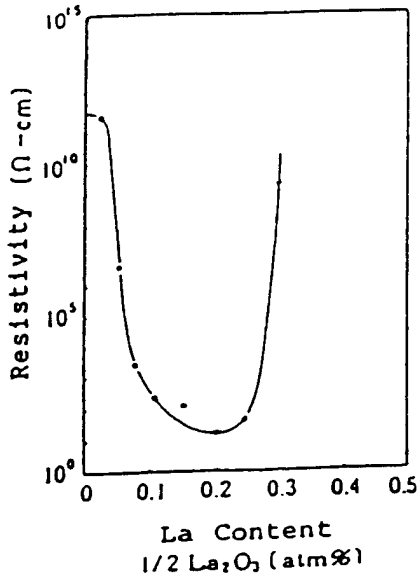


Fig.16 Resistivity change of BaTiO_3 ceramics with La_2O_3 doping concentration.

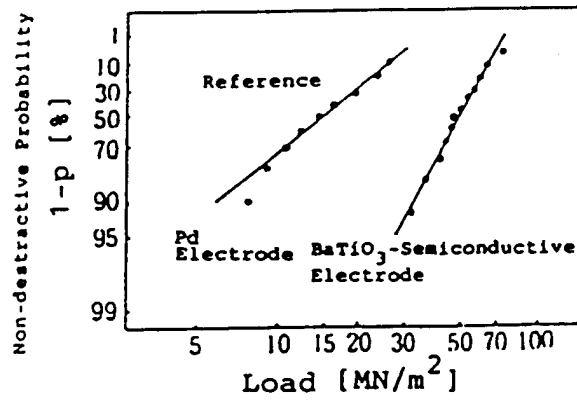


Fig.17 Weibull plots of multilayer piezoelements with ceramic electrodes.

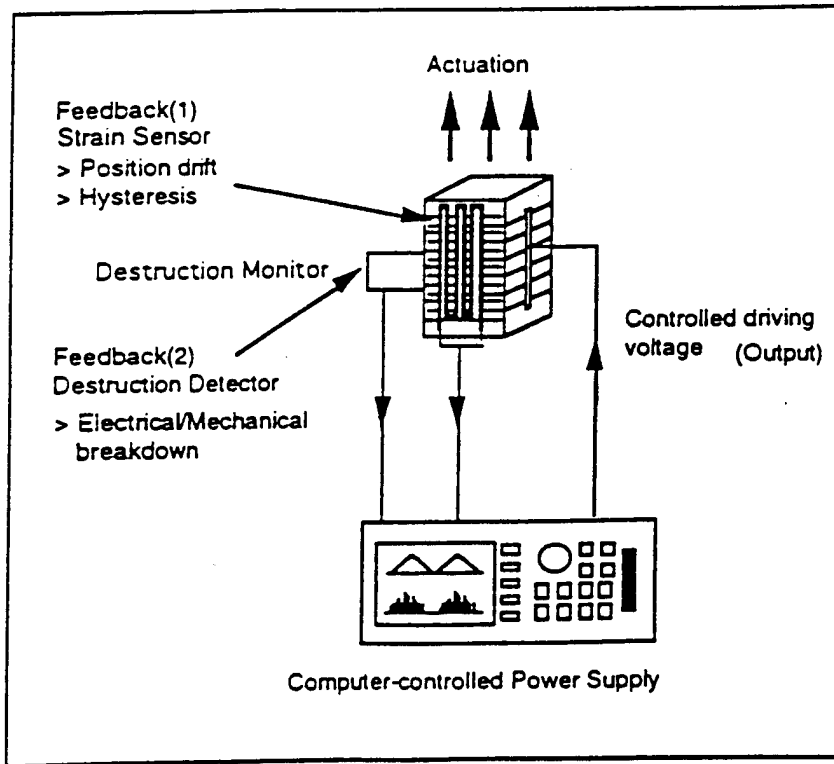


Fig.18 Intelligent piezoelectric actuator system with two feedback circuits.

multilayered piezo-actuator ($\text{Pb}((\text{Ni}_{1/3}\text{Nb}_{2/3})\text{Zr,Ti})\text{O}_3$) near the internal electrode edge, as schematically illustrated in Fig. 19.15) The sensor part is embedded in this actuator, and it can be called really a "smart" structure. Changes in the AE count and the surface potential are plotted as a function of drive cycle in Fig. 20, where a drastic increase and a sudden drop are observed, respectively, according to the crack propagation inside the multilayer sample.

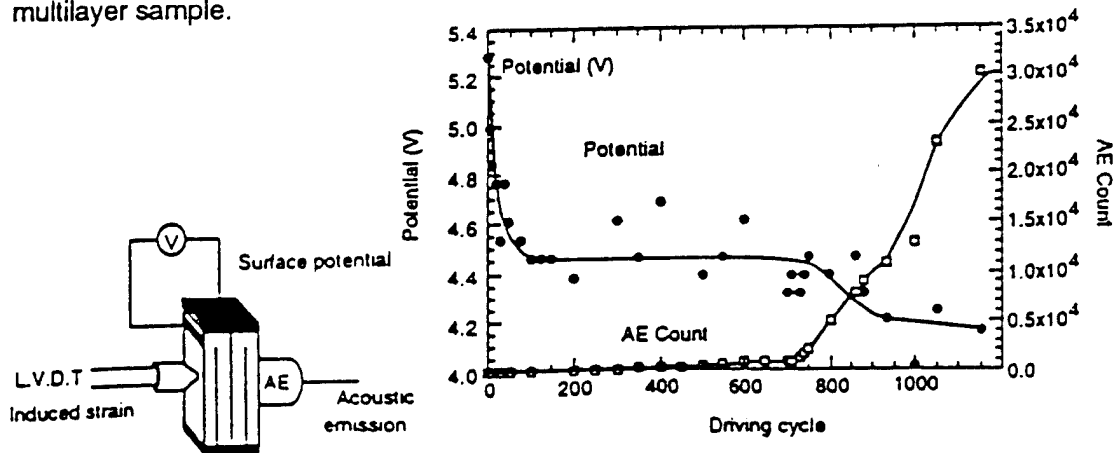


Fig.20 Changes in AE count and surface potential with driving cycle measured in a multilayered piezoelectric PNNZT sample.

Fig.19 Sample arrangement for measuring the induced strain, acoustic emission and surface potential.

SUMMARY

Problems in the multilayered ceramic transducers and possible solutions are summarized:

1. The sample with a particle/grain size above a certain critical range (0.1 μm) should be used for practical ferroelectric/piezoelectric devices.
2. Electrode configurations not to generate large internal stresses should be adopted, or stiff ceramic electrodes will be another promising technology.
3. To obtain the reliability of piezoelectric multilayer actuator systems, the AE measurement or the surface potential monitoring can be introduced for detecting the crack initiation/propagation.

This work was partly sponsored by the Office of Naval Research through Contract No. N00014-92-J-1510.

REFERENCES

- 1) K. Utsumi: Private Communication at 4th US-Japan Seminar on Dielectric & Piezoelectric Ceramics (1989).
- 2) K.Utsumi, Y.Shimada, T.Ikeda and H.Takamizawa: *Ferroelectrics* **68**, 157 (1986).

- 3) T.Kittaka: Private Communication at 4th US-Japan Seminar on Dielectric & Piezoelectric Ceramics (1989).
- 4) M.Tohda, S.Ichikawa, K.Uchino and K.Kato: *Ferroelectrics* 93, 287 (1989).
- 5) T.Yano, I.Fukui, E.Sato, O.Inui and Y.Miyazaki: *Electr. & Commun. Soc. Proc.*, 1-156 (Spring, 1984).
- 6) T.Sato, H.Ishikawa, O.Ikeda, S.Nomura and K. Uchino: *Appl. Optics*, 21, 3669 (1982).
- 7) H.Goto, K.Imanaka and K.Uchino: *Ultrasonic Techno* 5, 48 (1992).
- 8) K.Ohmura, Y.Murai, K.Uchino and J.Giniewicz: *Int'l Display Res. Conf. Proc.*, IEEE, 138 (1989).
- 9) K.Uchino, E.Sadanaga, K. Oonishi and H. Yamamura: *Ceramic Trans.*, Vol.8 Ceramic Dielectrics, 107 (1990).
- 10) T.Yamakawa and K.Uchino: *Proc. Int'l Symp. Appl. Ferroelectrics '90*, 610 (1991).
- 11) A.Furuta and K.Uchino: *J. Amer. Ceram. Soc.* 76, 1615 (1993).
- 12) S.Takahashi, A.Ochi, M.Yonezawa, T.Yano, T.Hamatsuki and I.Fukui: *Jpn. J. Appl. Phys.* 22, Suppl.22-2, 157 (1983).
- 13) K.Abe, K.Uchino and S.Nomura: *Ferroelectrics* 68, 215 (1986).
- 14) H.Aburatani, S.Harada, A.Furuta, Y.Fuda and K.Uchino: *Jpn. J. Appl. Phys.* 33, 3091 (1994)
- 15) K.Uchino and H.Aburatani: *Proc. Int'l Conf. Intelligent Mater. '94* (1994) (in press).

APPENDIX 39

PIEZOELECTRIC ACTUATORS/ ULTRASONIC MOTORS -- Their Developments and Markets --

Kenji Uchino
International Center for Actuators and Transducers
Intercollege Materials Research Laboratory
The Pennsylvania State University, University Park, PA 16802

Abstract -- Recent development trend of piezoelectric actuators/ ultrasonic motors is reviewed from the Japanese patent disclosure, and their future market is predicted, which may reach up to \$ 10 billion in the year of 2000.

INTRODUCTION

Eighteen years have passed since the intensive development of piezoelectric/ electrostrictive actuators started, and the focus has been shifted to practical device applications presently. Piezoelectric shutters (Minolta Camera) and automatic focusing mechanisms (Canon) in cameras, dot-matrix printers (NEC) and part-feeders (Sanki) have been commercialized and mass-produced already by several tens thousand pieces per month. During these commercialization, new designs and drive/control techniques of the ceramic actuators have been mainly developed in these a couple of years [1 - 3]. A number of patent disclosures have been found particularly in Japanese industries such as NEC, TOTO Corporation, Matsushita Electric, Brother Industry, Toyota Motors, Tokin, Hitachi Metal, Toshiba.

The piezoelectric actuators and ultrasonic motors have been developed by private industries in Japan, aiming at the applications to precision positioners and compact motors, and are too practical to be supported by the Japanese government. Only a big national project relating to this area is currently on "Micromechanisms", which mostly covers the silicon micro-machining-related micromotors. On the contrary, the developments in the USA are mainly supported by the military-related government institutions, are mainly focused on active vibration control.

This paper reviews recent development trend of the piezoelectric actuators/ ultrasonic motors viewed from the Japanese patent disclosure, and predicts their future market.

DEVELOPMENT TREND VIEWED FROM THE PATENT DISCLOSURE

Table 1 summarizes 550 patents concerning piezoelectric actuators and ultrasonic motors disclosed during January 1988 - July 1990 in Japan, which is classified with respect to the patent submitter and the technical content. Tabulation was made using 4 large categories; material, design, drive/control and application, each of which is further classified into composition, fabrication process; multilayer, displacement magnification mechanism, bimorph, others: drive technique, control technique; servo displacement transducer, pulse-drive motor and ultrasonic motor.

Most of the top-ten companies (NEC, TOTO Corporation, Matsushita Electric, Brother Industry, Toyota Motors, Tokin, Hitachi Metal, Toshiba, Nippon Denso, Fuji Electric) have already started to supply the products of piezoelectric actuators/ultrasonic motors or their application devices. Only TOTO Corporation and Fuji Electric have not disclosed their target explicitly.

Development Trend in the Technical Content

The patent disclosure was graphed with respect to the technical content for 508 patents during 1972 - 84 in Fig.1 and for 550 patents during 1988 - 90 in Fig.2, respectively. It is noticeable that the device application shares most of the patents in Fig. 1, while it shares only 1/4 in Fig.2. The actuator design is significant in the recent years and shares more than half of the patents. Regarding the application, servo displacement transducers and pulse drive motors share 40 % and 43 %, respectively, in Fig.1, and the ultrasonic motors share only 5 %. On the contrary, in Fig.2 the servo displacement transducer and the pulse motor share only 8 % each, and the ultrasonic motor's ratio is increased up to 11 %.

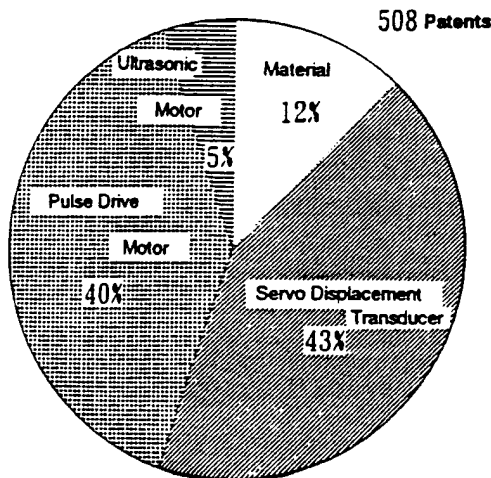


Fig.1 The ratio of 508 piezo-actuator related patents with respect to the technical content disclosed during 1972 - 84.

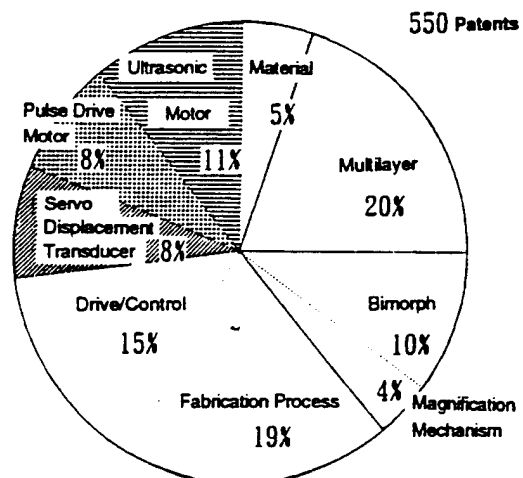


Fig.2 The ratio of 550 piezo-actuator related patents with respect to the technical content disclosed during 1988 - 90.

Table 1 Summary of the patent disclosure relating to piezoelectric actuators and ultrasonic motors disclosed during January 1988 - July 1990 in Japan. Classification is made with respect to the patent submitter and the technical content.

Technical Content Patent Submitter	Total	Material		Design			Drive/Control		Application							
		Composition	Fabrication Process	Multilayer	Magnification Mechanism	Bimorph	Others	Drive Technique	Control Technique (Sensor System included)	Servo Displacement Transducer		Pulse Drive Motor		Ultrasonic Motor		
										Optical Usage	Mechanical Usage	Optical Usage	Mechanical Usage	Propagating Wave	Standing Wave	Vibratory Piece
NEC	69			35	6		16	2	1	3	1		2		3	
TOTO Corp.	40						16	6	2				16			
Matsushita Electric	30	11				8	2	1			3			3		2
Brother Industry	27				2		15	8	2							
Toyota Motors	25			7			6	4	5		3					
Tokin	23			7		3	9	1					1	1	1	
Hitachi Metal	20			12							1		7			
Toshiba	19				1	1	6	1		2	5		1			2
Nippon Denso	16			10	1			3	1		1					
Fuji Electric	16			8		1	3	1	1		1					1
Hitachi	15					1	3	3	3		3				1	1
Murata Mfg.	12			3	1	2	3	3								
Minolta Camera	11					5	1						5			
Ube Industry	10					9			1							
Tosoh	10	7	1			2										
Malcon Electronic	10															10
NTK	9			2	1		5								1	
Olympus	9			3		3	1									
Canon	8				1		2	1	1				1		1	1
MITI-Ind.Lab.	8										8				1	1
JUKI	8							8								
Yokokawa Electric	8		1	1		2	2		1	1						
Mitsubishi Electric	7		3			2							2			
Matsushita Denko	6			1												
Mitsubishi Kasei	6			3		2	1								4	1
Sumitomo Spec. Metal	5			2			2	1								
Toshiba Ceramics	4		1			3										
Japan Auto-Parts R&D Lab.	4			2			2									
NEC Home Elec.	4										1			2		1
Fujitsu	4		2	1		1										
Miki Pulley	4															
Rion	4														4	
ALPS Electric	3			1											3	1
Kansai NEC	3							2	1						2	
COPAL	3			1				1			1					
Shimadzu	3				1			1		1						
OMRON	3					1	1	1								
Others	84	3	1	9	7	8	14	7	6	1	10		6	2	2	8
Total	550	21	9	108	21	54	110	55	25	8	37	1	41	8	33	19

The development of the piezoelectric actuators on the first stage was focused on inexpensive mass-production devices such as computer-related apparatus, displays, sensors by electronic manufacturing companies. Typical examples are found in dot-matrix printers by NEC, swing CCD image devices by Toshiba, VCR tracking heads by Sony and Matsushita Electric and piezoelectric relays by Omron. Recently, however, on the second stage chemical companies including organic/petro-chemical industries have started to be involved in these electro-ceramic areas (TOTO Corporation, Tokin, Hitachi Metal, Murata Manufacturing Co., Ube Industry, Tosoh, NTK, Mitsubishi Kasei, Sumitomo Special Metal, Toshiba Ceramics). Using the fine manufacturing technology of raw ceramic powders, they are trying to expand their territory to the device application in collaboration with optic or mechanical industries. When used in precision cutting machines, the quality and reliability of the actuator are essential rather than its price.

Recent Developments in the Leading Companies

In the following the recent development contents of the leading companies are described in detail.

NEC -- Their patents cover all the areas; design, drive/control and application. As the manufacturing pioneer of the multilayer piezoelectric actuators which were initially proposed by K. Uchino of The Pennsylvania State University (formerly Sophia University), NEC is still keeping the leading position in the piezoelectric actuator area. The development is focused on the design of the multilayer devices and their fabrication process, as well as the displacement magnification mechanism. A dot matrix printer was the first piezo-actuator product. A sketch of the printer head appears in Fig.3(a) [4]. The printing element is composed of a multilayer piezoelectric device, in which 100 thin ceramic sheets 100 μ m in thickness are stacked, together with a sophisticated magnification mechanism (Fig.3(b)). The magnification unit is based on a monolithic hinged lever with a magnification of 30, resulting in an amplified displacement of 0.5 mm and an energy transfer efficiency greater than 50%. The drive/control technique relating to the printer application is also remarked.

TOTO Corporation -- Most of the patents are related to the short stroke continuous drive type plungers, which will be suitable to their toilet chambers. Cylinder type ceramic actuators and a pulse voltage control are focused to be used.

Matsushita Electric -- Different from the recent research trend, they submitted 11 patents relating to the piezoelectric materials. Their materials slightly doped with magnetic ions have been remarkably improved in aging of actuator characteristics. The principle is the usage of the spin-orbit interaction of the magnetic ions under an external magnetic field. The bimorph design has mainly been developed aiming to the applications to VCR head control and ultrasonic motors.

Brother Industry -- Their patents are on the basic mechanisms combining parallel springs with piezoelectric actuators and their driving techniques. Practical applications have not been disclosed yet.

Toyota Motors -- The designs and fabrication processes of multilayer actuators have been intensively investigated, and using these actuators new fuel jet valves are now on development as well as their control techniques. A smart electronic shock absorber of automobile suspension (Fig.4) was commercialized by Toyota Motors[5]. The roughness of the road is detected as a vibration acceleration with a 5-layered piezosensor, and the signal is fed-back to a 88-layered piezoactuator through a power amplifier, in order to change the shock-absorption control valve. This feedback system can provide the controllability and the comfortability of a car simultaneously.

Tokin -- As one of the main suppliers of piezoelectric actuators, they submitted the patents mainly on the device designs such as bimorphs and multilayers, and their fabrication processes. Particular attention is paid on a fabrication process of cylinder type actuators and the application to card punchers. Figure 5 shows a Tokin's cylinder type piezoelectric gyroscope, which can be used to detect the noise motion of a handy video camera[6]. Among the 6 electrode strips, two of them are used to excite total vibration and the other two pairs of electrode are used to detect the coriolis force or the rotational acceleration cause by the hand motion. By using the gyro signal, the image vibration can be compensated electrically on a monitor display.

Hitachi Metal -- Their research has been concentrated on the multilayer actuator design and its application to fluid jet devices.

Toshiba -- Various patents can be found covering fabrication technique of ceramic devices, piezoelectric fans, ring laser gyros, 2-dimensional piezo-drive devices etc.

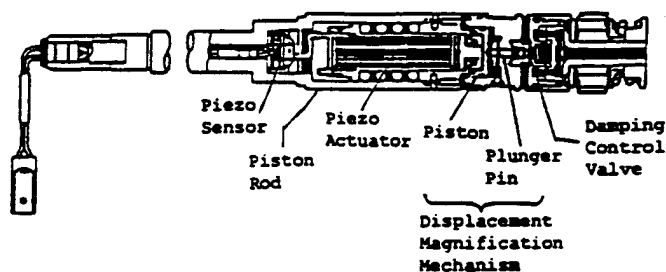


Fig.4 Smart electronic shock absorber of automobile suspension with a piezoelectric sensor/actuator system (Toyota).

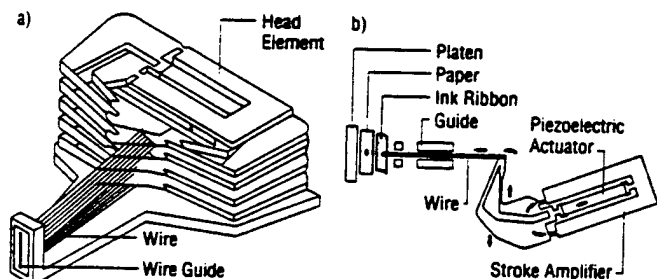


Fig.3 Structure of a printer head (a), and a differential-type piezoelectric printer-head element (b) (NEC).

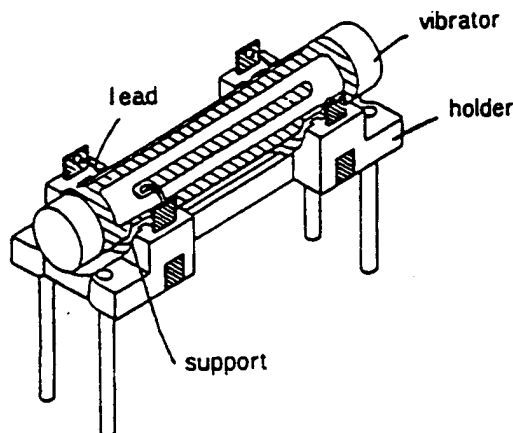


Fig.5 Piezoelectric ceramic cylinder vibratory gyroscope (Tokin).

Nippon Denso -- Most of their patents concern the designs and fabrication processes of multilayer piezo-actuators. Multi-valve mechanisms for fluid control are their original application area. The above-mentioned Toyota adaptive automobile suspension was developed in collaboration with Nippon Denso.

Fuji Electric -- Designs and fabrication processes of multilayer piezoelectric actuators are being developed. Various applications can be found in their patents including piezoelectric pumps, mechanical claspers, piezoelectric relays, micro-manipulators etc.

Hitachi -- Their research is to manufacture precision positioners with the development of the piezo-actuator designs and the control technique.

Murata Manufacturing -- Patents on the actuator designs such as multilayers and bimorphs.

Minolta Camera -- All patents relate to the camera shutters using a piezo-bimorph. Figure 6 shows the structure of the new shutter, which possesses advantages in simplicity and compactness in comparison with the conventional mechanical spring type [7].

Ube Industry -- A unique company who is developing intensively bimorph type piezoelectric actuators.

Tosoh -- Bimorph fabrication is remarked firstly. Original monomorph actuators have also been developed using semiconductive piezoelectric ceramics in collaboration with K. Uchino. A monomorph device has been developed to replace the conventional bimorphs, with simpler structure and manufacturing process. The principle is a superposed effect of piezoelectricity and semi-conductivity (Fig.7(a)) [8]. The contact between a semiconductor

and a metal (Schottky barrier) causes non-uniform distribution of the electric field, even in a compositionally uniform ceramic. Suppose that the ceramic possesses also piezoelectricity, only one side of a ceramic plate tends to contract, leading to a bending deformation in total. A monomorph plate with 30mm in length and 0.5 mm in thickness can generate 200 μ m tip displacement, in equal magnitude of that of the conventional bimorphs [9]. The recent "rainbow" actuators originally proposed by G. Haerding and manufactured by Aura Ceramics [10] are a modification of the semiconductive piezoelectric monomorphs, where half of the piezoelectric plate is reduced so as to make a thick semiconductive electrode to cause a bend (Fig.7(c)) [11].

Ultrasonic Motor Developments

Shinsei Kogyo -- The pioneering company of the ultrasonic motors is not fabricating them, but marketing them, obtaining the royalty of the basic patents from Canon, Fukoku, and Nasca. Their product, the propagating-wave type (surface-wave or "surfing" type) combines two standing waves with a 90 degree phase difference both in time and in space, and is controllable in both rotational directions (Fig.8) [12]. By means of the traveling elastic wave induced by the thin piezoelectric ring, a ring-type slider in contact with the "rippled" surface of the elastic body bonded onto the piezoelectric is driven in both directions by exchanging the sine and cosine voltage inputs, which makes it suitable for installation in cameras as an automatic focusing device.

Fukoku -- Manufacturer of the Shinsei's ultrasonic motors (\$ 500) by a production rate of 20,000 pieces/year. No particular research is held in this company.

Canon -- They are utilizing the Shinsei's ultrasonic motors for automatic camera focusing systems. Various investigations about the camera mounting are being done, especially on reducing the rotation sounds in any cases. About 80 % of the exchange lenses in "EOS" series installed the ultrasonic motors already in 1992. The production amount 300 K pieces/year and the average lens cost \$700 can provide the total sales at the moment as \$ 210 million.

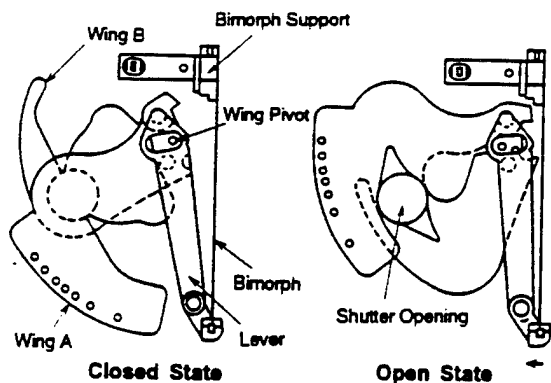


Fig.6 Compact camera shutter using a piezoelectric bimorph (Minolta Camera).

(a) (b) (c)

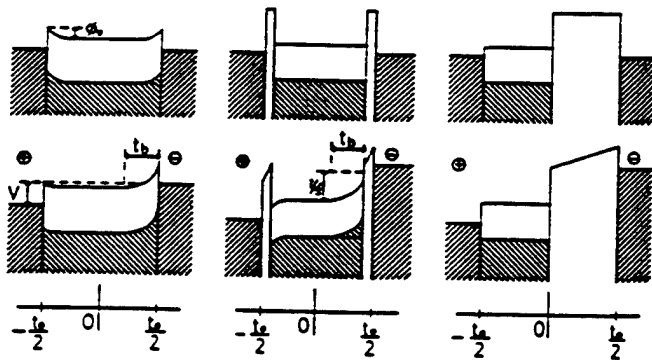
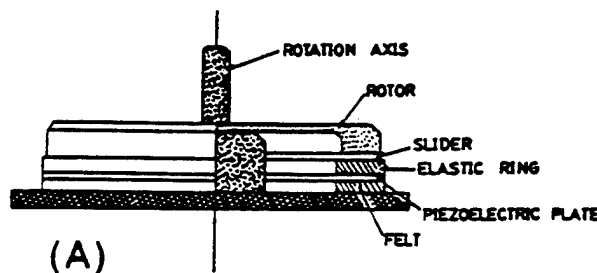
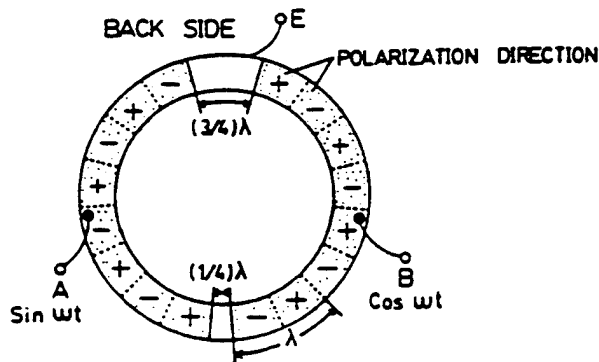


Fig.7 Electron energy band (Schottky barrier) models in monomorph devices (n-type semiconductor). (a) Schottky type, (b) Metal-Insulator-Semiconductor structure with very thin insulative layers, and (c) MIS structure with a thick insulative layer (K.Uchino & Tosoh).



(A)



(B)

Fig.8 Design of the surface wave type motor (a), and its electrode configuration (b) (Shinsei Kogyo).

Seiko Instruments -- They have trially commercialized miniature ultrasonic motors (10 mm in diameter) at relatively expensive prices (\$1500) and at the production amount of just several hundred pieces/year. If the installation into watches is realized, the market size will be incredibly large.

Nasca -- They are manufacturing the Matsushita's motors trially (\$ 500 - \$1500, several 100 pieces/year). The research has been done by Matsushita Electric.

THK -- Axial ultrasonic motors have been commercialized by combining the screw systems with Shinsei's ultrasonic motors (currently several 100 pieces scale).

SUN-SYN -- They developed precision x-y stages using linear type ultrasonic motors, which were originally proposed by K. Uchino, ALPS Electric and Nissan Motors. An ultrasonic linear motor is equipped with a multilayer piezoelectric actuator and fork-shaped metallic legs as shown in Fig.9 [13]. Since there is a slight difference in the mechanical resonance frequency between the two legs, the phase difference between the bending vibrations of both legs can be controlled by changing the drive frequency. The walking slider moves in a way similar to a horse using its fore and hind legs when trotting. A trial motor 20 x 20 x 5 mm³ in dimension exhibited a maximum speed of 30 cm/s and a maximum thrust of 0.9 kgf with a maximum efficiency of 20%, when driven at 98kHz of 6V (actual power = 0.7 W).

Malcon Electronics -- Standing wave type ultrasonic motors are their target, and now under development.

AlliedSignal -- The only company in the USA who is manufacturing the ultrasonic motors.

Rion and Piezotech were reported to have developed various different ultrasonic motors, but are not commercializing them yet.

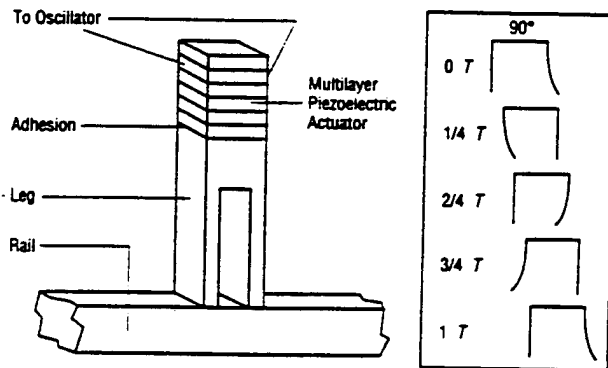


Fig.9 Ultrasonic linear motor of a vibratory coupler type (K.Uchino & Nissan Motors).

MARKET OF PIEZOELECTRIC ACTUATORS/ ULTRASONIC MOTORS

A couple of years ago Mr. Sekimoto, President of NEC, expressed his desire to the piezoelectric actuators in his New Year's speech that the market-share of piezoelectric actuators and their employed devices would reach up to \$ 10 billion (\$ 10¹⁰) in the near future.

Ceramic Actuator Elements

Presently NEC and Tokin are producing multilayer actuators roughly at 1 million pieces/year rate in each company. They are sold averagely by \$ 100 per piece. Consequently, the total market value reaches \$ 200 million. In 5 years the production rate will be expected to increase by 10 times, instead of the cost decrease by 1/4, leading to the total market growth up to \$ 500 million.

Using these multilayer actuators, various electronic devices will be manufactured with the additional value by presumably 10 times. For example, the dot-matrix printer by NEC costs averagely \$ 3,000 using the multilayer actuators of \$ 100. The production amount was about 100 K pieces/year in 1986, leading the total sales of \$ 300 million. Therefore, the sales of the final products using the piezoelectric actuators will be expected to reach \$ 5 billion in total in 2000.

Camera-Related Applications

Piezo-bimorph type camera shutters have been widely commercialized by Minolta Camera. The production amount of "Mac Dual" series is about 300 K pieces/year. Although the actuator itself costs inexpensive (\$ 1/ piece), the camera costs about \$ 350, then consequently total sales exceed \$100 million.

Canon's automatic focusing systems utilizing an ultrasonic motor are very famous. About 80 % of the exchange lenses in "EOS" series installed the ultrasonic motors already in 1992, and all the camera motors will be replaced by the ultrasonic motors by 2000. The production amount 300 K pieces/year and the average lens cost \$700 can provide the total sales at the moment as \$210 million.

Ultrasonic Motors

The actual market of ultrasonic motors opened in June 1986 when Shinsei Industry started to supply the trially manufactured ultrasonic motors using a propagation wave type. After that, Shinsei Industry has developed various applications including a remarkable success in Nuclear Magnetic Resonance medical instruments. Mass-produced samples (1500 pieces) were firstly employed for automatic curtain drawers in the New Tokyo Municipal Building in 1990; this accelerated the wide commercialization.

In 1991, an automobile application, which must be one of the key usages of the ultrasonic motors, was realized for head-rest control in Toyota New Crown. Canon succeeded in EOS exchange lens applications, and are presently developing much smaller inexpensive motors which will be applicable to automatic winding of the film. Applications of the ultrasonic motors to cameras will be undoubtedly successful in these three years. Seiko Instrument has started to distribute their miniaturized 10 mm motors, especially suitable for watch applications. Sanki's part-feeders are now sold at a rate of 20 K pieces/year averagely by \$ 500/piece, resulting in the total sales of about \$10 million. One of the future largest markets of the ultrasonic motors will be the automatic window shutter system. The system unit price of \$2,000 multiplied by 100 K sets/year can provide the sales amount of \$ 200 million. Future big market includes the applications to floppy drive, CD/laser disk drive etc.

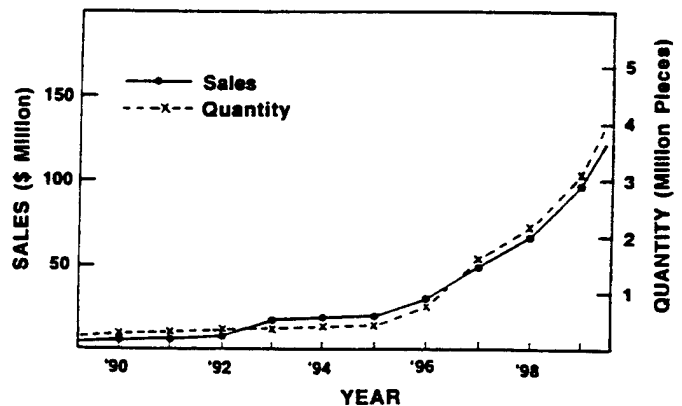


Fig.10 Market-share prediction of ultrasonic motors (motor part only).

Matsushita Electric proposed a big dream to replace all the conventional miniaturized electromagnetic motors, most of which are now produced by Mabuchi at a production rate of 1 billion pieces/year. Even if the each motor cost is very low (\$ 3/each), the total sales are remarkably large (\$ 3 billion/year). Just 10 % replacement of the conventional electromagnetic motors with the new ultrasonics motors can provide \$ 300 million sales per year; this will again provide \$ 3 billion sales as final device products.

Figure 10 shows the expected market size of the ultrasonic motor itself. The amount in 2000 will reach up to \$150 million, suggesting the total sales of the final products will exceed \$ 2 billion.

SUMMARY

Taking account of the estimated annual sales of \$500 million for ceramic actuator elements, \$300 million for camera-related devices and \$150 million for ultrasonic motors, piezoelectric/electrostrictive actuators and ultrasonic motors are expected to increase in market share to more than \$ 1 billion in 2000. Regarding the final actuator-related products, \$10 billion by Mr. Sekimoto will not be very different from the realistic amount, and a bright future is anticipated in many application fields.

Finally, the author would like to appreciate all the companies who supplied the data listed in this paper.

REFERENCES

- [1] K.Uchino, Piezoelectric/Electrostrictive Actuators, Morikita Publishing, Tokyo (1986)
- [2] K.Uchino, Bull.Am.Ceram.Soc., 65(4), 647 (1986)
- [3] K.Uchino, MRS Bull., 18(4), 42 (1993)
- [4] T.Yano, I.Fukui, E.Sato, O.Inui and Y.Miyazaki, Proc. Electr. & Commun.Soc., p.1-156 (Spring,1984)
- [5] Y.Yokoya, Electronic Ceramics, 22, No.111, 55 (1991)
- [6] Tokin Corporation, Catalogue "Ceramic Gyro"
- [7] Minolta Camera, Catalogue "Mac Dual I II"
- [8] K.Uchino, M.Yoshizaki, K.Kasai, H.Yamamura, N.Sakai and H.Asakura, Jpn.J.Appl.Phys., 26(7), 1046 (1987)
- [9] K.Uchino, M.Yoshizaki and A.Nagao, Ferroelectrics, 95, 161 (1989)
- [10] Aura Ceramics, Inc., Catalogue "Rainbow"
- [11] K.Uchino, M.Yoshizaki and A.Nagao, Jpn.J.Appl.Phys., 26, Suppl.26-2, 201 (1987)
- [12] Y.Akiyama (Editor), Ultrasonic Motors/Actuators, Triceps, Tokyo 1986
- [13] M.Tohda, S.Ichikawa, K.Uchino and K.Kato, Ferroelectrics, 93, 287 (1989)

APPENDIX 40

NEW PIEZOELECTRIC COMPOSITE ACTUATOR DESIGNS FOR DISPLACEMENT AMPLIFICATION

A. Dogan*, J. F. Fernandez**, K. Uchino and R.E. Newnham
International Center for Actuators and Transducers-Materials Research Laboratory
The Pennsylvania State University, University Park, PA 16802

* Supported by Turkish Science and Technology Council (TUBITAK) and USA-NAVY
**Current address: Electroceramic department, Instituto de Ceramica y Vidrio, CSIC,
28500 Arganda del rey, Madrid, Spain)

ABSTRACT:

The moonie actuator is a versatile performer that fills the gap between the multilayer actuator and the bimorph actuator. This paper describes the effect of geometrical change in the endcap on the moonie's actuator characteristics. The effect of cavity dimensions, which are the key parameters for transformation and amplification of radial motion into axial motion, on the characteristics of the moonie actuator were investigated. Actuator properties of the newly designed cymbal actuator were investigated with different ceramic driving element. Characteristics of the different composite ceramic actuator designs were compared based on their displacement, response time and generative forces.

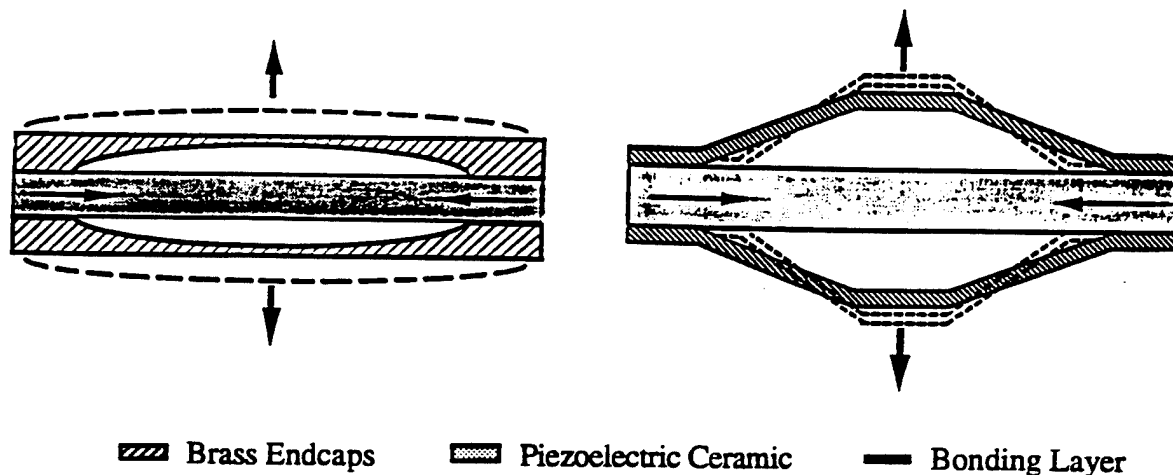
1. INTRODUCTION

Piezoelectric ceramics are widely used as a sensor many years. In recent years, there are lots of attention for the actuator application of the piezoelectric ceramics. Piezoelectric ceramic exhibits Poisson's effect; expansion in longitudinal direction and shrinkage in transverse direction, when an electric field is applied parallel to the polarization direction. There are two actuator designs which use this phenomenon to enhance the displacement for practical applications: multilayer ceramic actuators with internal electrodes and bimorph actuators. The advantages of the multilayer actuator are its generative force and quick response speed. However, small displacement and high capacitance of multilayer actuators make them impractical for certain applications. On the other hand, bimorph actuators show larger displacement. However, low generative forces and small displacement are their disadvantages. There is a need for an actuator with intermediate level displacement and generative force. The moonie and cymbal type of flextensional and roto-flexensional actuators were designed to fill the gap between multilayer and bimorph actuators [1-3]. The ceramic-metal composite moonie and cymbal actuators consist of ceramic driving element, epoxy or metal alloy bonding layer and metal, polymer or glass endcaps. Piezoelectric, electrostrictive, and antiferroelectric-ferroelectric type of ceramic materials can be used as a driving element. The basic configuration of the moonie and cymbal actuators are shown in Figure 1. The metal endcaps serve as mechanical transformer for converting and amplifying the lateral motion of the ceramic into a large axial displacement normal to the endcaps. Both the d_{31} ($=d_{32}$) and d_{33} coefficients of the piezoelectric ceramic contribute to the axial displacement of the composite.

The objective of this study is to evaluate the actuator characteristics of the moonie and cymbal transducers. Cavity beneath the endcaps plays an important role for transformation and amplification of lateral motion into axial motion. The effect of cavity dimensions on the characteristics of the moonie were studied systematically altering the cavity diameter and cavity depth while keeping the endcap thickness constant.

2. EXPERIMENTAL PROCEDURE

The composite actuators were made from electroded PZT-5A (Niobium doped Lead Zirconate Titanate), 0.9PMN-0.1PT (Lead Magnesium Niobate-Lead Titanate) and PNZST ($\text{Pb}_{0.99}\text{Nb}_{0.01}[(\text{Zr}_{0.6}\text{Sn}_{0.4})_{0.94}\text{Ti}_{0.06}]_{0.98}\text{O}_3$) (12.7 mm in diameter and 1 mm in thickness) and metal endcaps (12.7 mm in diameter with thickness ranging from 0.3 to 3.0 mm). The endcaps for moonie were machined from brass with composition 30% Zn-70% Cu. A punch die designed was used for the fabrication of the cymbal endcaps. The ceramic disk and the endcaps were bonded together around the circumference with Emerson & Cuming epoxy (Eccobond 45), taking care not to fill the cavity or short circuit the electrodes. The displacement of a composite actuator at 0.01 Hz was measured with a Linear Voltage Differential Transducer (LVDT) having a resolution of approximately 0.05 μm . Fastest response speed of the actuators was calculated from the resonant frequency data which was obtained with a Hewlett-Packard Impedance/Gain-Phase Analyzer HP-4194A.



Dimensions: (all in mm) Endcap diameter; $d_m = 12.7$ mm, PZT diameter; $d_p = 12.7$ mm
 Cavity diameter; $d_c =$ variable; 3.0, 5.0, 7.0, 9.0 / Cavity depth, $h =$ variable; 0.3, 0.5, 0.7, 0.9
 Metal cap thickness; $t_m = 1.0$, PZT thickness; $t_p = 1.0$ Bonding layer thickness; $t_b = 0.020$

Figure 1 The cross sectional view of the moonie (on the left) and cymbal (on the right) actuator. Arrows show the displacement direction

3. EVALUATION OF THE EFFECT OF GEOMETRY ON THE CHARACTERISTICS OF THE MOONIE TRANSDUCER

By altering the geometric parameters, it is possible to change the effective compliance of the composite moonie structure and tailor the desired actuator properties. The effect of the endcap thickness on the performance of the moonie actuator has been studied experimentally in correlation with FEA methods. The results has been reported in earlier publications [3-7]. The displacement shows an inverse relation with endcap thickness. The displacement of the moonie actuator increases with decreasing thickness, because of the increased flexibility of the endcaps. A moonie actuator with 0.3 mm thick brass endcap and with the fixed cavity diameter ratio at

80%, which is the ratio of the inner diameter of the endcap to the outer diameter, exhibits a 22 μm displacement under an applied electric field of 1.0 kV/mm. Generative force of the moonie actuator decreases drastically with decreasing endcap thickness. Although the flexural motion and displacement are largest at the center of the endcaps, the generative force is the lowest at that point. Displacement decreases dramatically when moving from the center to the edge. Conversely, generative force increases when moving from the center to the edge, where it approaches that of PZT ceramic. Therefore, it becomes possible to tailor the desired actuator properties by changing the contact area over the brass endcaps.

Brass endcaps with 3, 5, 7, and 9 mm cavity diameters and 0.3, 0.5, 0.7, and 0.9 mm crescent shaped cavity depths were fabricated by matrix combination while keeping the thickness constant at 1.0 mm, and diameter fixed at 12.7 mm. Figure 2 shows the relation between displacement and cavity diameter. The displacement amplification is exponentially related to the cavity diameter of the endcaps (at constant cavity depth) and linearly related to the cavity depth (at constant cavity diameter). Fastest response time-cavity diameter relations at various constant cavity depths of the moonie actuators is shown in Figure 3. Response time increases rapidly with increasing cavity diameter and decreases slightly with increasing cavity depth.

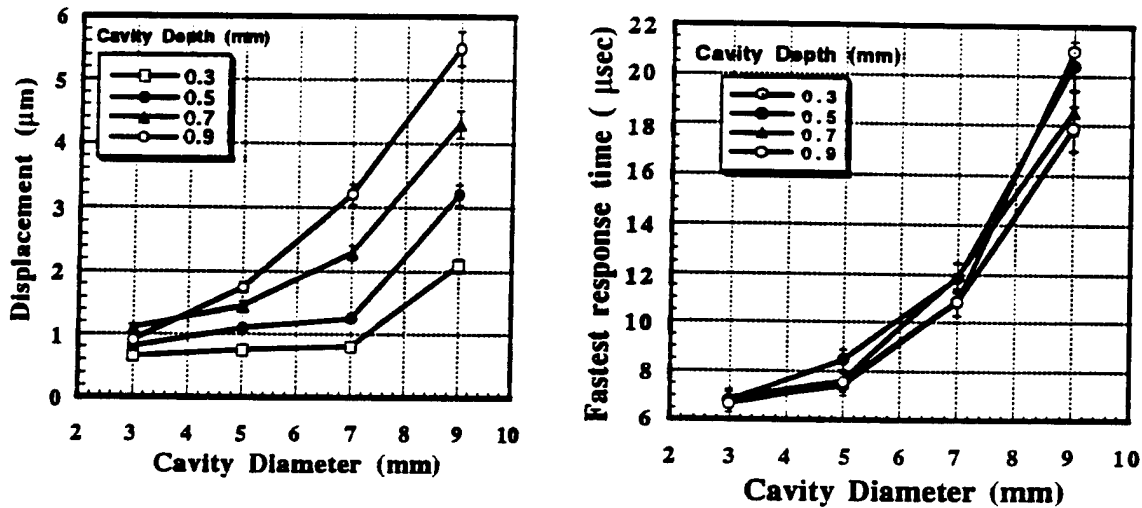


Figure 2. The displacement-cavity diameter relation of the moonie actuator (on the left)
 Figure 3. Fastest response time-cavity diameter relation of the moonie actuator (on the right)

The effective coupling factor, k_{eff} , can be derived from the series (resonant) and parallel (antiresonant) resonant frequencies of the transducer [9]. The effective coupling factor for the first resonance mode of moonie actuators with varying cavity depth and cavity diameters were calculated from their admittance spectra. Figure 4 shows the calculated effective coupling factor, k_{eff} , of the moonie actuator as a function of the cavity diameter at various cavity depths. The planar coupling factor of PZT-5A disc with 12.7 mm in diameter and 1.0 mm in thickness is around 0.65. The coupling factor decreases to 0.54 because of the load effect when the PZT-5A ceramic disc is sandwiched between brass endcaps. The moonie actuator with a cavity diameter of 3.0 mm, and a cavity depth of 0.9 mm has the highest effective coupling factor of 0.42. As the cavity diameter increased, the effective coupling factor decreased linearly down to 0.11 for a cavity diameter of 9.0 mm with a cavity depth of 0.3 mm. Effective coupling factor depends heavily on the cavity diameter and shows low sensitivity to the cavity depth.

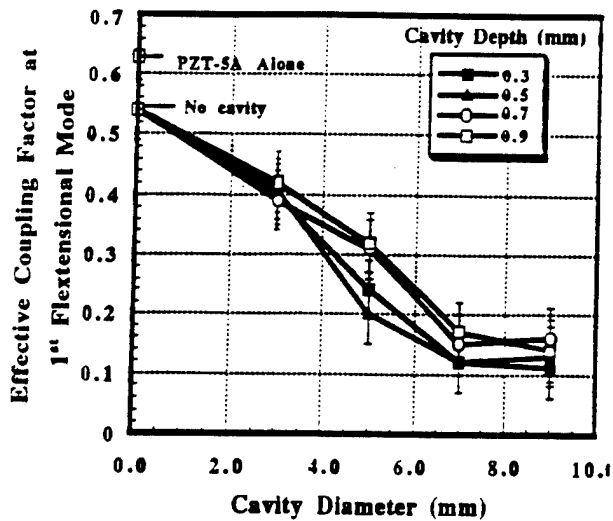


Figure 4 Effect of cavity diameter on the effective coupling factor, k_{eff} , of the moonie transducer at various cavity depths. (on the left).

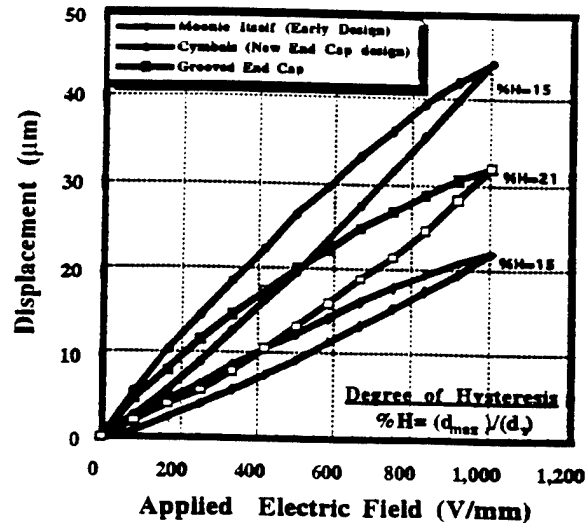


Figure 5 Displacement hysteresis of different endcap designs, (on the right).

4. CYMBAL ACTUATOR

Finite element analysis in correlation with experimental results showed that there is a high compressive stress on the endcaps just above the bonding layer. Mechanical losses due to this stress concentration reduces the effective force transfer and from the PZT to the endcap. A new actuator design with truncated conical endcaps was developed, named the "Cymbal" [3-4]. The cymbal actuator exhibits higher displacement with larger generative force along with cost effective manufacturing. Displacement hysteresis of the different endcap designs are shown in Figure 5. With the cymbal endcaps displacement values enhanced twice as much as moonie' value. Displacement characteristics of the cymbal actuators with different ceramic materials as the driving unit are shown in Figure 6. Cymbal actuator with PZT-5A exhibits linear displacement. The cymbal actuator with the PMN-PT type ceramic driving element shows larger displacement with lower losses. However, it exhibits non-linear displacement characteristics according with the relaxor characteristics of the PMN-PT ceramic. PNZST is an antiferroelectric-ferroelectric type phase transition material. Unique properties of this material is that the volumetric expansion under applied electric field. With cymbal endcap design this volumetric expansion is converted to the negative axial displacement.

5 SUMMARY

Displacement of the moonie actuator is approximately inversely proportional to endcap thickness, exponentially proportional to the cavity diameter, and linearly proportional to the cavity depth. Response time of the moonie actuator increases with increasing cavity diameter. Moonie shows position dependent behavior with maximum displacement at the center and maximum force at the perimeter. Desired actuator properties can be easily tailored by changing the contact area over the endcaps. The moonie actuator can give displacements of 20 to greater than 100 μm , maximum generative force of 3 N to several N's, and response time of 20 to 100 μsec . By altering some of the dimensions on the moonie design, it is easy to tailor an actuator with desired properties. Cymbal actuator shows twice as big as displacement than moonie for the studied size and much higher generative force due to increased contact surface.

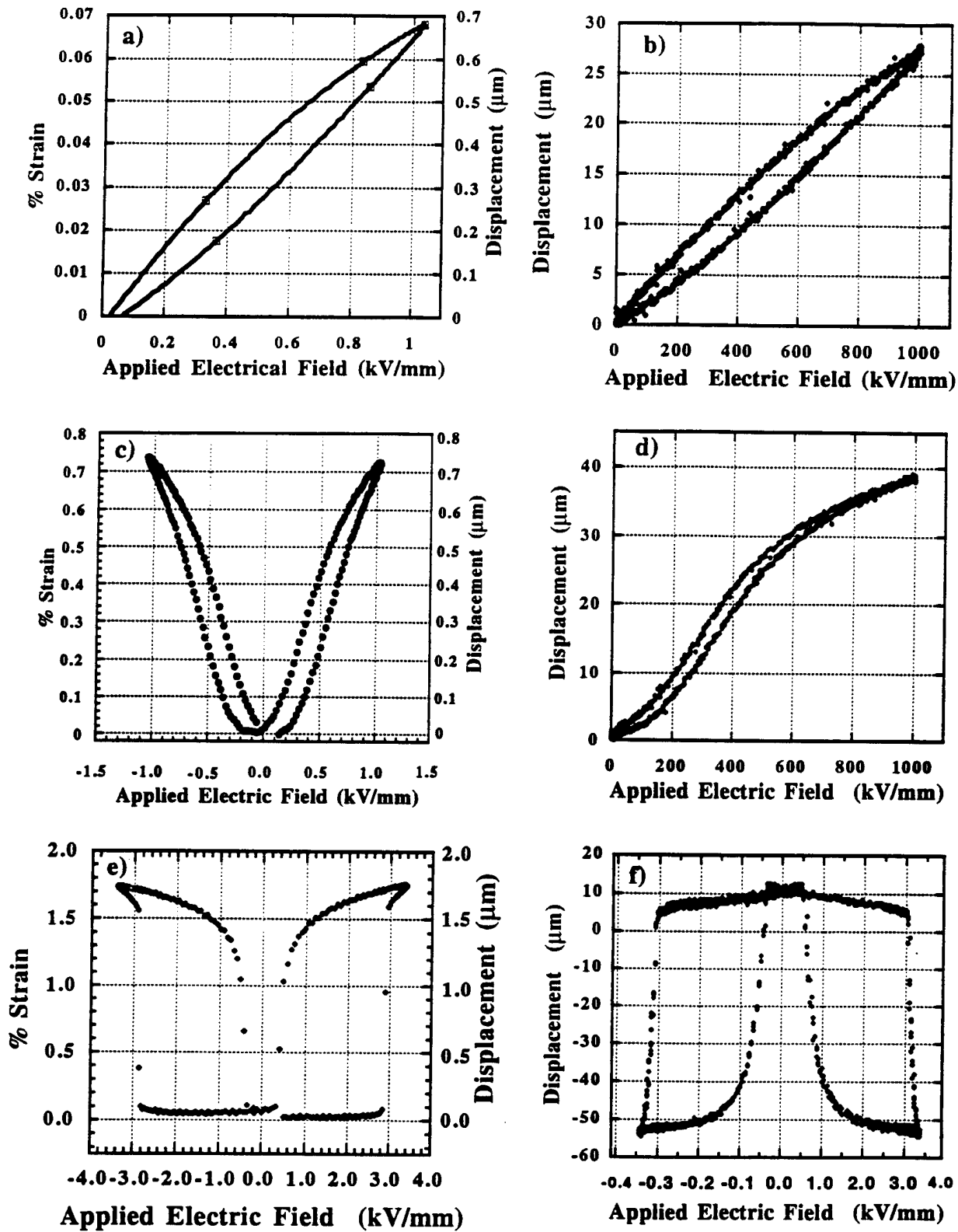


Figure 6. Displacement hysteresis various ceramic discs and cymbal actuators with this ceramics as driving element a) PZT-5A, b) Cymbal with PZT-5A, c) PMN-PT, d) Cymbal with PMN-PT e) PNZST, f) Cymbal with PNZST

Several features of the various solid state actuator designs are listed in Table I. Similar dimensions for each actuator were selected to make a fair comparison. Advantages of the moonie and particularly the cymbal actuators are the easy tailoring the desired actuator properties by altering the cavity size and endcap dimensions with cost effective manufacturing.

Table 1 Comparison of the Solid State Actuator Designs

Features	Multilayer	Bimorph	Rainbow	Cymbal	Moonie
References	[10]	[10]	[11]	[3-4]	[5-8]
Dimensions	5x5x12.7 (LxWxT)	12.7x10x1 (LxWxT)	Φ 12.7 mm T= 0.5 mm	Φ 12.7 mm T= 1.7 mm	Φ 12.7 mm T= 1.7 mm
Driving Voltage (V)	100	100	450	100	100
Displacement (μm)	10	35	20	40	20
Generative Force (N)	900	0.5-1	1-3	15	3
Fastest Response Time (μsec)	1- 5	100	100	5-50	5-50
Cost	high	med.	med.	low	low

ACKNOWLEDGMENTS

The authors would like to express their gratitude for the support to the following agencies and organizations: Office of Naval Research Contract no. N00014-92 J 1510, National Science Foundation Grant no. DMR-9223847, Spanish Science Ministry (CICYT MAT94-807 and DGICYT PR94-028), Turkish Science and Technology Council (TUBITAK) and Middle East Technical University, Ankara-TURKEY.

REFERENCES

- [1] R.E.Newnham, Q.C.Xu and S. Yoshikawa, *U.S Patent # 4,999,819 (March 12,1992)*.
- [2] Y.Sugawara, K.Onitsuka, S.Yoshikawa, Q.Xu, R.E.Newnham, and K.Uchino, *J.Am.Ceram.Soc., vol. 75, no.4, pp. 996-999, (1992)*.
- [3] A. Dogan Ph.D. thesis The Pennsylvania State University (PSU), 1994
- [4] A. Dogan and R.E. Newnham "Flexensional Cymbal Transducer" PSU Invention disclosure No. 94-1395,1994
- [5] A.Dogan, Q.C. Xu, K.Onitsuka, S.Yoshikawa, K.Uchino and R.E.Newnham, *Ferroelectrics, vol. 156, pp. 1-6, (1994)*
- [6] R.E.Newnham, A.Dogan, Q.C. Xu, K.Onitsuka, S.Yoshikawa, K.Uchino IEEE - UFFC , Baltimore 1993
- [7] K.Onitsuka, A.Dogan, J.Tressler, Q.C.Xu, S.Yoshikawa, and R.E.Newnham, *Ferroelectrics, vol. 156, pp. 37-42, (1994)*
- [8] A.Dogan, S.Yoshikawa, K.Uchino and R.E.Newnham, IEEE-UFFC Proceedings Vol II pp 935-939, France 1994
- [9] Mason, W.P., *Physical Acoustics* Vol 1 Part A, Academic Press, New York, (1964)
- [10] Information was extracted from Tokin Co. product catalog 1993
- [11] Haertling G. *Bull of Am. Ceramic Soc. Vol 73 No 1, pp 93-96, 1994 (1994)*

APPENDIX 41

Metal-Ceramic Composite Transducer, The "Moonie"

KATSUHIKO ONITSUKA, AYDIN DOGAN,* JAMES F. TRESSLER, QICHANG XU, SHOKO YOSHIKAWA AND ROBERT E. NEWNHAM
Materials Research Laboratory, The Pennsylvania State University, University Park, PA 16802

ABSTRACT: A new type of metal-ceramic composite transducer, the "moonie," has been developed by sandwiching a poled lead zirconate titanate (PZT) ceramic between two specially designed metal end caps. Piezoelectric coefficients an order of magnitude larger than PZT itself are obtained. The metal-ceramic composites are being developed as fish finders, hydrophones, actuators, and transducers with integrated sensing and actuating capabilities. This paper describes the moonie principle, optimization of the moonie design using finite element analysis, and the performance of the device for several different applications.

INTRODUCTION

THE moonie transducer consists of a piezoelectric or electrostrictive ceramic disk sandwiched between two metal end caps, each having a crescent-shaped cavity on its inner surface (hence the name "moonie"). These metal end plates serve as mechanical transformers for converting and amplifying the lateral displacement of the ceramic into an axial motion normal to the plates. Both the d_{33} and d_{31} coefficients of the piezoceramic contribute to the axial displacement of the composite. The cavities are used as a mechanical transformer for transforming the high acoustic impedance of the ceramic to the low acoustic impedance of the surrounding medium (Newnham and Ruschau, 1991; Sugawara et al., 1992; Xu et al., 1991; Newnham et al., 1992; Onisuka, 1993).

Figure 1 shows the basic configuration of the moonie transducer. The ceramic element can be either a piezoelectric ceramic or an electrostrictive ceramic either in single layer or multilayer form. Electrostrictive ceramics generally show less hysteresis than PZT but are highly nonlinear. Multilayer elements consist of a number of thin ceramic layers with internal electrodes; thus allowing for lower drive voltages.

APPLICATIONS OF THE MOONIE

Table 1 compares three applications of the moonie transducer: hydrophone, actuator, and fish finder. The materials and dimensions listed in Table 1 were chosen after considering the important features required for each application. Bonding materials and dimensions are the key factors in tailoring the properties. Finite Element Analysis (FEA) was used to optimize the geometry of the moonie transducer.

Associate Editor: K. Reifsnider.

*Author to whom correspondence should be addressed.

Imanaka et al. utilized the multilayer moonie actuator to control the scanning angle for a micro-optical scanner. Figure 2 shows the schematic diagram of the optical scanner unit containing the multilayer moonie actuator. By replacing the usual multilayer actuator with a multilayer moonie, reduction of the operating voltage and miniaturization of the optical scanner unit size were achieved (Goto and Imanaka, 1991; Imanaka, 1991; Imanaka, 1992).

FINITE ELEMENT ANALYSIS (FEA)

A theoretical analysis of the PZT-metal composite was performed using the finite element analysis programs SAP90 and MARK. A quarter-section axially symmetric model to define the moonie structure is shown in Figure 3. The resonance frequencies of moonies with different dimensions were calculated using dynamic analysis. Mesh refinement for the stress analysis on the moonie hydrophone, especially in the stress concentration area, was performed to confirm the magnitude of the stress values. When the generated strain exceeds the elastic limit, non-linear behavior of the material should be considered. In this paper, geometrical non-linear analysis was also performed to calculate the displacement of moonie actuators when applying an electric field across the electrodes of the moonie.

CALCULATED AND EXPERIMENTAL RESULTS

Moonie Fish Finder

A fish finder is an underwater transducer which converts a high voltage electrical pulse to mechanical motion. The mechanical motion creates a sound wave that is transmitted efficiently through the water in the desired direction. The sound wave reflects off targets, such as fish or the bottom of the water, and travels back to the transducer. The reflected sound wave "echo" mechanically deflects the transducer and

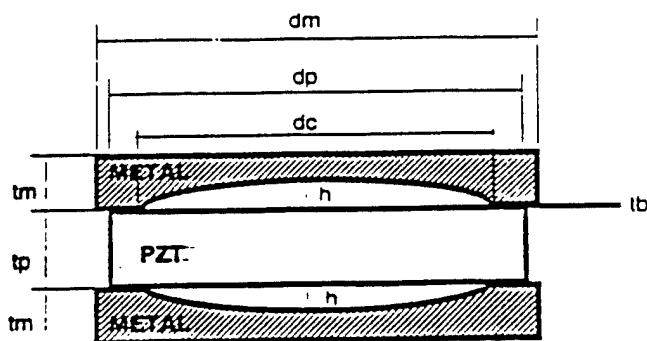


Figure 1. Cross-sectional view of the moonie transducer.

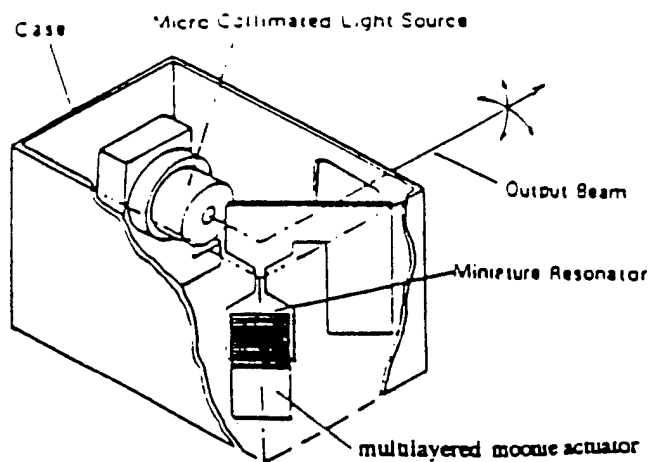


Figure 2. Schematic illustration of the optical scanner unit incorporated with the multilayer moonie actuator (Goto and Imanaka, 1991; Imanaka, 1992).

a very low voltage pulse is created. The distance to the target is determined by measuring the time difference between the transmitted pulse and received echo (Airmar Co. 1989). In some fish finder applications, transducers having a wide main lobe without side lobes are used in searching for fish over a wide area.

Using FEA dynamic analysis, the lowest three vibration modes were calculated and are illustrated in Figure 4. In the first vibration mode, the center of the transducer has maximum displacement. The first vibration mode is found to be useful as a fish finder because it has a wider main lobe than the conventional fish finder design (Onitsuka, 1993).

The resonance frequencies of the moonie are dependent upon such parameters as the metal cap diameter, metal thickness, cavity diameter and depth, and PZT diameter and thickness. By using FEA, the appropriate shape and dimensions can be designed for fish finders with selected resonance frequencies. Figure 5 shows that there is good agreement between experimental and calculated frequencies for the first resonant mode. In Figure 6, the first resonance frequencies measured in actuators with different brass end cap thicknesses are also shown to be in excellent accordance with the calculated results.

Moonie Hydrophone

One important sensor application is the hydrophone, a device used to detect weak pressure waves in fluids. In many

hydrophone applications, there is a great demand for piezoelectric transducers with high pressure tolerance, high dielectric constant (K), high hydrostatic piezoelectric charge coefficient (d_h), high hydrostatic voltage coefficient (g_h), and subsequently a high figure of merit ($d_h \cdot g_h$). PZT ceramics have high d_{33} and d_{31} , but their $D_h (= d_{33} + 2d_{31})$ values are very low because the d_{31} is approximately half the magnitude and is opposite in sign to d_{33} (Airmar Co., 1989).

In the last decade, several piezoelectric ceramic-polymer composites with different connectivity patterns have been developed for hydrophone and medical transducer applications (Newnham, 1986; Gururaja et al., 1987; Banno, 1983; Zhuang et al., 1983). The advantages of these composites over ceramics include a higher figure of merit ($d_h \cdot g_h$) to enhance the sensitivity, increased mechanical compliance, smaller acoustic impedance for matching to water or tissue, and lower transverse electromechanical coupling coefficient. Disadvantages of these ceramic-polymer composite transducers, however, are a lower dielectric constant and a lower pressure tolerance than their ceramic counterparts.

PZT-brass composite moonies with dimensions $d_m = d_p = 11.0$, $d_c = 7.6$, $t_p = 1.1$, $t_m = 1.2$ and $h = 0.15$ (all in mm) were fabricated to examine their performance as hydrophones. The brass end caps were bonded to a PZT-5

Table 1. Applications of the moonie transducer.

	Hydrophone	Actuator	Fish Finder
Function	Pressure sensor	Mechanical actuator	Transceiver
Metal	Brass	Brass	Aluminum
Ceramic	PZT-5	PZT-5, PMN-PT	PZT-4
Bonding	Ag paste	Ag paste, Epoxy	Epoxy
Diameter (mm)	11	11	27-45
Thickness (mm)	5	2-5	10-20
d_{33} (pC/N)	2500	4500	1500
Feature	High sensitivity	High displacement	Low side lobes

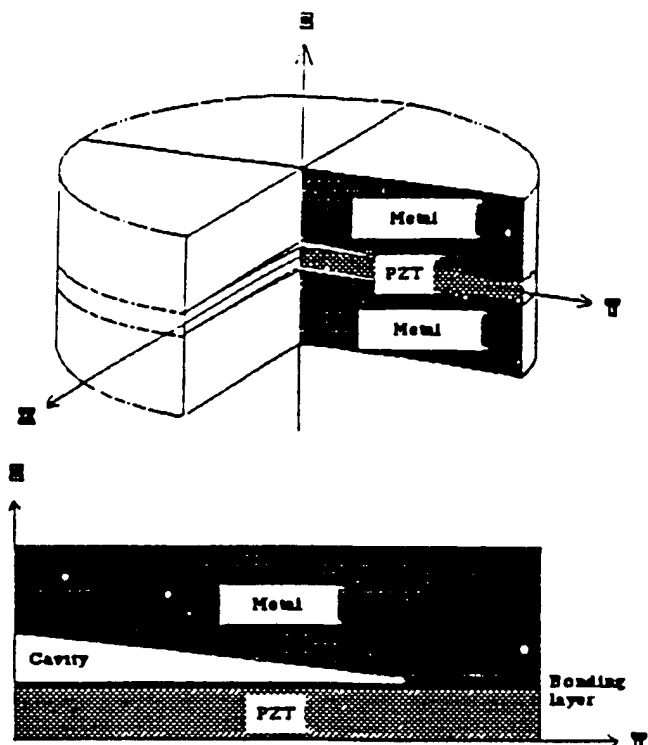


Figure 3. Cross-sectional view of the moonie (top) and one quarter of the axisymmetric model for FEA (bottom).

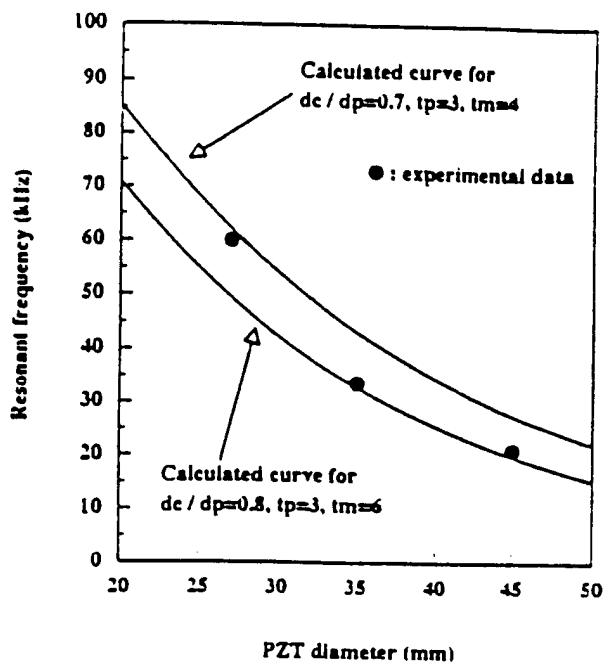


Figure 5. Comparison of the first resonance frequencies calculated by FEA with experimental values plotted as a function of the PZT diameter.

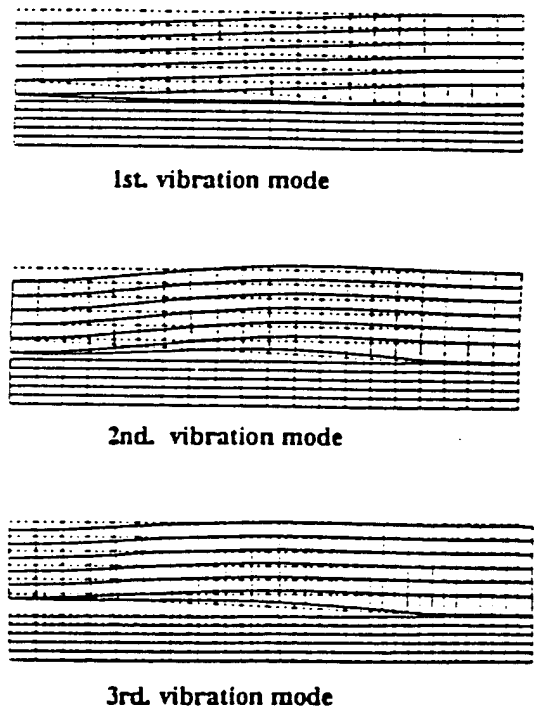
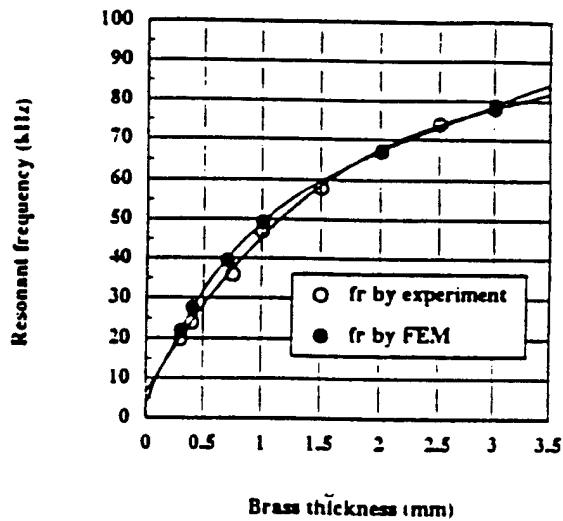


Figure 4. Quarter section views of the three vibration modes calculated by FEA.



Dimensions: $d_o=10.8, d_m=11.2, d_i=8.5, t_1=1, t_2=0.02,$
 $h=0.2$ (all in mm)

Figure 6. Comparison of the first resonance frequency values calculated by FEA with the experimental values plotted as a function of the brass end cap thickness.

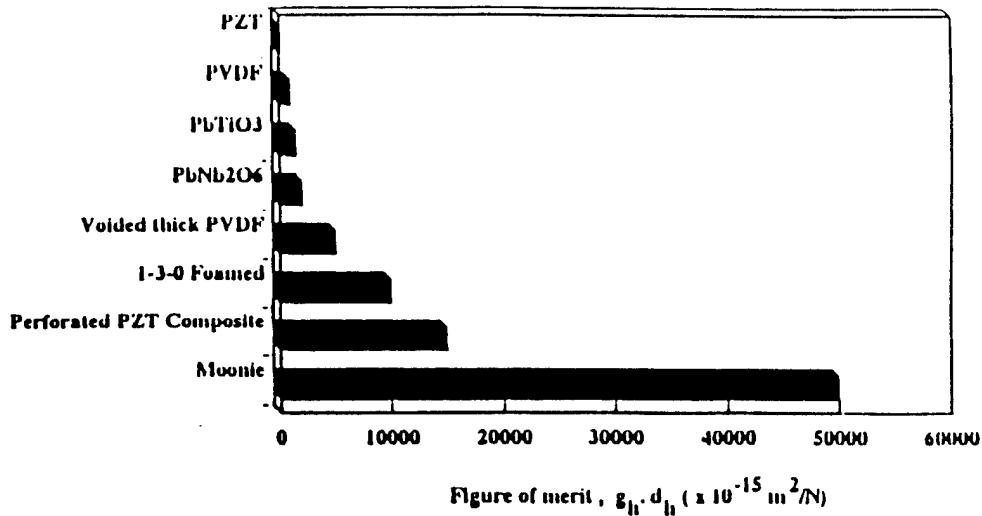


Figure 7. Comparison of the figures of merit of different materials and composites for hydrophone application (Xu, 1991; Newnham, 1986; Gururaja et al., 1987; Banno, 1983; Zhuang et al. 1983).

disk with capacitor electrode silver paste and fired at 600°C for 10 minutes. Brass was chosen for its relatively low thermal expansion coefficient (approximately 15 ppm/°C).

The moonie composite enhances d_h by converting a portion of the z-directional stress into large radial and tangential stresses of opposite sign, thereby causing the d_{31} and d_{32} contributions to d_h to add rather than subtract. Figure 7 shows a comparison of the figures of merit of different materials and composites. The moonie exceeds $50,000 \times 10^{-15} \text{ m}^2/\text{N}$ in the figure of merit, which is 500 times larger than the PZT ceramic alone (Xu, 1991).

Figure 8 shows the experimental results for d_h and g_h plotted as a function of hydrostatic pressure up to 1000 psi (approx. 7.0 MPa). The moonie hydrophone transducer exhibits a high figure of merit as well as a high pressure tolerance with very little aging under static hydrostatic pressures of 350 psi (2.5 MPa) (Xu, 1991).

Figure 9 shows the FEA results of the stress analysis when unit hydrostatic pressure was applied to the surface of

the transducer. In the longitudinal z-direction (Figure 9a), the stress distribution in the PZT is rather complex. The stress distribution only in the PZT ceramic is shown because the total stress induced in the PZT by hydrostatic pressure is important for the hydrophone application. There are 38 units of compressive stress concentration at the inner edge of the bonding. On the other hand, at the outer edge of the PZT, 0.7 units of extensive stress concentration are induced. Since ceramics are usually weakest under tensile stresses, the outer edge of the PZT must be reinforced. In the radial direction (Figure 9b), mainly extensive stresses, shown as the + region in Figure 9b, are induced in the PZT ceramics, except near the bonded region. A similar stress distribution was obtained in the tangential direction. The extensive forces in the radial and tangential direction in the PZT, when coupled to the moonie structure, make the moonie a highly sensitive hydrophone (Newnham et al., 1992).

Moonie Actuator

Actuators are electromechanical transducers which develop useful strains by controlling an applied electric field. Figure 10 illustrates the two common types of piezoelectric actuator, the multilayer ceramic actuator with internal electrodes, and the cantilevered bimorph actuator, together with a new type of multistacked multilayered moonie (multi-multi moonie). Multi-multi moonies with large displacements are made by inserting multilayered ceramic actuators between moonie end caps and stacking several moonies together. Normal multilayer actuators produce a large force, but only small displacements. Conversely, bimorphs produce large displacements but the forces are very small. The moonie actuator combines the advantages of both by providing both large displacements and a reasonably large generative force (Uchino, 1989).

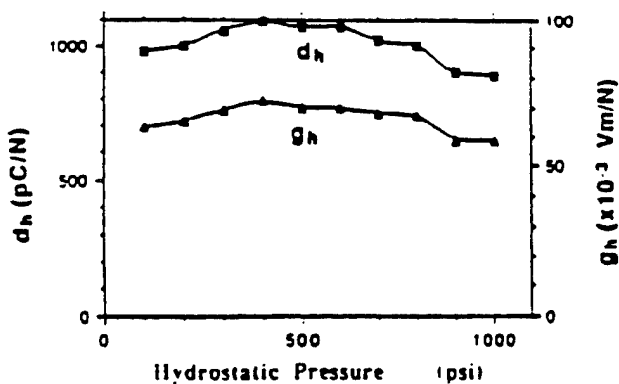


Figure 8. d_h and g_h of the moonie hydrophone as a function of hydrostatic pressure.

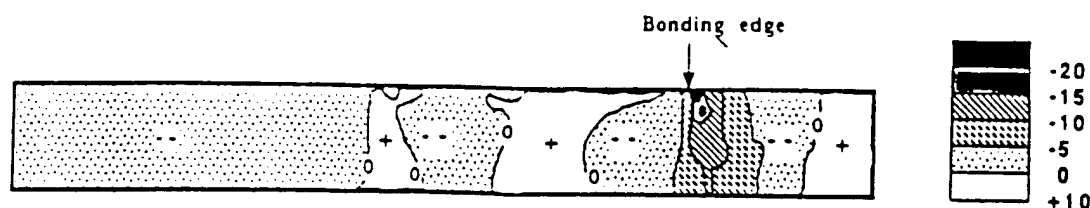


Figure 9a. Longitudinal z-directional stress distribution in the PZT ceramic under unit hydrostatic pressure.

The desirable properties of actuators are:

1. Large displacement (large strain)
2. Small hysteresis (position reproducibility)
3. Small size and weight
4. High power
5. Quick response time
6. Low driving voltage
7. Wide working temperature range
8. No aging

The dependence of the effective d_{33} coefficient and the first resonance frequency on the brass thickness is shown in Figure 11. The dimensions of the PZT moonies were $d_m = 11.2$, $d_p = 10.8$, $d_c = 8.5$, $t_p = 1.0$, $t_m = 0.3$ to 2.5 , $t_b = 0.02$, and $h = 0.2$ (all in mm). Silver filled epoxy was used as the bonding agent. By reducing the thickness of the end caps, the d_{33} values increase dramatically. An effective piezoelectric coefficient, d_{33} , of about 13,000 pC/N was obtained for a brass thickness of 0.3 mm.

Figure 12 shows the relationship between displacement and brass thickness for a single layer moonie actuator. By decreasing the brass thickness, the displacement increases in the same manner as the effective d_{33} coefficient. A single moonie actuator with a brass cap thickness of 0.3 mm can produce a 22 μm displacement under applied electric field of 1 kV/mm.

Figure 13 shows the relationship between displacement (measured over the center of the cap) and applied load for a moonie actuator having 0.3 mm thick brass caps. Although the displacement is very high at the center of the actuator, the generative force is low. Generative force increases while displacement decreases when the location of the measuring point is moved from the center to the edge of the cap. In the middle of the end cap, the moonie can sustain a load of 300 grams force by sacrificing one third of its displacement, going from 22 to 13 μm .

The load effect was also calculated using both linear and non-linear FEM analysis. Both results show the same linear decrease in displacement with increasing load. The discrepancy between the calculated and experimental results is attributed to an increase in the area of the applied load as the force was increased, as opposed to the FEM analysis, which always assumed a point load.

Figure 14 shows the displacement versus electric field curves for a doubly-stacked actuator driven by PZT-5A disk. A displacement of about 40 μm can be obtained under a field of 1 kV/mm, which is twice the single moonie displacement and nearly 20 times that of the uncapped ceramic.

Integrated Sensor and Actuator

The elimination of mechanical vibration or acoustic noise has achieved considerable attention in recent years, both on the macroscopic (e.g., smart shock absorbers) and microscopic (e.g., active optic systems) scale. The fundamental parameters that must be considered for a vibration control device are its response time, as well as the force and vibration displacement amplitude that must be canceled. Once these criteria have been met for a particular application, it then becomes desirable to reduce costs by miniaturizing and/or reducing the power delivered to the device.

Using this information, it became our objective to fabricate a vibration control device based on the moonie actuator. In order to produce the most efficient device, the sensing and actuating functions were integrated into a single composite. The prototype design is shown in Figure 15. The actuator portion of the device consists of the standard moonie, 11 mm in diameter and 3 mm thick. The sensor is a separate piece of piezoceramic (PZT), 0.1 mm thick, which was imbedded within the upper end cap. The sensor detects sinusoidal vibrations normal to the actuator surface,

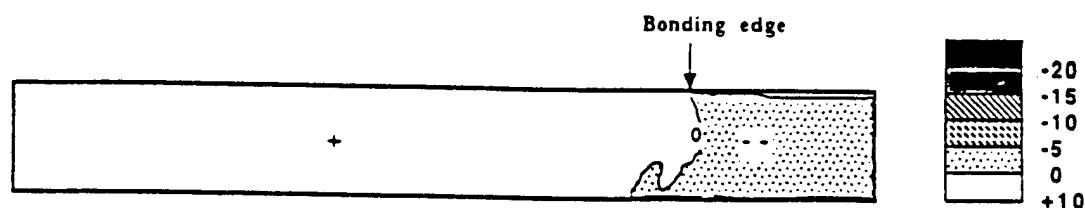
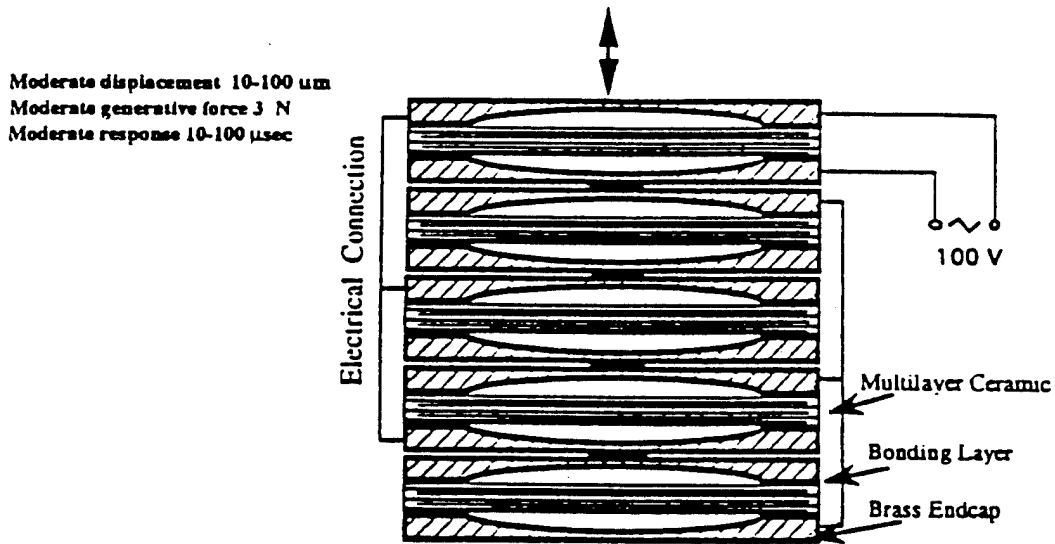
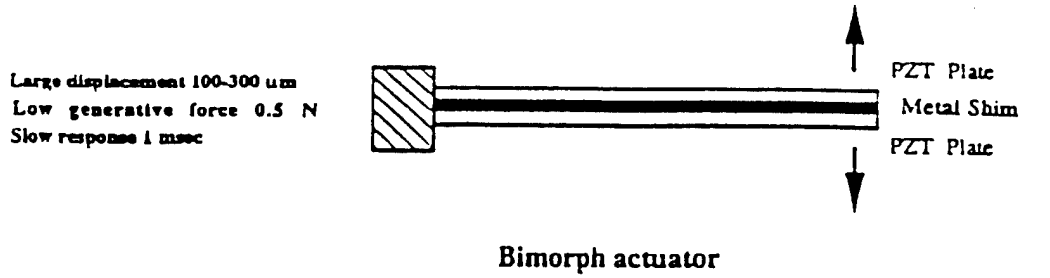


Figure 9b. Radial r-directional stress distribution in the PZT ceramic under unit hydrostatic pressure.



Multilayer-multistacked Moonie Actuator

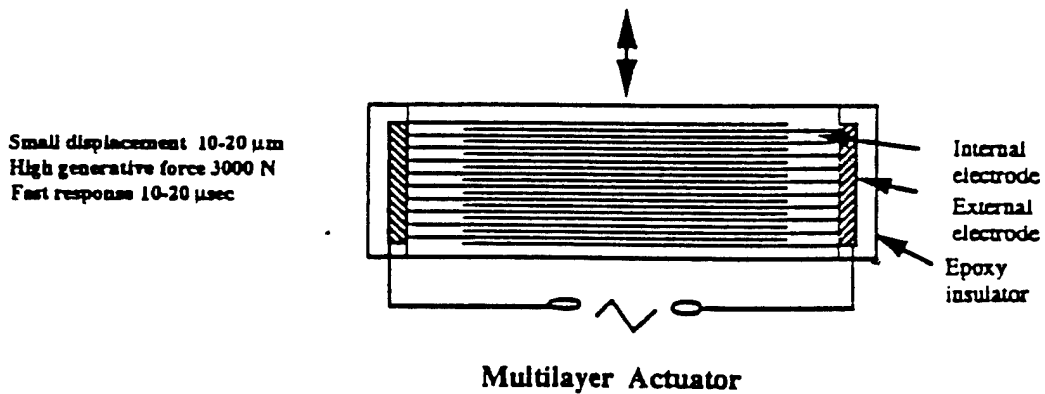


Figure 10. Two common types of actuator along with the multi-multi moonie actuator.

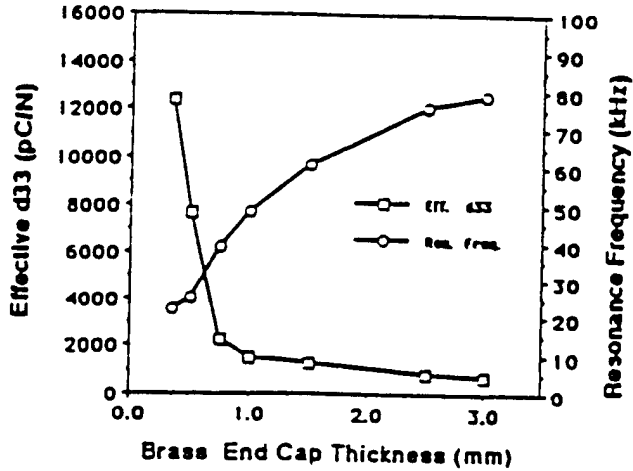
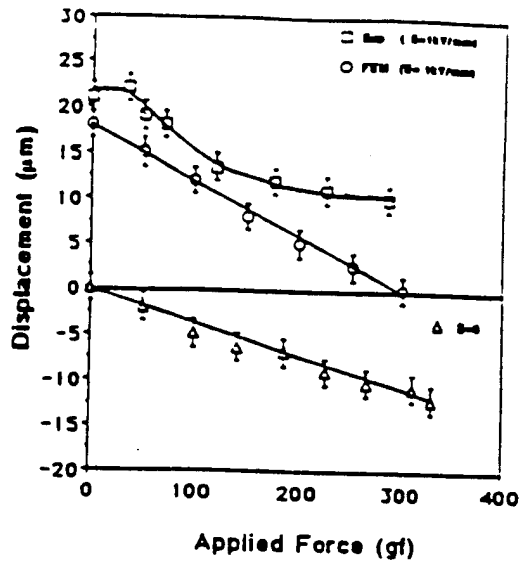
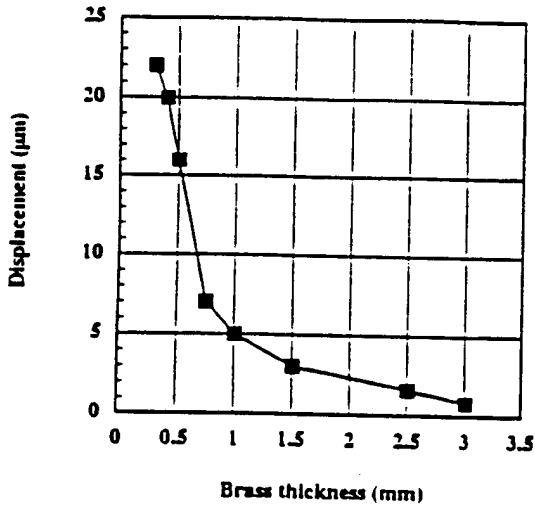


Figure 11. Dependence of the effective d_{33} and the first resonance frequency on end cap thickness.



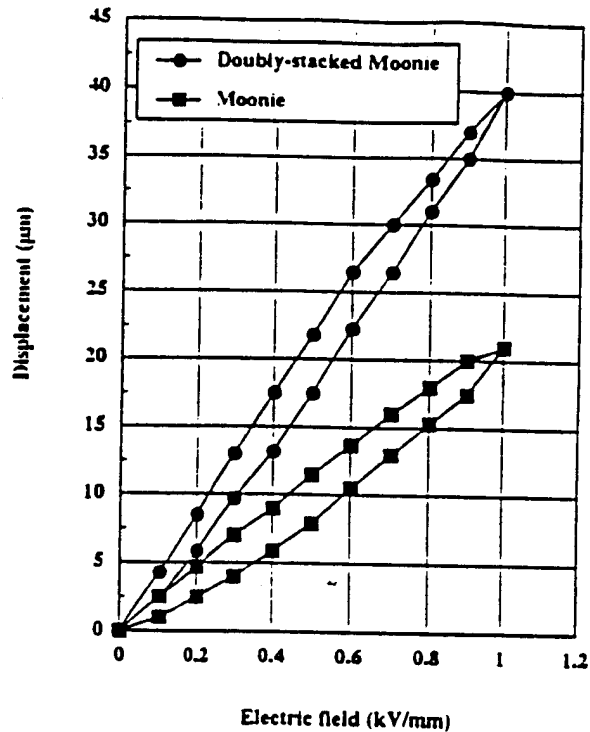
Dimensions: $d_1=10.8$, $d_2=11.2$, $d_3=8.5$, $t_1=0.3$, $t_2=1$, $t_3=0.02$, $h=0.2$ (all in mm)

Figure 13. Effect of load on displacement, as measured over the center of the end cap, under an applied electric field of 1 kV/mm (upper) and no applied field (lower).



Dimensions: $d_1=10.8$, $d_2=11.2$, $d_3=8.5$, $t_1=1$, $t_2=0.02$, $h=0.2$ (all in mm)

Figure 12. Maximum displacement measured at the center of the epoxy bonded moonie actuator as a function of end cap thickness (under an applied electric field of 1 kV/mm).



Dimensions: $d_1=10.8$, $d_2=11.2$, $d_3=8.5$, $t_1=0.3$, $t_2=1$, $t_3=0.02$, $h=0.2$ (all in mm)

Figure 14. Displacement hysteresis of the moonie and doubly-stacked moonie actuator.

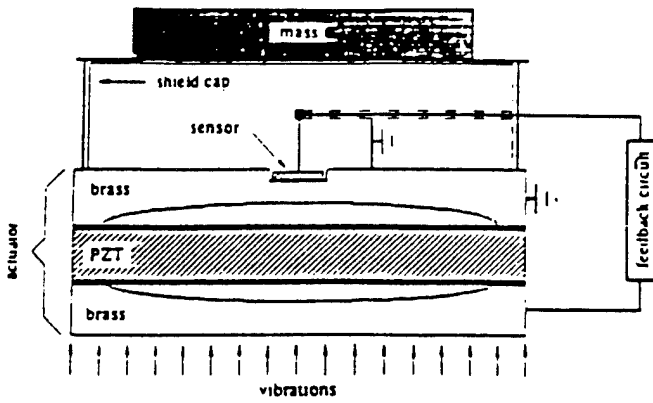


Figure 15. Schematic illustration of the integrated sensor and actuator.

as shown in Figure 15, then via a feedback loop, sends a signal of appropriate amplitude and phase back to the actuator so that the latter effectively cancels the external vibration.

The ability of the moonie actuator to actively control external vibrations was tested by adhering the device atop a vibrating multilayer actuator 11 mm in diameter and consisting of 12 PZT layers each 0.375 mm thick. The vibration frequency and displacement amplification of this external vibration source was manually controlled by driving the multilayer actuator with a sinusoidal AC field. The dynamic frequency range of the sensor was found by applying a sinusoidal AC field to the moonie actuator and observing the resulting vibration signal on an oscilloscope. The response remained relatively flat between 100 and 6000 Hz.

The data in Figure 16 show that the integrated sensor/actuator device can indeed be used to cancel external vibrations. The horizontal axis shows the 1 kHz electric field applied to the moonie actuator when the field applied (at 1 kHz) to the multilayer vibration source was either 75 V/mm,

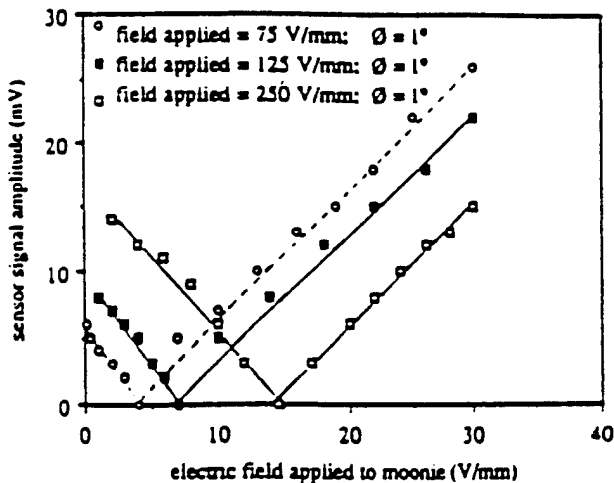


Figure 16. Net sensor signal response for three different fields applied to the multilayer vibration source as a function of electric field applied to the moonie at a frequency of 1 kHz.

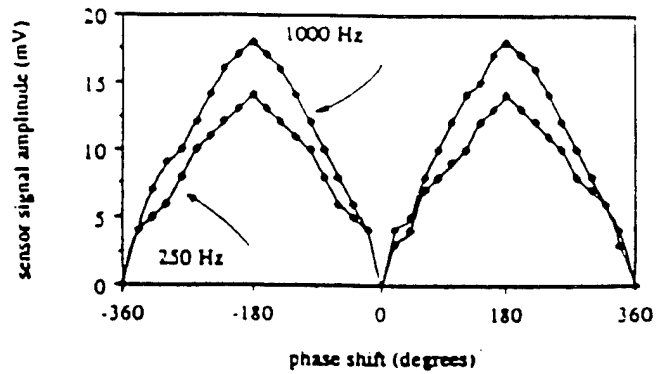


Figure 17. Sensor signal response as a function of phase shift of the electric field applied to the moonie as referenced to the drive of the external vibration source.

125 V/mm, or 250 V/mm. The vertical axis shows the corresponding net vibration signal amplitude, which comes from the sum of the multilayer and moonie vibrations. The results show that whenever the applied fields and phase shift into the moonie are adjusted to the appropriate magnitude, the net vibration signal goes to zero, indicating that the integrated sensor/actuator device has effectively canceled the external vibration. The reason the phase shift is 1° rather than the expected 180° was due to the polarization direction of the sensor being opposite that of the actuator.

Figure 17 shows how the net vibration signal amplitude changes with phase shift (as referenced to the drive of the multilayer actuator vibration source) when the applied field into the multilayer is 125 V/mm and the field applied to the moonie is 7.05 V/mm. These data show that when the phase shift between the two fields is slightly greater than 0° , there is no net vibration signal. This indicates that the moonie and multilayer actuator have the same displacement amplitudes and are vibrating exactly 180° out-of-phase with each other, resulting in no net vibration signal.

Figure 18 shows the applied electric field and phase shift (feed back signal) needed to be supplied to the moonie actu-

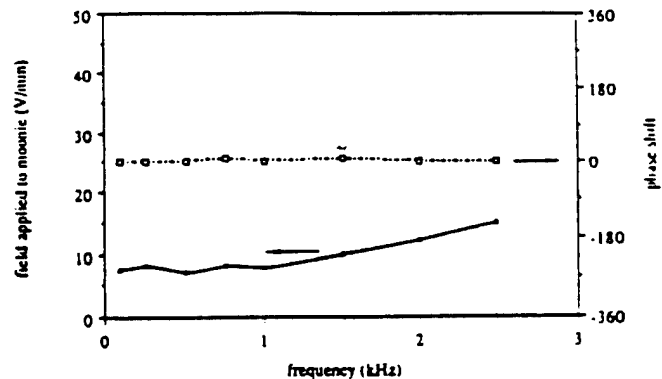


Figure 18. Field and phase shift applied to the moonie actuator needed to cancel the external vibration when the field applied to the multilayer vibration source is 75 V/mm.

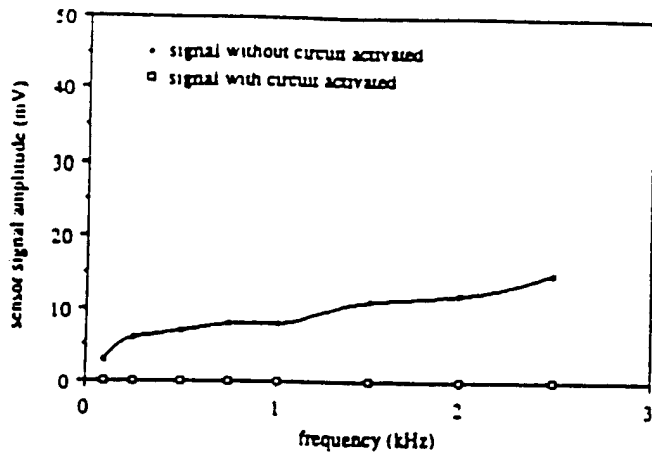


Figure 19. Sensor signal response both with and without the feedback circuit activated.

ator in order to cancel the external vibration over the shown frequency range when the field applied to the multilayer was 75 V/mm.

Figure 19 superimposes the subsequent sensor signal amplitude detected from the multilayer vibration source both with and without the feedback signal activated. These data show that when the feedback field given in Figure 18 is activated, the multilayer vibration signal can be completely suppressed over this frequency range. The reason 2500 Hz was chosen as the maximum frequency was the inability to maintain adequate coupling between the moonie and multilayer actuator at higher frequencies.

The minimum and maximum electric fields into the moonie actuator for which the sensor signal remained sinusoidal were 200 V/mm and 370 V/mm, respectively, and were independent of frequency. These fields thus define the dynamic displacement range that the sensor is capable of detecting as being between 0.35 nm and 0.65 μm (as calculated by finite element analysis) (Onitsuka, 1993).

Lastly, the response time of the device, 20 μsec , was estimated from the resonance frequency of the actuator, 50 kHz.

SUMMARY

1. The moonie design has been shown to work well for both sensing and actuating functions.
2. Three specific applications for the moonie have been developed: hydrophone sensors, transceivers for fish finders, and actuators.
3. Finite Element Analysis has been shown to be an effective design method for analyzing the flexensional resonance frequencies of the composite moonie type transducers.

4. PZT-brass moonie hydrophones with redistributed stresses show a very high figure of merit as well as high hydrostatic pressure tolerance.
5. A single moonie actuator with brass caps 0.3 mm thick has effective d_{33} coefficients of about 13,000 pC/N, and can produce a 22 μm displacement under applied electric field of 1 kV/mm. By decreasing the brass thickness, the displacement increases in the same manner as the d_{33} coefficient.
6. A doubly-stacked actuator produces a 40 μm displacement under a field of 1 kV/mm, which is twice the single moonie displacement and nearly 20 times that of the uncapped ceramic.
7. The newly designed integrated sensor/actuator device can effectively cancel external vibrations of small displacement amplitudes and low forces in the frequency range 100–2500 Hz.

REFERENCES

- Airmar Technology Co. 1989. Application Notes, pp. 8–10a.
- Banno, H. 1983. "Recent Developments of Piezoelectric Ceramic Products and Composites of Synthetic Rubber and Piezoceramic Particles", *Ferroelectrics*, 50(1–4):329–338.
- Gururaja, T. R., A. Safari, R. E. Newnham and L. E. Cross. 1987. "Piezoelectric Ceramic Polymer Composites for Transducer Application", *Electroceramics*, L. Levinson, ed., New York: Marcel Dekker, pp. 92–128.
- Goto, H. and K. Imanaka. 1991. "Super Compact Dual Axis Optical Scanning Unit Applying a Torsional Spring Resonator Driven by a Piezoelectric Actuator", *Proc. of SPIE*, 1544:272–281.
- Imanaka, K. 1991. "Compact Optoelectronics Instrumentation", *Business Japan* (June):72–73.
- Imanaka, K. 1992. "Micro Hybrid Integrated Devices and Components; Micro Photonic Devices", *Proc. of SPIE*, Vol. 1751.
- Newnham, R. E. 1986. "Composite Electroceramics", *Ann. Rev. Mat. Sci., Annual Reviews, Inc.*, pp. 47–68.
- Newnham, R. E. 1991. "Smart Electroceramics", *J. Am. Ceram. Soc.*, 74(3):463–480.
- Newnham, R. E., Q. C. Xu, K. Onitsuka and S. Yoshikawa. 1992. "A New Type of Flexensional Transducer", *Proc. of Third International Workshop on Transducers for Sonics and Ultrasonics*, Orlando, Florida, May 6–8, p. 123.
- Onitsuka, K. Ph.D. thesis. 1993. "Effect of Bonding and Geometry on the Flexensional Transducer, 'Moonie'", The Pennsylvania State University.
- Sugawara, Y., K. Onitsuka, S. Yoshikawa, Q. C. Xu, R. E. Newnham and K. Uchino. 1992. "Metal Ceramic Composite Actuators", *J. of Am. Ceram. Soc.*, 74(4):996.
- Xu, Q. C., S. Yoshikawa, J. R. Belsick and R. E. Newnham. 1991. "Piezoelectric Composites with High Sensitivity and High Capacitance for Use at High Pressure", *IEEE Trans. on UFFC*, 38:634–639.
- Xu, Q. C., A. Dogan, J. Tressler, S. Yoshikawa and R. E. Newnham. 1991. "Ceramic-Metal Composite Actuator", *Ultrasonic Symposium Proceedings*.
- Uchino, K. 1989. "Recent Topics of Ceramic Actuators", *Ferroelectrics*, 91:281–292.
- Zhuang, Y. G. Hew and Q. C. Xu. 1983. "Sandwich PZT/Polymer Composite Transducer", *Ferroelectrics*, 49:241–249.

APPENDIX 42

TAILORING HIGH DISPLACEMENT PERFORMANCE OF CERAMIC-METAL
PIEZOCOMPOSITE ACTUATORS "CYMBALS"

J. F. Fernandez*, A. Dogan, J.T.Fielding, K. Uchino, R. E. Newnham.

International Center for Actuators and Transducers. Materials Research Laboratory,
The Pennsylvania State University, University Park, PA 16802.

* (Current address: Electroceramic Department, Instituto de Ceramica y Vidrio, CSIC, 28500
Arganda del Rey, Madrid, SPAIN)

ABSTRACT

The unique design of metal-ceramic actuators exhibits very high displacement and large generative forces. This new design metal-ceramic composite actuator, named "Cymbal", consists of a piezoelectric disk sandwiched between two cone-truncated shaped metal endcaps. The radial motion of the piezoelectric ceramic is converted into a flextensional motion, rotational motion or both motions in the metal endcap. On the basis of previous studies of ceramic-metal composites, a simplified model approach was developed in order to evaluate properties of cymbals and as criteria for material selection.

The effect of the stiffness for the metal, piezoelectric coefficients and epoxy characteristics were evaluated as a function of the main actuator parameters. It was found that the higher the transverse piezoelectric coefficient, the higher the displacement of the actuator. The stiffness of metal affects negatively the displacement but allows the composite to support higher loads. There is a Thermally Induced Displacement (TID) of the piezocomposite with temperature that is related to the thermal expansion mismatch between the metal endcaps and the ceramic. By

selecting appropriate materials it is possible to avoid this TID. Very low or negligible temperature dependence of the displacement was attained by using PZT ceramics with low temperature dependence on its properties or by using metal with higher stiffness and lower thermal expansion coefficients than the ceramics.

1. INTRODUCTION

In recent years, piezoelectric and electrostrictive ceramics have been used in many actuator applications as displacement transducers, pressure sensors, shape controllers and precision micropositioners. When an electrical field is applied parallel to the polarization direction in a piezoelectric ceramic, a expansion in longitudinal direction and shrinkage in transverse direction occurs. There are two actuator designs which use this phenomenon to enhance the displacement for practical applications: multilayer ceramic actuators and Bimorph actuators. The advantage of multilayer actuators are its generative force and quick response speed. However, small displacement and high capacitance of multilayer actuators make them impractical for certain applications. On the other hand, Bimorph actuators show larger displacement but low generative forces. There is a need for and actuator with intermediate level displacement and generative force.

A new type of metal-ceramic composite actuator, which is based on the concept of flextensional transducer has been reported (1-2). In this metal-ceramic composite the PZT ceramic is sandwiched between metallic endcaps with shallow cavities, with 2(0)-2-2(0) connectivity (3). Because the shallow cavities have a moon shape, the composites is named "moonie". The radial motion of the piezoelectric ceramic is converted into a flextensional motion in the metal endcap. As a result, a large displacement is obtained at the device center in the direction perpendicular to the ceramic disk.

Due to large difference in the thermal expansion coefficient between the metal, brass, $20 \times 10^{-6} / ^\circ\text{C}$, and the ceramic, PZT, $6 \times 10^{-6} / ^\circ\text{C}$, a significant thermally-generated stress is

produced in the composite during the cooling process when silver paste bonding is used. If no stress relaxation occurs below the glass softening temperature, typically 400 °C, thermally induced compressive stresses are generated in the PZT, while tensile stresses are generated in the endcaps (4). These prestresses help to maintain the PZT polarization during exposure to high hydrostatic pressure, which is required for hydrophone applications. However this tensile stress concentration can easily damage the outer edge of the PZT. The dimensional change produced during the poling process of the PZT increases this tensile stress concentration, reaching values close to the fracture strength of the ceramic.

As actuators, metal-ceramic composites need to achieve higher displacement and reduce the stress concentration in order to attain higher generative force and reliability. It was found that the introduction of a ring-shaped groove on the endcaps enhanced markedly the displacement (5). At the same time, assembly techniques using room temperature bonding curing epoxies with prepoled ceramic were successfully developed. However, because the polymers have a low melting point, the epoxy bonding method is only useful for low temperature applications. In addition, the temperature characteristics of the moonie are related to those of the ceramic elements (6-7). The thermal expansion coefficient mismatch between the metal and ceramic is the origin of the Thermal Induced Displacement or TID (7).

New metal-ceramic designs using truncated-cone shaped endcap, named "cymbals" (8), figure 1, have demonstrated higher displacements, effective piezoelectric coefficients, and generative forces (7-8). In cymbal actuators the radial motion of the ceramic is converted into flextensional and rotational motion of the metal endcap.

In this paper a simplified model was developed in order to understand basic motion in cymbals type actuators and to evaluate how different materials parameters affect performance of ceramic-metal composites. The temperature dependence of the new design metal-ceramic "cymbal" actuators, were investigated in order to avoid the temperature dependence of properties.

2 SIMPLIFIED MODEL APPROACH.

In order to focus the research on materials effects of cymbal performance, a simplified model approach was developed. By optical microscope observation of polished cross section of punched brass cymbal endcaps, it was observed the existence of a curvature near the bonding ring area of the endcap, that have been draw schematically in figure 2. Obviously, that curvature produce negative effects as undefinition of the bonding area with will be traduced in low load tolerance of the composite and low strength of the bonding. That shape favor the appearance of leakage epoxy into the cavity that created spurious resonant peaks in the frequency response. The curvature is also the origin of deformations in the cymbal endcap that affect both the stress transmission between metal and ceramic and the vibration modes. As a consequence of the related effects change of the amplification characteristics appears with the associated problems on reproducibility. By the contrary, the higher the diameter of the cavity the higher the displacement of the ceramic-metal composite.

In order to avoid such a problems, it is necessary to have a very good definition of the bonding area ring of the metal endcap, and at the same time reduces as much as possible the deformation of metal that form the cavity. And schematic two dimensions wiew of that endcap is shown in figure 2 for comparation with previous designed.

When the piezoelectric ceramic is electrically driven if it possible to assume that tow-force member load axially the endcap due to the bonding and the symmetry of the structure, but the endcap is loaded eccentrically that means that the stress distribution cannot be uniform in the top part of the cavity. The conditions of equilibrium of the internal forces in a given section must be equivalent to a force P applied at the centroid of the section and a couple M of moment $M=Ph$, where h corresponds to the cavity depth (figure 3.a and 3.b). As a result, rotation of the segments, flexion of each segment or both motions will be produced depending on the stiffness of the metal and on the geometry.

Let consider the structure of figure 3.c, in which each segment are pin-connected in the extremes. In that case and if the structure is axially unloaded, the motion is pure rotational

without mechanical losses. When the PZT is electrically driven by a field parallel to the polarization direction, the longitudinal shrinkage is transferred to the metal endcaps by the bonding. Compressive stresses are generated in the PZT while extensive stresses are generated in the endcaps. The bonding materials must be able to endure these stresses exerted in opposite direction: otherwise, some microcracks may form and debonding can occur. By increasing the bonding area for a determined lap tensile strength bonding, it is possible to define a threshold bonding area that prevents debonding. The highest efficiency in transfer the transverse motion in the ceramic is attained when the bonding area is enough large to consider that the part of the endcap that form the cavity follow completely the shrinkage of the ceramic in the cavity. However, if the bonding area is too much larger that the bonding area threshold very high stress concentration will occur in the bonding area.

In order to make the most simplified calculation a bidimensional model (figure 2) it is necessary to take into account with the following approaches:

a) Hinge approach: the endcap motion is pure rotational, that means that mechanical losses are not included.

b) Threshold bonding approach: the transverse shrinkage of the ceramic, Δd_c , is completely amplified to longitudinal displacement by the endcaps.

The displacement is the addition of the longitudinal expansion of the ceramic plus the change of the cavity depth due to transverse shrinkage under the approaches made, according with

$$d = 2\Delta h + \Delta h_c \quad [1]$$

where Δh is the cavity depth change and Δh_c is the longitudinal expansion of the ceramic under applied electrical field, E , given by

$$\Delta h_c = d_{33} E h_c \quad [2]$$

where d_{33} is the longitudinal piezoelectric coefficient. The cavity depth change could be calculated following the expression

$$\Delta h = \left[p^2 - (p \cos(\theta + \Delta\theta) + (\Delta d_c / 2))^2 \right]^{1/2} - h \quad [3]$$

Where

$$\Delta d_c = -d_{31} E d_c \quad [4]$$

From the expression [3] it is easy to understand that the higher the cavity diameter, the lower the cavity depth and the higher the transverse piezoelectric coefficient, will produced the higher displacement. In that sense, the ceramic-metal composite works like a pure displacement amplifier.

Thermally Induced Displacement (TID) is consequence of the thermal expansion mismatch between ceramic and metal. It is possible to calculate that TID from

$$TID = h_c \Delta t_c + 2 h_m \Delta t_m + 2 \left[(\Delta t_m p)^2 - ((\Delta t_c d_c - \Delta t_m \Delta d_t) / 2)^2 \right]^{1/2} - 2(h+h_m) \cdot h_c \quad [5]$$

whit

$$\Delta t_c = 1 + \alpha_c \Delta T \quad [6]$$

and

$$\Delta t_m = 1 + \alpha_m \Delta T \quad [7]$$

where α_c and α_m are the thermal expansion coefficients of the ceramic and the metal respectively.

If the PZT is electrically driven, the expression [3] can be rewritten as the Thermal Displacement Dependence, TDD:

$$d(T) = 2 \left((\Delta t_c p)^2 - \left[(\Delta t_c d_c - \Delta t_m d_t) / 2 - (d_{31}(T) E \Delta t_c d_c) / 2 \right]^2 \right)^{1/2} - 2 \left((\Delta t_c p)^2 - \left[(\Delta t_c d_c - \Delta t_m d_t) / 2 \right]^2 \right)^{1/2} + d_{33}(T) E \Delta t_c h_c \quad [6]$$

when $d_{31}(T)$ and $d_{33}(T)$ are the corresponding piezoelectric coefficients at different temperatures. In the above expression TID was included. For a $\Delta T=0$, expression [6] transform in expression 1 where the angle was replaced for the cavity depth variation. From the above expression, it is clear that avoiding the temperature dependence of the ceramic-metal composites could be reached by elimination of the mismatch between thermal expansion coefficients of ceramic and metal, and by the reduction of piezoelectric coefficients thermal dependence, mainly d_{31} coefficient.

It is obvious that the stiffness of the metal endcaps play a important role in the endcap motion. In order to rotate segment AB at the B point. The forces acting consist of couples formed by P and P' (figure 3d), of moment $P(L/2)\sin\Delta\theta$, which tends to move the segment away from the starting position and the couple M exerted by the spring which tends to bring the segment back to its original position. The moment of the couple is $M=k(2\Delta\theta)$, where k is the spring constant. The system is stable if couples are balance each other and the value of the load in such case is called the critical load (9) and is denoted by P_{α}

$$P_{\alpha}(L/2)\sin\Delta\theta=k(2\Delta\theta) \quad [7]$$

or since $\sin\Delta\theta=\Delta\theta$

$$P_{\alpha}=4k/L \quad [8]$$

For an applied force $P>P_{\alpha}$ the segment will move away from the original position and, after some oscillations, will settle into a new equilibrium position. For a rectangular spiral torsion spring the moment is (10)

$$M=\pi Ybt^3\theta'/(3L) \quad [9]$$

where Y is the modulus of elasticity, b the material width, t the material thickness, θ' the angular deflection and L de length of the active spring material. From that expression the stress concentration is

$$\sigma_{\alpha}=2\pi Yt\theta'/L \quad [10]$$

The displacement of the endcaps will be reduced proportionally to the stiffness of the metal and to the thickness of the metal. The displacement calculus need to take into account such effect and will became more complex.

When the system is uniaxially loaded, that is the normal case for applications as actuators, the load will be transfer from the endcaps to the ceramics. The stress transfer will generated an expansion of the ceramic in transverse direction. Because of the strength of the ceramic, there

is a limit on that energy transfer. As a consequence, a deformation of the metal endcap will occur. That deformation will produce buckling in the three segment that form the cavity. After removal of the load, the system will return to its original symmetry plastic deformation does not occur. From Euler's formula (9), the critical load that produces buckling in a segment is

$$P_{\alpha} = \pi^2 Y I / L^2 \quad [11]$$

when Y is the modulus of Elasticity, and I is the moment of Inertia. For a metal sheet of thickness t, $I = (1/12) A t^3$, when A is the area. The critical stress for producing buckling is given by

$$\sigma_{\alpha} = P_{\alpha} / A = (1/12) \pi^2 Y t^2 / L^2 \quad [12]$$

The motion of metal endcap when the ceramic is electrically driven and the composite is axially loaded, could be understood from the stress concentration of the system and need to be evaluated taking into account the geometry and the stress distribution of the cavity in spherical coordinates. The relations that defined the condition to prevent buckling and to favor rotation of the endcaps will be matter of a more improved and complex mathematical model that is not the goal of that present study. However, if critical stress for buckling and torsion are similar it is possible to found from expression [10] and [12] that the angular deflection depends on the thickness and inversely on the length of the segment

$$\theta' = (1/24) \pi t / L \quad [13]$$

The above expression establish a critical geometry that produce rotation motion, flexion motion or both motion of the endcap. Further analysis of the motion of the cymbals could be done by Finite Element Analysis on the basis of the ideas here expressed.

3. EXPERIMENTAL PROCEDURE.

Poled ceramic disks, having 12.7 mm in diameter and 1 mm in thickness, of three different ceramic commercial compositions were investigated. Table I resumes the most important

parameters of the piezoelectric compositions used. Dielectric constant and dielectric losses were measured using HP 4194A Impedance/Gain Phase Analyzer; d_{31} was measured by the resonance method (11) and d_{33} by using a Berlincoumeter.

Different metals and alloys were selected according to both the thermal expansion coefficients and the stiffnesses. Molybdenum, Tungsten and Zirconium were the pure metals selected, and Brass, 70%Cu-30%Zn, Kovar, 54%Fe-29%Ni-17%Co, and Low Carbon Steel, ASTM A 599 electroplated with tin, were the alloys selected. Table II resumes main physical properties obtained from technical literature (12-13). Truncated-cone shape of the cymbal design (8), was achieved by punching first and then pressing (up to 100 MPa) metal sheets of approximately 250 μm . After punching, spurs generated in the border of the endcaps were carefully removed by grinding. Pressing process confers a well defined ring shaped bonding area of 2 mm and a cavity diameter of 8.7 mm. That bonding ring area was grinded using SiC sand paper of 400 mesh in order to remove possible oxide layer and to give a more adequate surface for epoxy bonding.

The ceramic disk and the endcaps were bonded together around the circumference with two different epoxies. The epoxy was distributed taking care do not to fill the cavity, otherwise properties could be drastically changed. Bonding process was performed under small pressure over the bonding ring area by using adequate rings. Characteristics of used epoxies as well curing process are listed in table III. Both epoxies are two component with similar lap tensile strength characteristics. Eccobond is a black color epoxy that contains dispersed CaCO_3 particles. Masterbond is a light brown pure epoxy phenolic with a wide temperature range of operation and needs to be cured at moderately elevated temperatures.

The displacement of a composite actuator was measured at 0.1 Hz in frequency under and applied field of 1 kV/mm with a Linear Voltage Differential Transducer, LVDT, at room temperature or with a photonic non contact sensor as a function of temperature. In both cases the resolution was 0.05 μm . The displacement under load was monitoring with an Eddy current sensor with a resolution of 0.2 μm . Temperature dependence experiments were performed in a specially designed temperature chamber in the range of -5°C to $+95^\circ\text{C}$.

Borosilicate Glass Standard Reference Materials 731 from NIST (14), was used as a temperature standard.

3. RESULTS AND DISCUSSION.

Figure 4 shows the metal sheet thickness and cavity depth for the different metals selected. After pressing the cavity depth of the endcap is approximately 270 μm , for zirconium, brass, low carbon steel and kovar; 250 μm for molybdenum and 175 μm for tungsten. Before pressing none of the endcaps show defined bonding area ring. After pressing the cavity depth was reduced from as punched one for metals with modulus of elasticity below 300 GPa. That effect indicates that the curvature observed in the as punched endcaps diminished. Metals with higher modulus of elasticity, even if they got a better defined bonding ring, do not decrease the cavity, on the contrary as happens with tungsten endcaps, the cavity depth could be increased as a consequence of higher and more uniform pressure than in the punching process. Otherwise punching and pressing give more reproducible metal endcaps, that is very important in order to get reliable composites.

Figure 5 shows the effect of Young's modulus of metal endcaps and hardness-softness of ceramic materials on the displacement of composite cylindrical actuators. For the same metal endcap, there is dependence of the displacement on the d_{31} piezoelectric coefficient of the ceramic. The higher the contraction of the PZT in the radial direction is, and thereafter the shrinkage of the cavity, the higher the displacement is. The theoretical approached displacements for the same cavity size are 26, 19 and 10 μm for PZT 5H, PZT 5A and PZT 8D respectively, these data fit reasonably the measured ones, figure 5. From that result it seems that the mechanical losses generated on the bonding and on the endcaps are almost equilibrated with the circular shape of the design. To prove that assumption, brass and zirconium endcap were made removing part of the endcap in order to get only 40% of the bonding ring and that the contribution to the displacement only were conferred by shrinkages

in one direction of the ceramic disks without contribution of the 90° rotated direction. That type endcaps had a bowtie cymbal shape and were bonded with eccobond to PZT 5H. The displacement of the bowtie cymbals was 28,5 and 26,6 μm for zirconium and brass respectively, less than 10% higher than displacements of 26,2 and 25,4 μm for zirconium and brass cymbal regular endcaps. In both cases the resonance spectrum give a flextensional peak plus PZT transverse resonance peak. The frequency values of the flextensional peaks were lower for the partially stress removed endcaps (15).

It seems that there is a saturation of the displacement for cymbals made with metals with modulus of elasticity near to the value of the modulus of elasticity of PZT. The decrease of the displacement with the increase of the stiffness of the metal endcap is related to higher mechanical losses in the endcap motion. That behavior is almost linear for cymbals bonded at room temperature with eccobond that is in agreement with the linear dependence of the different motion of the endcaps with the modulus of elasticity of the metals. The displacement of the stiffest metal is approximately 52-57% of that achieved using least stiff metal endcaps, and it is practically independent of the ceramic type. In the case of composites bonded with masterbond a different behavior was exhibited. In general lower displacement values was observed than for the room temperature cured, epoxy bonded cymbals. And it seems that this decrease is significant for the cymbals made with PZT 5H, that shows the highest displacement. The reason for such behavior is attributed to the softness of the epoxy. Even though both epoxies have similar tensile lap strength, masterbond is a pure phenolic epoxy high temperature cured, while eccobond, having dispersed particles, possesses a higher flexibility. The thickness of the bondline using masterbond is slightly thinner than for the eccobond because of the decreasing of viscosity with the temperature, with ranges on 10-15 μm and 20-25 μm respectively. On the other hand, for cymbals assembled with endcaps having larger thermal expansion coefficient than the ceramic, stresses generated during the elevated temperature epoxy curing resulted in a pronounced decrease in attained displacement. In the case of brass, which has the highest mismatch of thermal expansion coefficient in relation to the ceramic, the displacement is drastically reduced.

The degree of hysteresis of the displacement is an important criteria for actuators that provides information about losses. It is defined (16) as

$$\Delta H \% = 100 \Delta X / X_{\max} \quad [14]$$

where X_{\max} is the displacement at maximum electric field, in the present case 1kV/mm, and ΔX is the difference in displacement between increasing and decreasing path of half maximum of the applied electric field. hysteresis data as well maximum displacement were recorded after more than 12 cycles to eliminate walk off. Figure 6 shows the degree of hysteresis for the cymbals actuators as a function of the metals endcap Modulus of Elasticity. It seems that there is a small dependence of the hysteresis with the stiffness of the metal. the lowest hysteresis values are register for ceramic-metal composites based on hard PZT ceramic. The main reasons for hysteresis losses in piezoelectric ceramic are domain reversal mechanisms. PZT-5A ceramic disks typically show 5-8% hysteresis losses. The losses is the epoxy bonding layer between the ceramic and the metallic endcaps, and mechanical losses on the solid hinge regions of the metal endcaps are the reasons of the increase of hysteretic behavior. Cymbals made with the previous design had hysteresis value of 15%. New pressed cymbal shape reduce a little bit the histeretic behavior. On the other hand epoxy effect has not been clarify excessively, very similar values had been obtained for eccobond and masterbond for samples based on soft piezoceramic materials. On the contrary, samples made with PZT 8D, hard piezoelectric, and masterbond shows and interesting behavior against samples made with eccobond. The hysteretic behavior increased with the modulus of elasticity for the samples bonded with high temperature epoxy. Thermal curing of the epoxy could be the reasons of such a behavior.

Figure 7 shows the displacement of kovar endcap, PZT-5H ceramic, bonded with eccobond, actuators under load. Net displacement of different metal endcap cymbals is shown in figure 8. The net displacement is the displacement produced by the actuator at each load one time that the deformation of the structure, displacement without applied electrical field, is subtracted. The deformation of the structure in a function of the load is shown in figure 9. As lower the modulus of elasticity of the metal higher the displacement and higher the

deformation of the metal. By the contrary, the maximum load, defined as the load until the net displacement is keeping higher than 90% of the initial displacement, increased with the modulus of elasticity of the metal. Figure 10 collects the data of maximum load and deformation for such a load for different metals endcaps. The values obtained are quite larger than the previous reported in original cymbal type actuator (7), 20 N. The reasons of such improvement it is attributed to a more efficiently stress transmission of the endcaps. The main discrepancies from a linear behavior in figure were given by the low carbon steel cymbals due to its high ductility against the rest of metals selected, and by the tungsten cymbal because of its lower cavity depth that means a different spring response of the endcaps. Low carbon steel is the only metals studied that have a maximum load that its critical for the performance, because of the permanent deformation of the endcap that makes impossible to the actuator recovers its initial properties. The other metals recovered the original displacement after were tested. Resonance spectra, that are very sensitive to symmetry changes were recorder before and after the load test with no variations except in the case of low carbon steel cymbals. On the other hand, PZT type do not have to much influence on the maximum load of the actuator as can be derived from the figure 11. For all the PZT types the maximum load is approximately 67 N in the case of Kovar endcaps.

For the composites bonded with masterbond, one time that the maximum load is reached debonding take place an the sample is destroyed. All samples debonded at the endcap face that is in contact with the load and a characteristic damage of the center of the PZT electrode occurs. Even the tensile lap strength is similar in both epoxies, the existence of particles in eccobond conferred to that epoxy higher flexibility, that could be traduced as a small rotation of the metal bonding ring. In that case the ceramic support more stress and relief it because of its higher strength. Masterbond is a more crystallize epoxy due to its curing process. The calculated stress in the bonding ring area of one endcap is 1.9 MPa for a load of 70 N, that is lower than the tensile lap strength of the epoxy. However, small microcracks generated in the bonding by air bubbles, deformation of the endcap, variation on the thickness of the epoxy, etc., could be the origin of a reduction of absorbed stress by the bonding. On the other hand,

the deformation of the metal endcap, mainly produced by buckling could be not symmetrically produced in both endcap. The reason to induce such a idea lies on the assumption that the load is connected in series with the upper metal endcap, the ceramic and the lower metal endcap. The higher strength of the ceramic could relief partially the stress and in that case the lower endcap support different stress distribution. If concentration of the stress is produced in the upper endcap, higher deformation of the endcap and possible bending of the ceramic could provoke the collapse of the structure as has been observed. Anyway more and new experiment will be required to clarify such a question that could open new and improved design for actuator applications.

By using expression [5] it is possible to calculate the Thermal Induced Displacement, TID, of the cymbal actuators. The data obtained for the different metal under study show (figure 12) that the reduction of the thermal expansion mismatch between the metal and the ceramics

TID measured data in table IV confirm the theoretical data and shows that is practically possible to avoid or to get a negative TID. The measured data were lower than the calculated. The reasons are attributed to the effect of the epoxy that have almost one order of magnitude higher thermal expansion coefficient that affect the stress transfer and because the deformation of the metal. The discrepancies between the calculated data and the measured are higher as higher the TID is. From the point of view of practical application, negative TID's are very interesting because the metal produces a compressive stress on the ceramic that can reduce the depolarization process due to the increasing of the temperature. At the same time, negative TID could easily overcome in the final device by combining the cymbal with carefully tailored materials.

Figure 13 shows the thermal dependence of the net displacement for different endcap materials bonded to PZT 5H with eccobond. There is a drastically decrease of the displacement for temperatures higher than 50°C attributed to the bonding layer that became more flexible at higher temperatures. The linear operation region of the actuator is restricted to temperatures between 15°C to 45°C for the materials with low mismatch of thermal expansion coefficient between metal and ceramic elements. For temperatures below 15°C, the increasing

of the displacement with the temperature is related to the temperature dependence of the piezoelectric ceramic, in particular of the d_{31} variation with temperature (17).

With masterbond it is possible to extend the operating temperature range of the cymbal actuator (figure 14). In that case it is observed that the temperature dependence of the net displacement is very close to that of the d_{31} of the ceramic in all the temperature range. That dependence is higher for the least stiff metal endcaps. Some deviations to such a behavior are observed for the metals with higher thermal expansion coefficient than the ceramic. Figure 15 shows various measured curves for brass, kovar and tungsten metal endcaps bonded with masterbond to several PZT ceramic types, as well the calculated data from expression [6] for kovar endcaps. From these curves it is possible to determine different ways to eliminate the thermal dependence of the cymbal actuators:

a) Reducing the temperature dependence of the radial coefficients of the PZT ceramic. If the bonding has no significant effect on the temperature characteristics and the stiffness of metal is low, the metal-ceramic composite follows the thermal characteristics of PZT ceramics, meaning that the cymbal works as a displacement amplifier. In such a case, piezoelectric ceramics with low temperature dependence are more powerful for temperature applications, such as PZT 8D and even PZT 5A.

b) Changing the cavity size: In the case of brass, it is possible to observe a very low temperature dependence for temperatures higher than 40°C. In such a case, the mismatch of thermal expansion coefficients between the metal endcaps and the ceramic produces a positive and high TID or in other words, the cavity size changes. It is possible to consider that the cavity size is changing slowly in relation to the cavity depth. As the cavity depth increases the displacement decreases (18). Inconvenient is that the net position of the actuator is increasing continuously because of the TID, even though the temperature dependence could be canceled for a fixed temperature range.

c) Using higher stiffness metal: The mechanical losses cause a reduction of the displacement, however tungsten endcaps provide a temperature independent behavior. One of

the most important characteristics of that composite is the existence of a slightly negative TID that can be easily compensated.

d) Combining multistack structures constructed using the above mentioned effect, it is possible to have very high displacement and negligible TID and temperature dependence.

Figure 16 shows the temperature dependence of selected samples, taking into account both the net displacement and the TID. It is possible to observe that real displacement without temperature dependence in study range have been obtained. Ceramic-metal composite type cymbal, with 2(0)-2-2(0) connectivity, get practical elimination of temperature dependence in the actuator applications of piezoelectric ceramics, making possible the extension of application now in use or considers new ones.

CONCLUSIONS

Properties and performance of ceramic-metal composites with connectivity 2(0)-2-2(0) can be tailored through the selection of materials. Because of the composite structure, the metal endcaps act as amplifier of the displacement generated by the piezoelectric ceramic. The metal endcaps transfer the transversal shrinkage of the ceramic to longitudinal displacement. The motion mechanism correspond with a rotation of the metals endcaps segment according with the simplified approach made. The higher the d_{31} of the PZT the higher the displacement. The stiffness of the materials reduced the attained displacement. But, on the contrary, the applicable maximum force increases with the stiffness of the metal endcaps and it seems to be independent of PZT ceramic type. Higher applicable force limits are reported (up to 85N, previous: 20N) based on more efficiently stress transfer bonding reached by elimination of the curvature of the endcaps in the vicinity of the bonding area.

Cymbal Actuator thermal behavior of displacement depends on the thermal characteristics of PZT ceramic element, particularly d_{31} temperature behavior. Thermal Induced Displacement, TID, was eliminated by using metals with similar thermal expansion coefficient than the ceramic as well, as been calculated that higher cavity reduced such TID. Low or negligible

temperature dependence of displacement in Cymbal Actuator was achieved based on metal endcaps with higher stiffness and lower thermal expansion coefficient than piezoelectric ceramics.

ACKNOWLEDGMENTS

The authors would like to express their gratitude for the support to the following agencies and organizations: Office of Naval Research Contract no. N00014-92 J 1510, National Science Foundation Grant no. DMR-9223847, Spanish Science Ministry (CICYT MAT94-807 and DGICYT PR94-028), Turkish Science and Technology Council (TUBITAK) and Middle East Technical University, Ankara.

REFERENCES

- [1] R. E. Newnham, Q. C. Xu and S. Yoshikawa, Transformed Stress Direction-Acoustic Transducer, U.S. Patent # 4,999,819, March 12, 1992.
- [2] Q. C. Xu, A. Dogan, J. Tressler, S. Yoshikawa and R. E. Newnham, "Ceramic-Metal Composite Actuators", *Ferroelectrics* 160,337-46(1994).
- [3] J. F. Fernandez, A. Dogan, J. F. Tressler, Q. M. Zhang and R. E. Newnham, "Hollow Piezoelectric Composites", *Sensors and Actuators A Physical* submitted.
- [4] K. Onitsuka, "Effects of Bonding and Geometry on the Flextensional Transducer, "Moonie"", Ph.D. Thesis, The Pennsylvania State University, University Park, PA (1993).
- [5] K. Onitsuka, A. Dogan, Q.C. Xu, J. Tressler, S. Yoshikawa and R.E. Newnham, "Design Optimization for Ceramic-Metal Composite Actuators (Moonie)", *Ferroelectrics* 156,37-42(1994).
- [6] A. Dogan, S. Yoshikawa, K. Uchino and R. E. Newnham, "The Effect on the Characters of the Moonie Transducer and Reliability Issue", *IEEE Transactions on*

- Ultrasonics, Ferroelectrics and Frequency Control*, Proceeding V.II pp 935-9, France (1994).
- [7] A. Dogan, "Flexensional "Moonie and Cymbal" Actuators", Ph.D. Thesis, The Pennsylvania State University, University Park, PA (1994).
- [8] A. Dogan and R. E. Newnham, "Flexensional Cymbal Transducer" USA Patent Application. PSU Invention Disclosure no. 94-1375, 1994.
- [9] F. P. Beer and E. R. Johnston Jr., *Mechanics of Materials*, MacGraw Hill Inc., New York 1991.
- [10] R. A. Walsh, *Electromechanical Design Handbook*, MacGraw Hill Inc., New York 1995
- [11] Q. C. Xu, A. R. Ramachandra and R. E. Newnham, "Resonance Measuring Technique for Complex Coefficients of Piezoelectric Composites" *J. of Wave-Material Interaction* 2,2,105-122(1987).
- [12] E. A. Brandes, *Smithell's Metals Reference Book*, 6th edition, Butterworth&Co, New York 1983.
- [13] Y. S. Touloukian, R. K. Kirby, R. E. Taylor, P. D. Desai, *Thermophysical Properties of Matter. The TPCR Data Series Vol.12: Thermal Expansions; Metallic Elements and Alloys*. JFI/Plenum, New York 1975.
- [14] NIST Standard Reference material 731. Gaithersburg, MD, June 1993.
- [15] J.F. Fernandez, A. Dogan, J. T. Fielding, K. Uchino and R. E. Newnham, *Frequency Response of Cymbal Actuator*, in preparation.
- [16] K. Uchino (1986)
- [17] D. Berlincourt; "Piezoelectric Crystal and Ceramics" *Ultrasonic Transducer Materials*, O. E. Mattiat, Plenum Press, New York (1971)
- [18] Q. C. Xu, S. Yoshikawa, J. and R. E. Newnham, "Piezoelectric Composites with High Sensitivity and High Capacitance for Use at High Pressures", *IEEE Transactions on Ultrasonics, Ferroelectrics and Frequency Control*, 38, 6, 634-639(1991).

Jose F Fernandez was born in Madrid, Spain on September 23, 1961. He received the B. S. degree in applied physics in 1985, M.S. degree in physics in 1987 and Ph.D in physics in 1990, all of them from Autonomous University of Madrid, Spain.

He is a staff member of the Electroceramics Department at the Instituto de Ceramica y Vidrio, CSIC, Arganda del Rey, Madrid, Spain. In 1994-95 he was a Visiting Scientist at the Materials Research Laboratory, Pennsylvania State University. His research interest are in the processing of ceramics, dielectric and piezoelectric ceramics and composite materials for electronic applications.

He is a member of the American Ceramic Society and Spanish Ceramic and Glass Society.

Aydin Dogan was born in Ankara, Turkey, on February 22, 1966. He received the B.S. degree in materials science & metallurgical engineering in 1988 and the M.S. degree in 1990, both from Middle East Technical University in Ankara-Turkey. He received its Ph.D. in Solid State Science at the Pennsylvania State University, University Park, PA, in 1994. His research interests include electronic ceramics, sensors and actuators, smart materials and systems, and ferroelectrics.

He is a member of the Materials Research Society and is a NATO- TUBITAK science fellowship recipient.

Joe T. Fielding

Kenji Uchino was born on April 3, 1950, in Tokyo, Japan. He received the B.S. degree in Physics in 1973, the M.S. and Ph. D. degrees in Physical Electronics in 1975 and 1981, respectively, from Tokyo Institute of Technology, Tokyo, Japan.

He is presently Director of the International Center for Actuators and Transducers and Professor of Electrical Engineering at the Pennsylvania State University, University Park, PA, and is vice-president of NF Electronic Instruments, Inc., State College, PA. Previously, he was a faculty member at Tokyo Institute of Technology and Sophia University, Tokyo, Japan. His research interests are in dielectrics, ferroelectrics and piezoelectrics, including basic research on materials, device design and fabrication processes, as well as applicational development of solid state actuators to precision positioners, ultrasonic motors, etc.

Robert E. Newnham was born in Amsterdam, NY, on March 28, 1929. He received the B.S. degree in mathematics in 1950 from Hartwick College, Oneonta, NY, the M.S. degree in physics and mineralogy from the Colorado State University, Fort Collins, CO, and the Ph.D. in crystallography in 1960 from Cambridge University, Cambridge, England.

He is ALCOA Professor of Solid State Science at the Materials Research Laboratory at the Pennsylvania State University, University Park, PA. Previously, he was a staff member of the Laboratory for Insulation Research at the Massachusetts Institute of Technology, Cambridge, MA. His research interests are in structure-property relations, electroceramics, and composite materials for electronic applications.

Table I. Piezoelectric properties of ceramics used as a drive element in cymbals.

CERAMIC	ϵ'	$\text{tg } \delta$	d_{31} (pC/N)	d_{33} (pC/N)
PZT 8D	1104	0.003	-107	289
PZT 5A	1802	0.016	-208	429
PZT 5H	3500	0.016	-285	581

Table II. Metal endcap characteristics

METAL ENDCAP	Density (g/cm ³)	α (10 ⁻⁶ K ⁻¹)	E (GPa)
Zirconium	6.49	5.9	77
Brass	8.53	19.9	110
Kovar	8.36	5.5	138
Low Carbon Steel	7.86	11.7	207
Molybdenum	10.22	5.1	324
Tungsten	19.30	4.6	405

EPOXY	Curing Process	Temperature Range	α (10^{-6} K^{-1})	Tensile Lap Strength MPa
Eccobond	24 h RT	-55 +95 °C	55	16.4

Table III. Characteristics of epoxies

Table IV. TID (μm) of different metal endcap PZT 5H cymbal actuators (from -5°C to 95°C).

EPOXY	Tungsten	Molybdenum	Kovar	Zirconium	LC Steel	Brass
Eccobond	-8.1	-0.5	-0.5	-0.5	4.8	48.9
Masterbond	-2.0	-2.0	-0.3	1.0	8.4	60.5

Figure Captions

- Figure 1. Displacement motion of cymbal ceramic metal composites. Arrows show the displacement direction and dashed lines shows the displacement motion.
- Figure 2 Schematic drawing of cross section cymbal endcaps for previous punched design and new punched and pressed design.
- Figure 3 Schematic view of load applied in different approaches to the cymbal case. a) Two force member is loaded axially, but eccentrically. b) Portion of the figure a) showing that the internal forces in a given section must be equivalent to a force P applied at the centroid of the section C . c) Ideally cymbal endcap formed with segments pin connected. d) Forces involved in a segment AB of the figure c).
- Figure 4. Thickness of the metal sheets used to the fabrication of cymbals endcaps, as well the cavity depth of the cymbal endcap as punched and after pressing treatment for different metal endcap Young Modulus.
- Figure 5 Displacement of cymbals actuators for different ceramics and metal endcaps
- Figure 6 Displacement hysteresis of cymbals actuators for different ceramics and metal endcaps
- Figure 7 Displacement-applied force relation of cymbal actuator.
- Figure 8 Net displacement in a function of the applied load for different metal endcap bonded with eccobond to PZT-5H ceramics.
- Figure 9 Deformation versus applied load for different metal endcap bonded with eccobond to PZT-5H ceramics.
- Figure 10 A) Maximum load and displacement and B) deformation, versus applied load for different metal endcap bonded with eccobond to PZT-5H ceramics.
- Figure 11 Net displacement in a function of the applied load for different PZT ceramic bonded with eccobond to kovar endcaps.

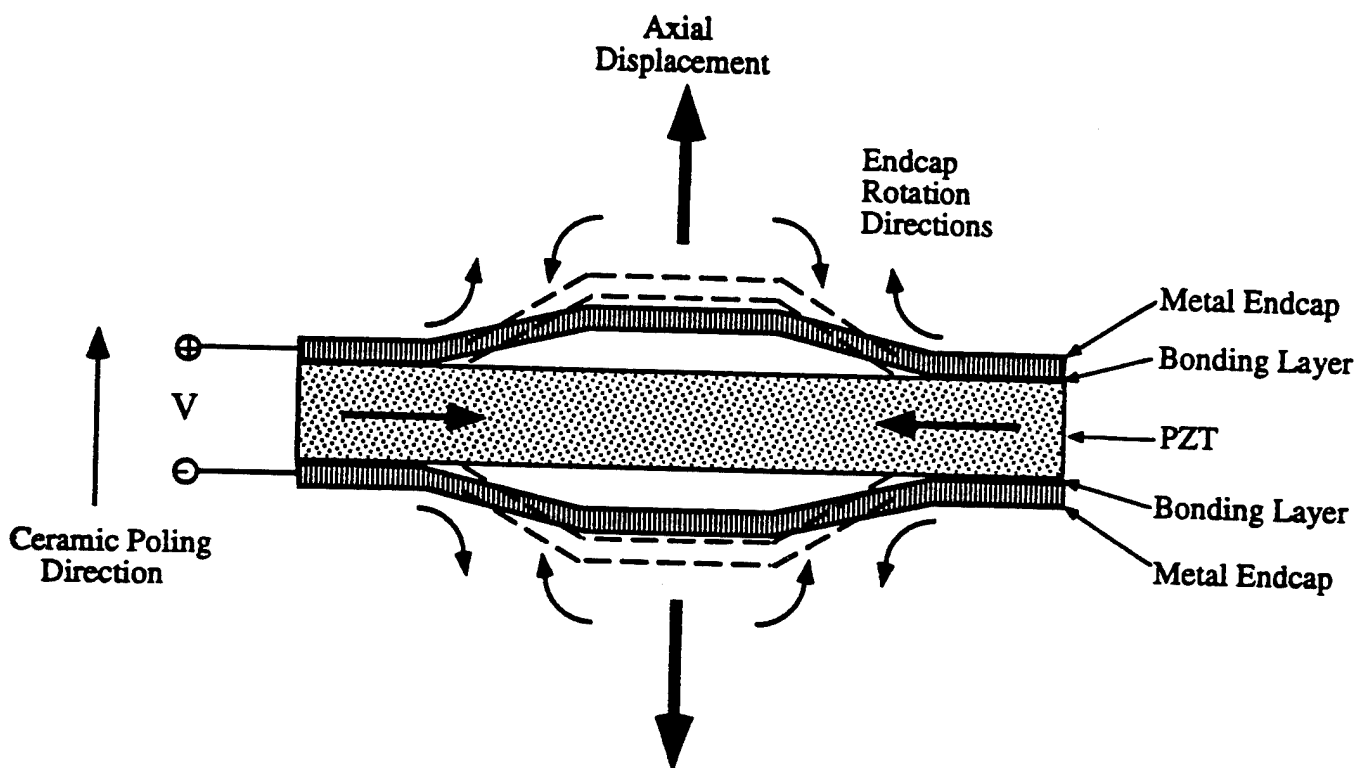
Figure 12 Calculated Thermal Induced Displacement for different metal endcaps. $\Delta T=50^{\circ}\text{C}$,
 $\alpha_c=6 \cdot 10^{-6} \text{ }^{\circ}\text{C}^{-1}$.

Figure 13 Displacement as a function of temperature for cymbals bonded with eccobond.

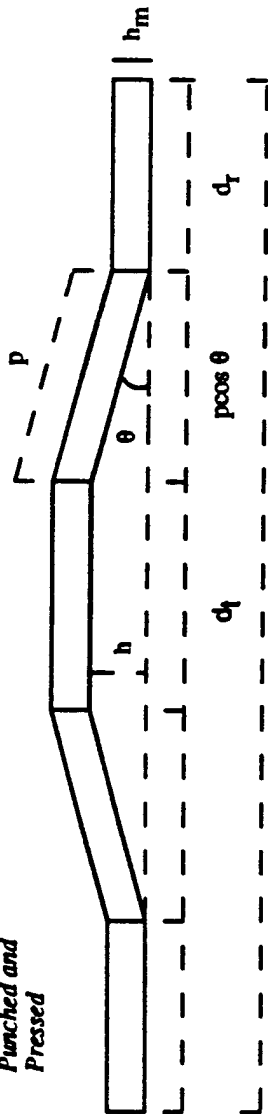
Figure 14 Displacement as a function of temperature for cymbals bonded with masterbond.

Figure 15 Displacement as a function of temperature for the cymbal bonded with masterbond showing the behavior of different PZT types for brass, kovar and tungsten endcaps. As well the calculated net displacement plus TID data for different PZT-kovar composites.

Figure 16 Temperature dependence of cymbal actuators showing net displacement plus TID.

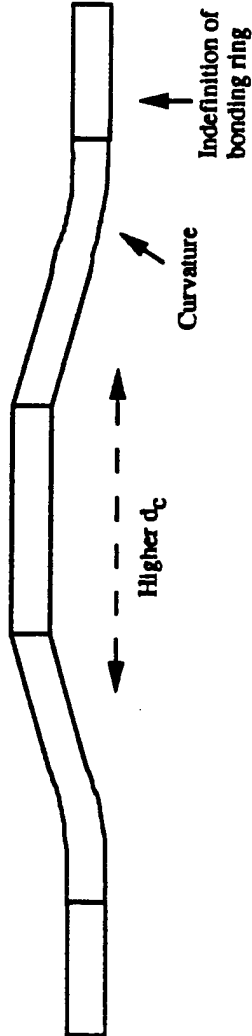


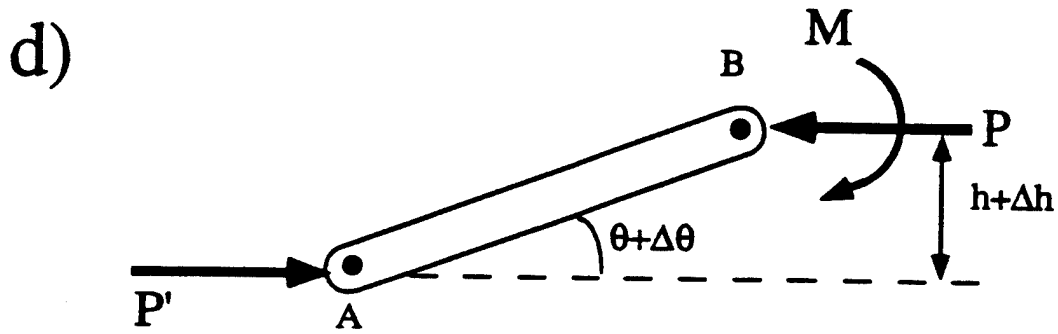
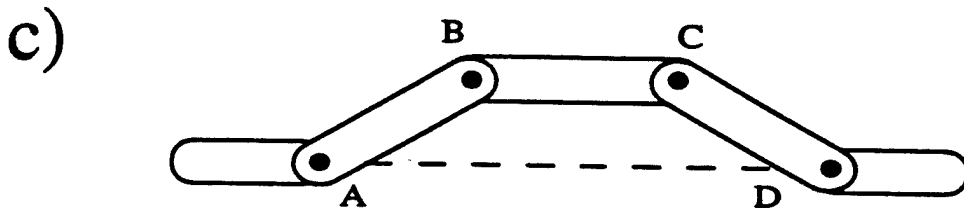
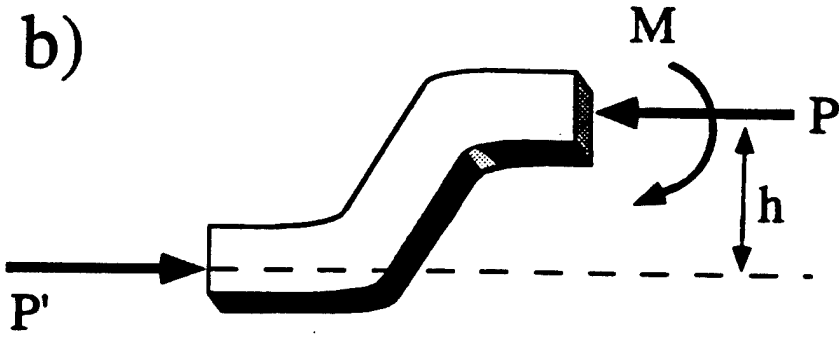
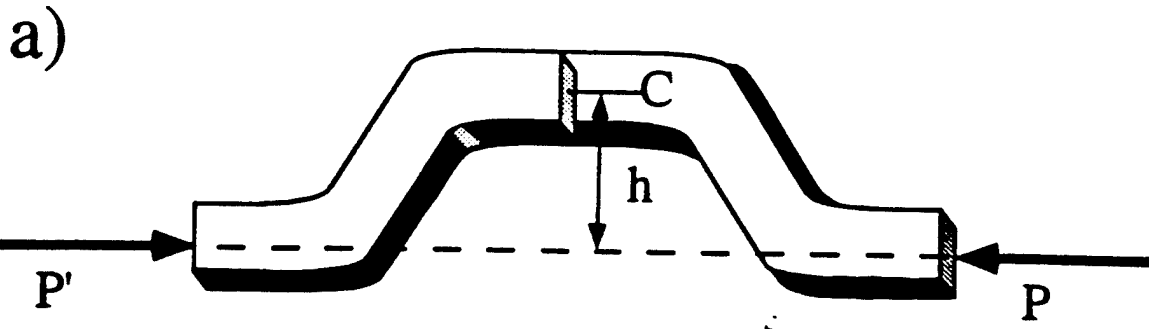
NEW
Punched and Pressed

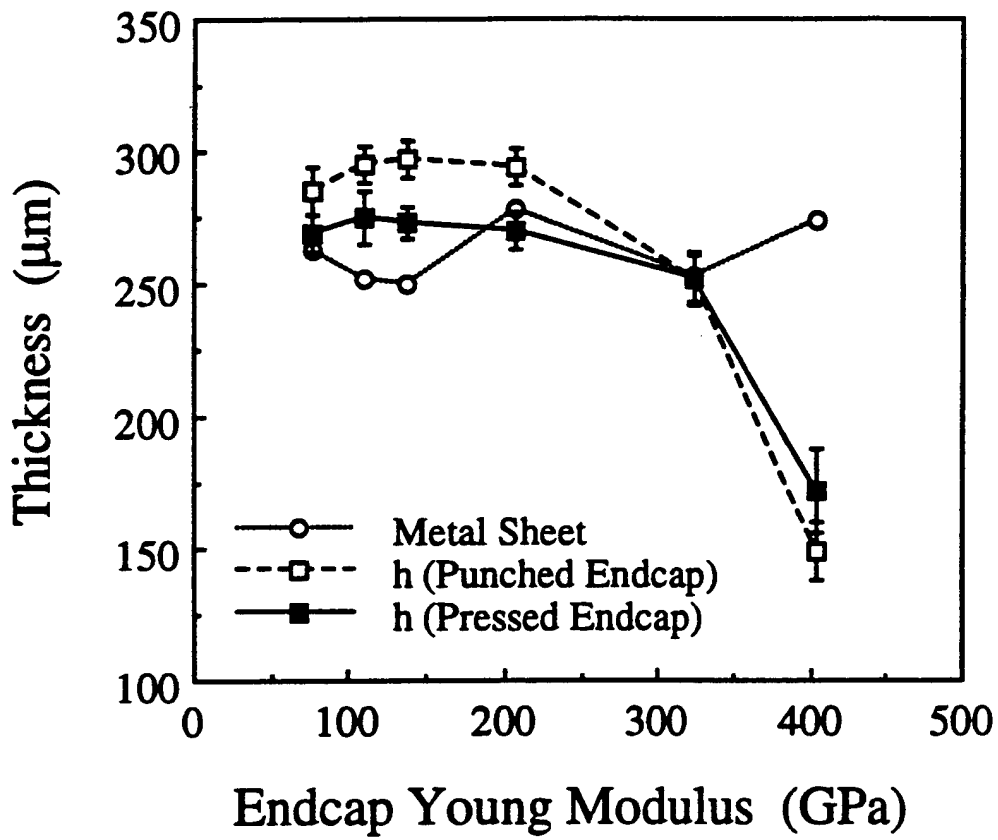


$$d = d_c + 2d_t = d_t + 2p \cos \theta + 2d_t$$

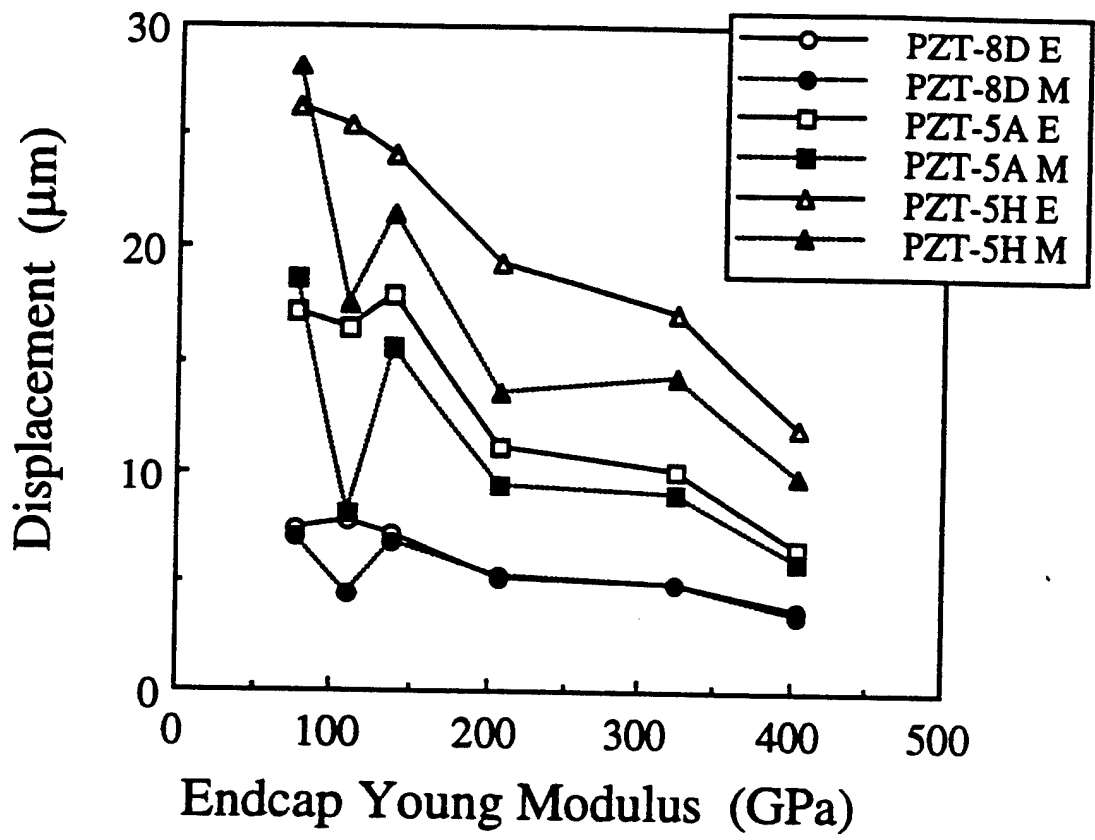
PREVIOUS
Punched



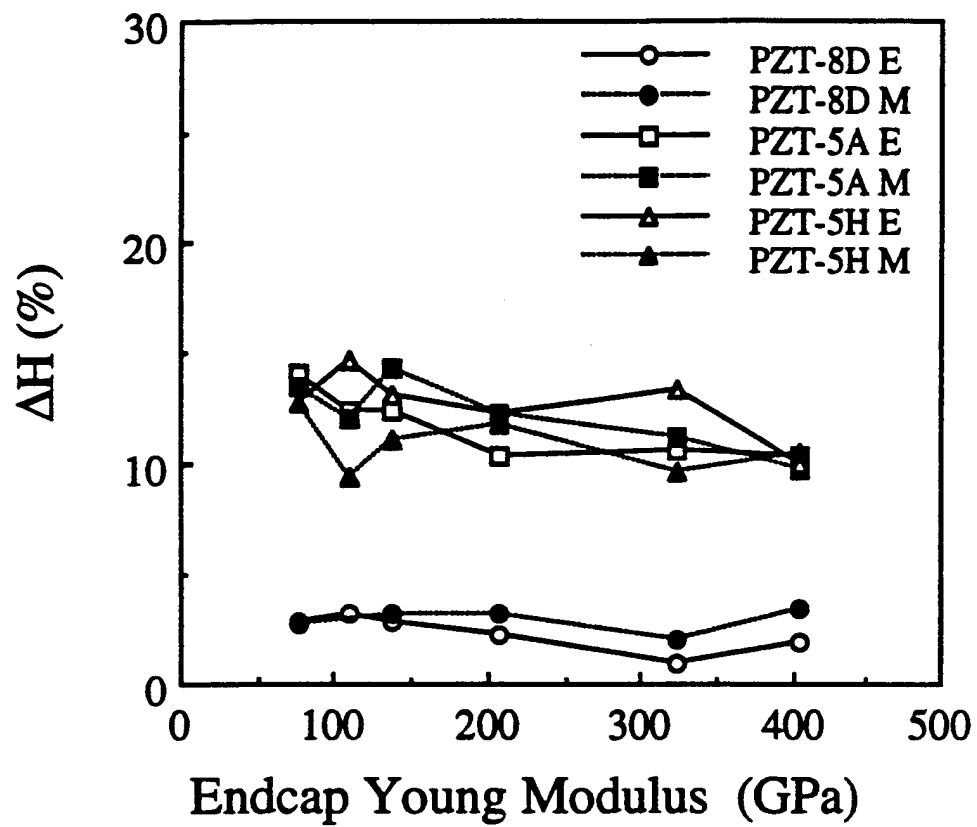




20

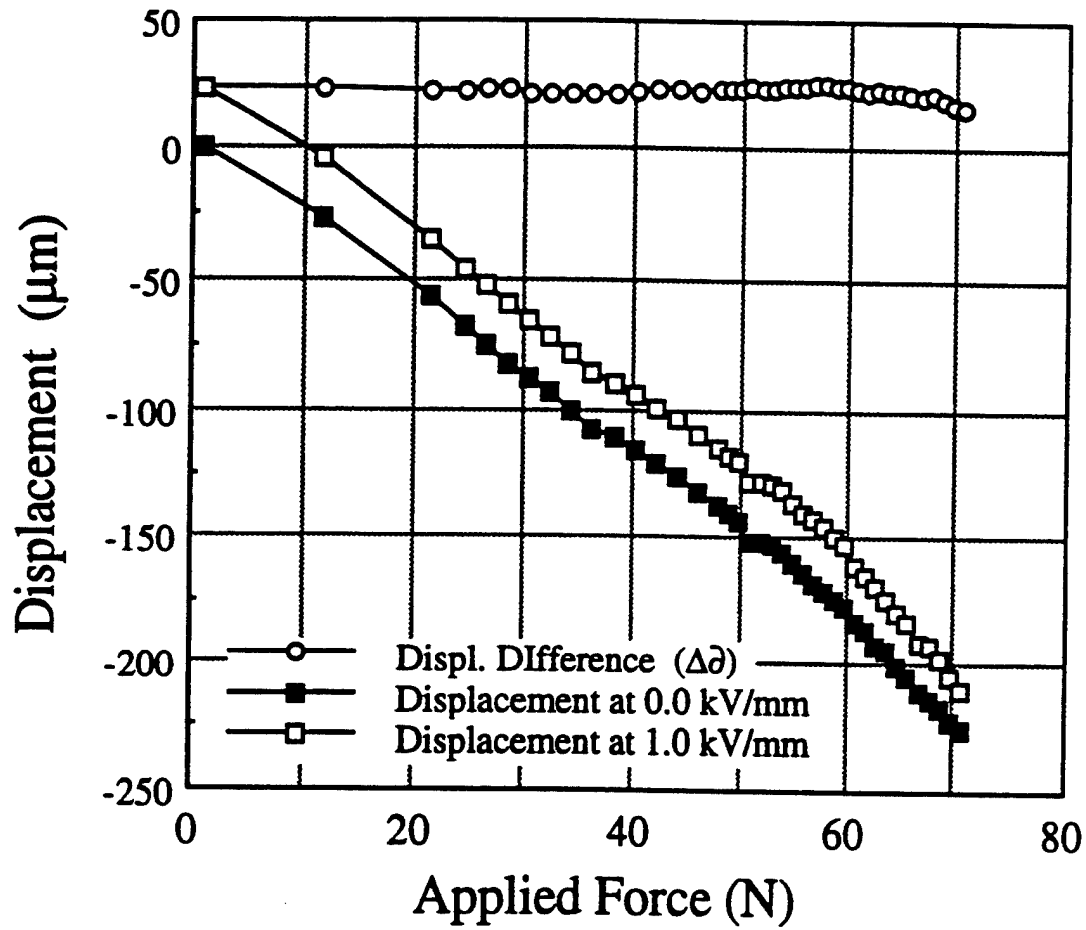


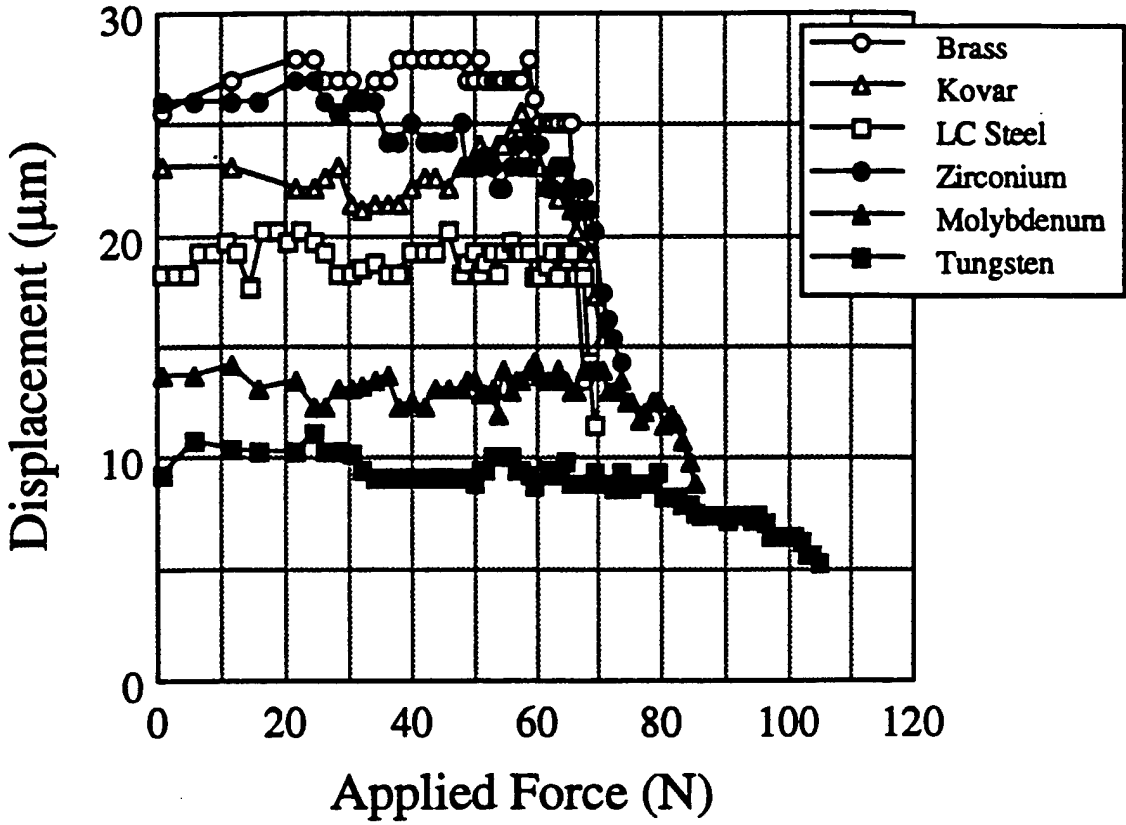
85



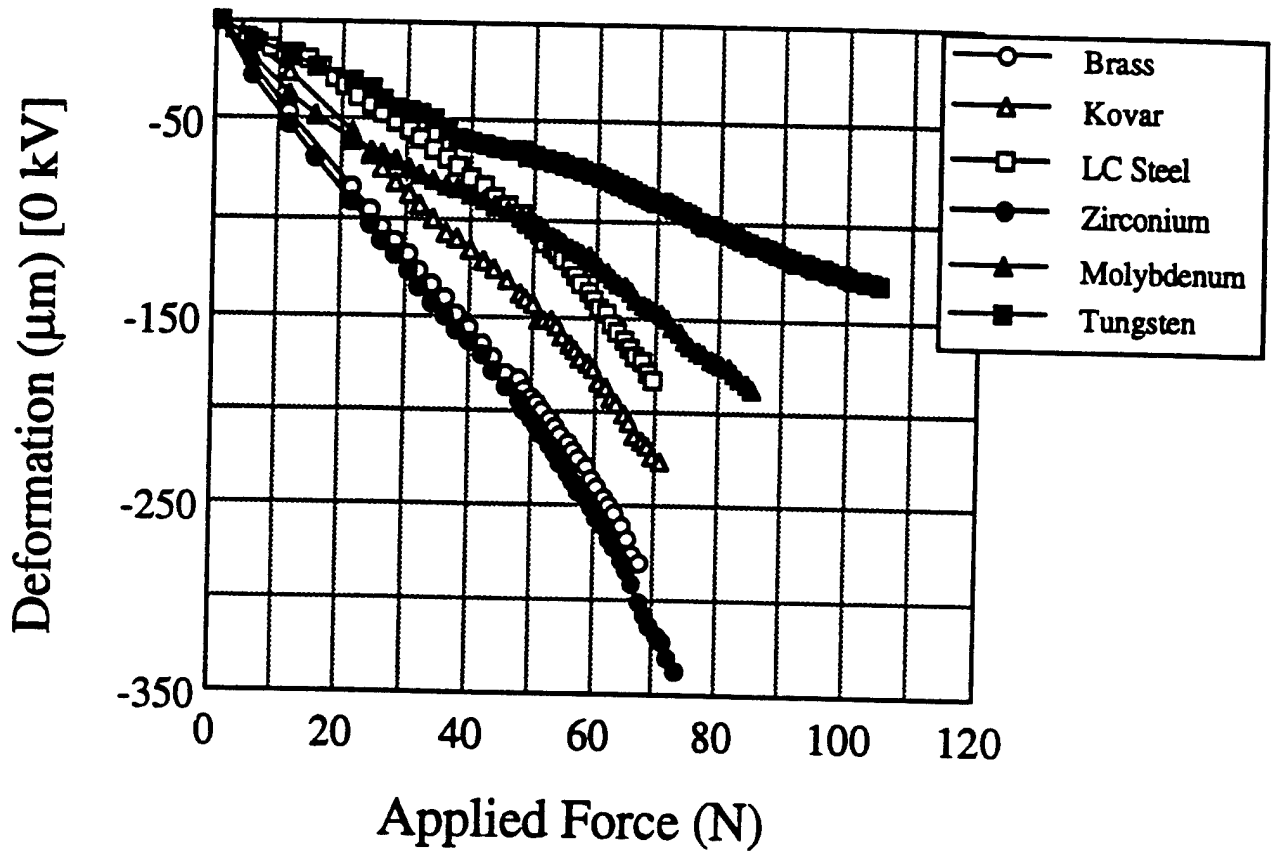
66

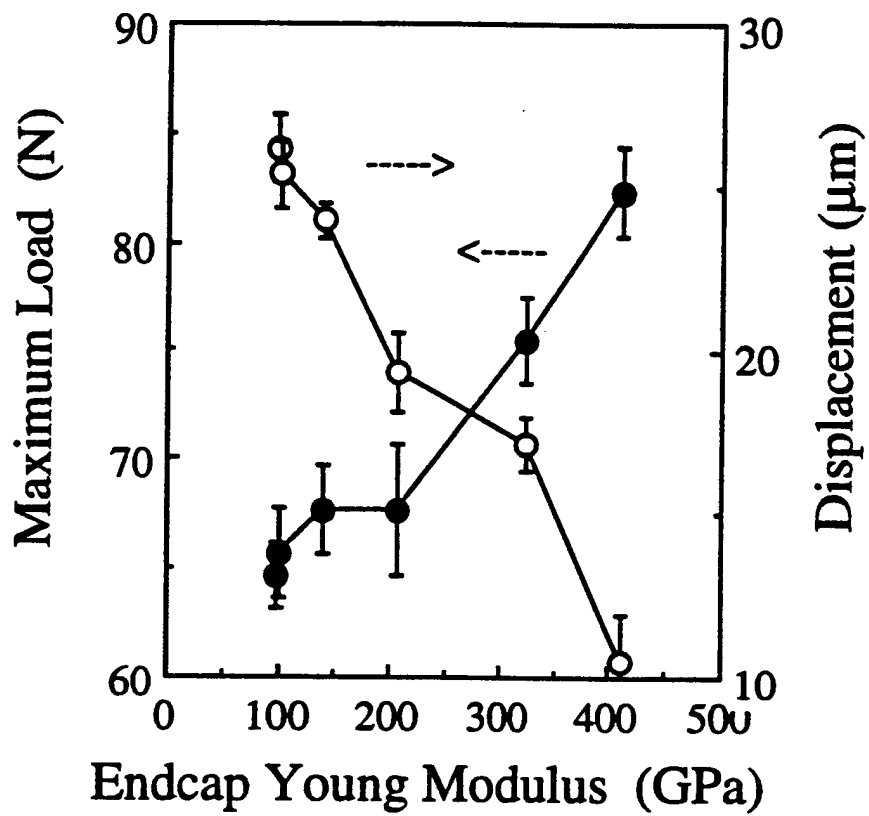
PZT 5H, Kovar Endcap, Eccobond



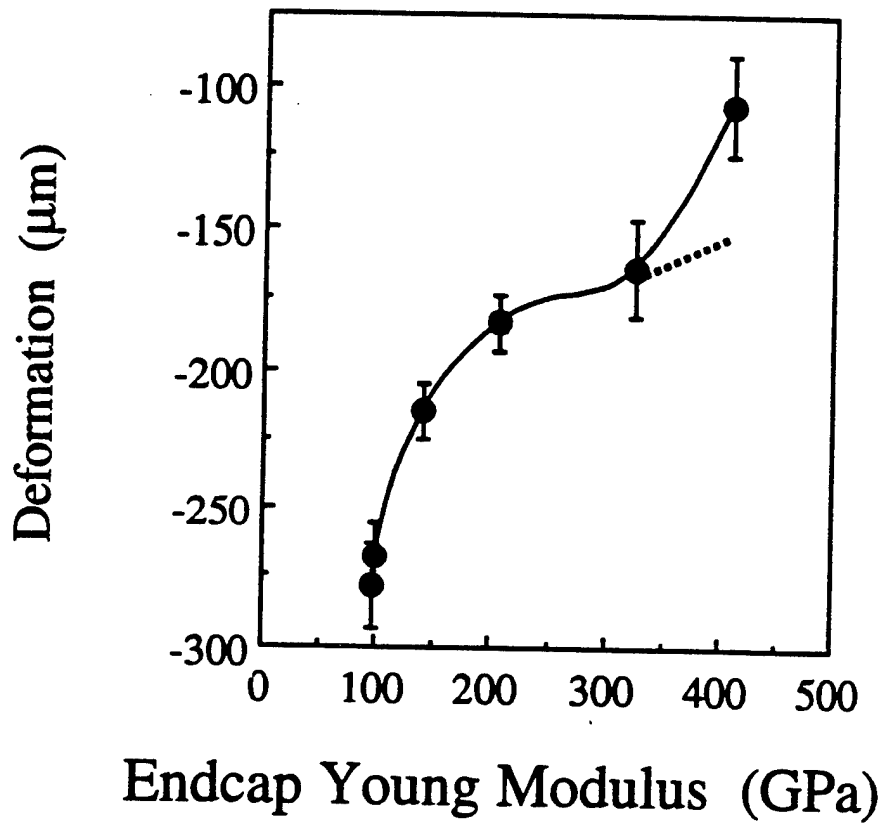


1.8

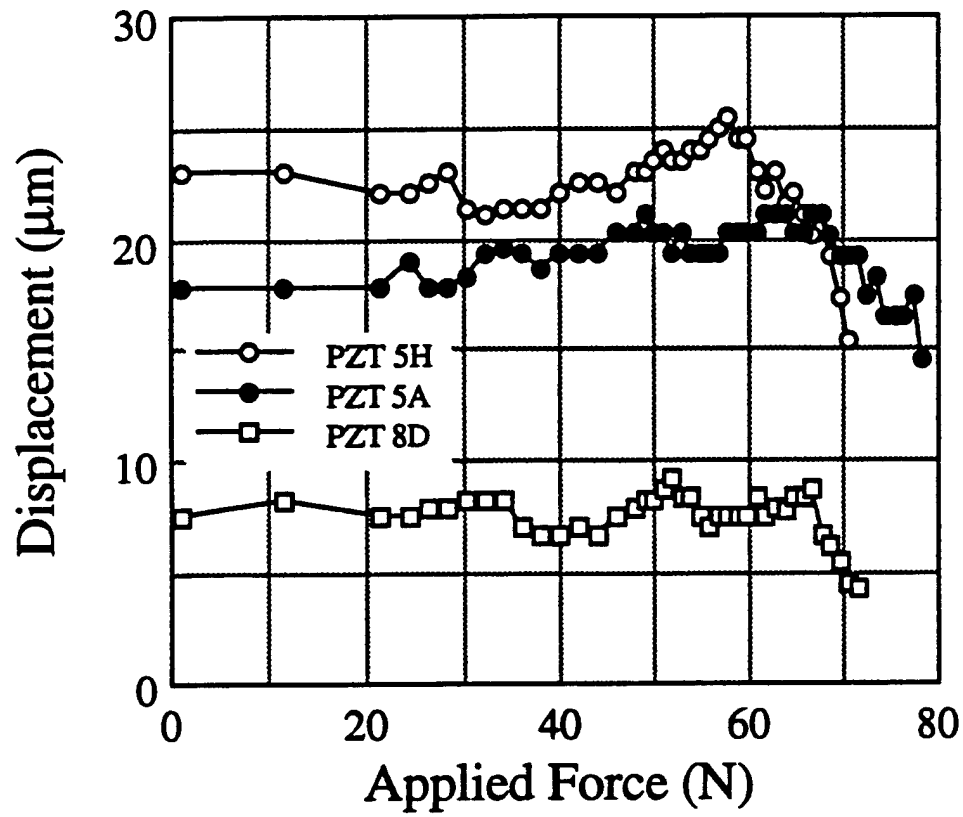




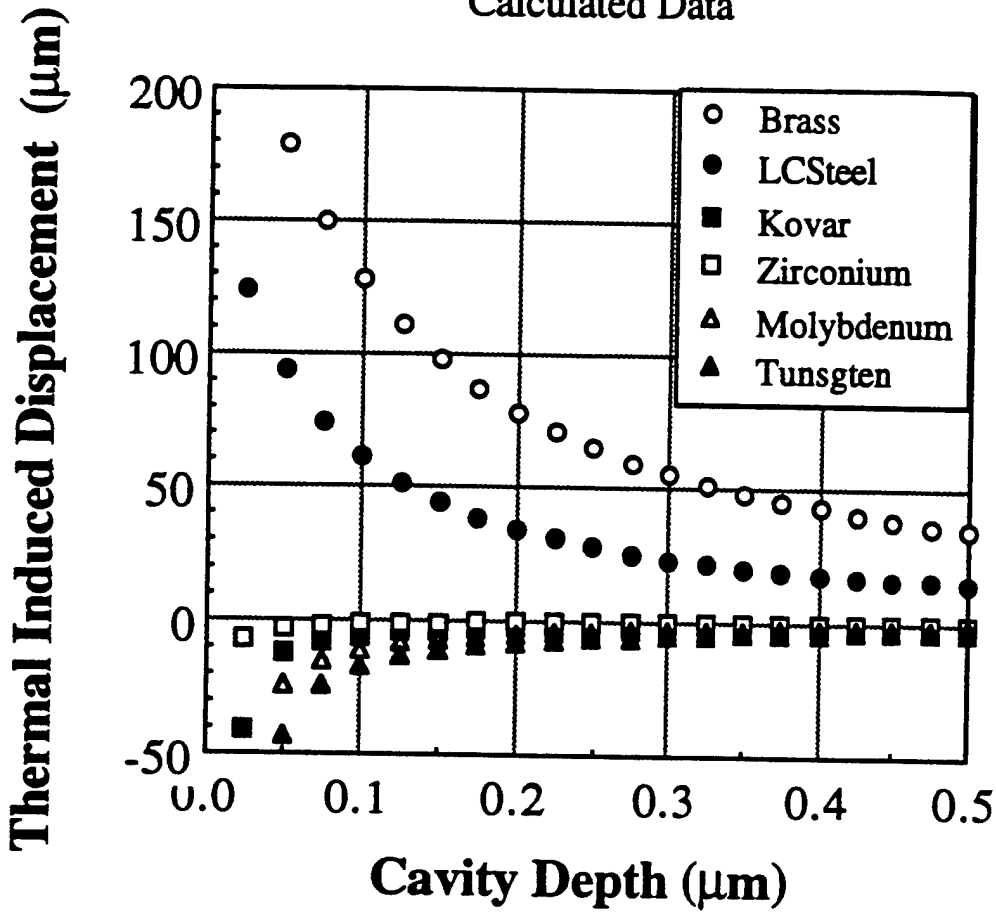
F10.c



F106

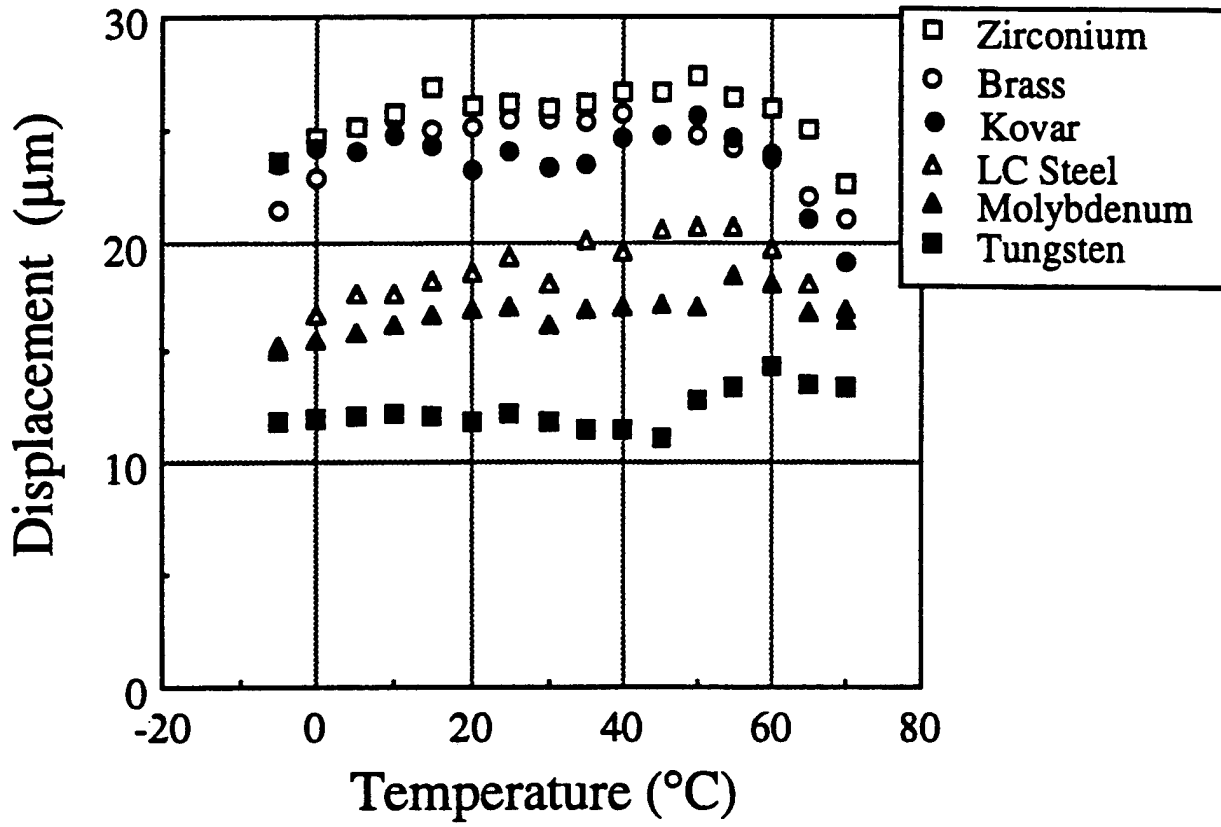


Calculated Data

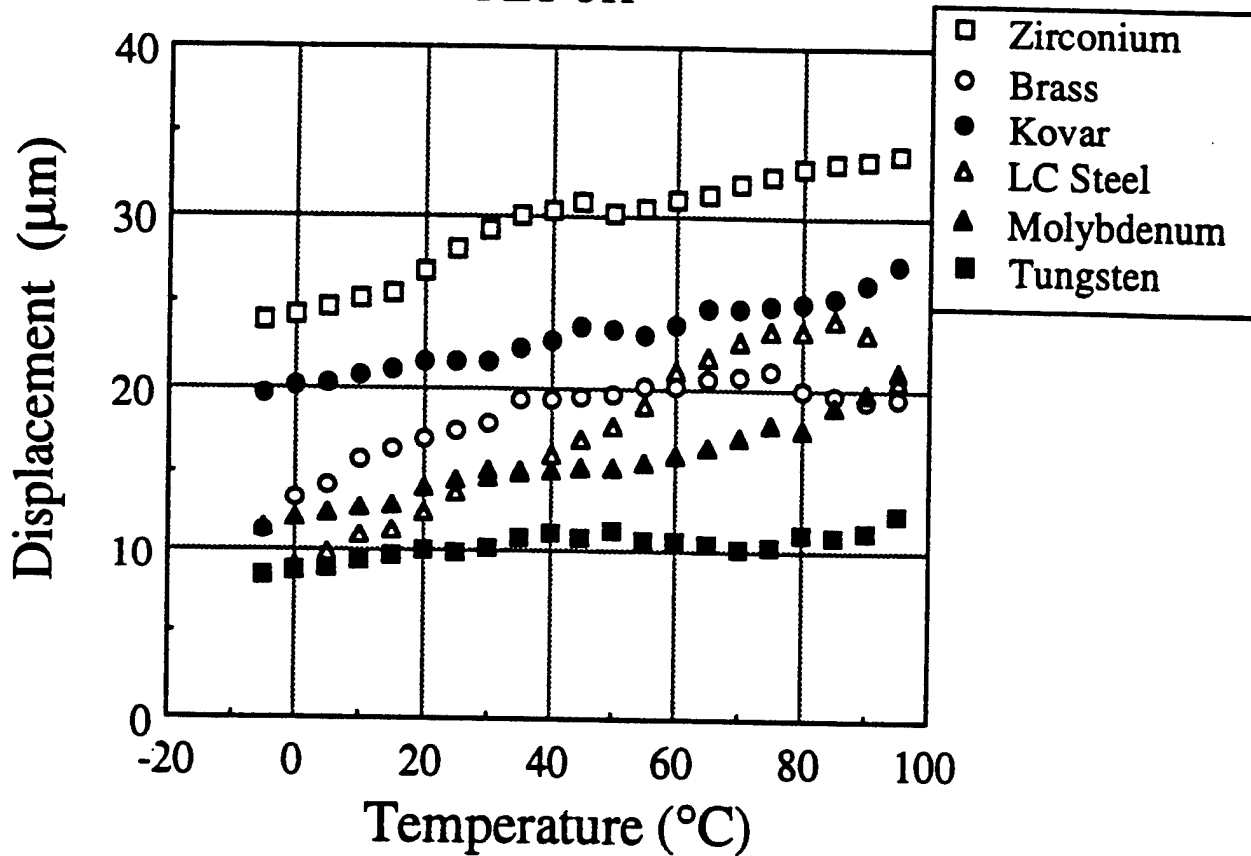


F 12

Bonded with Eccobond
PZT-5H

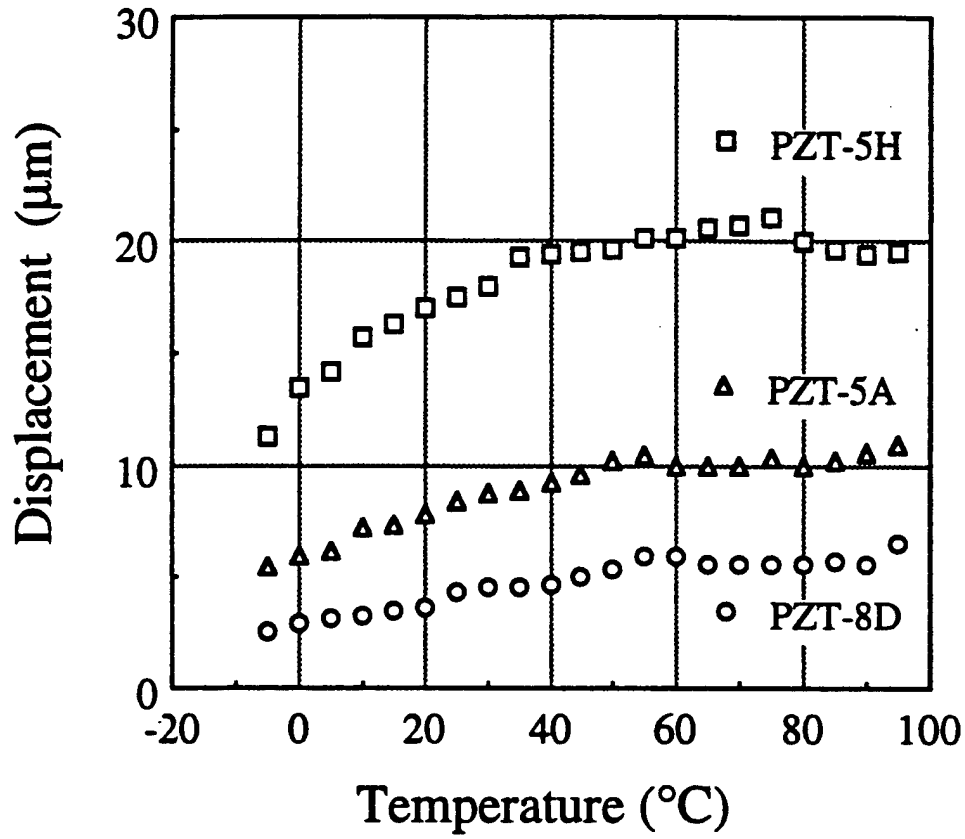


Bonded with Masterbond
PZT-5H

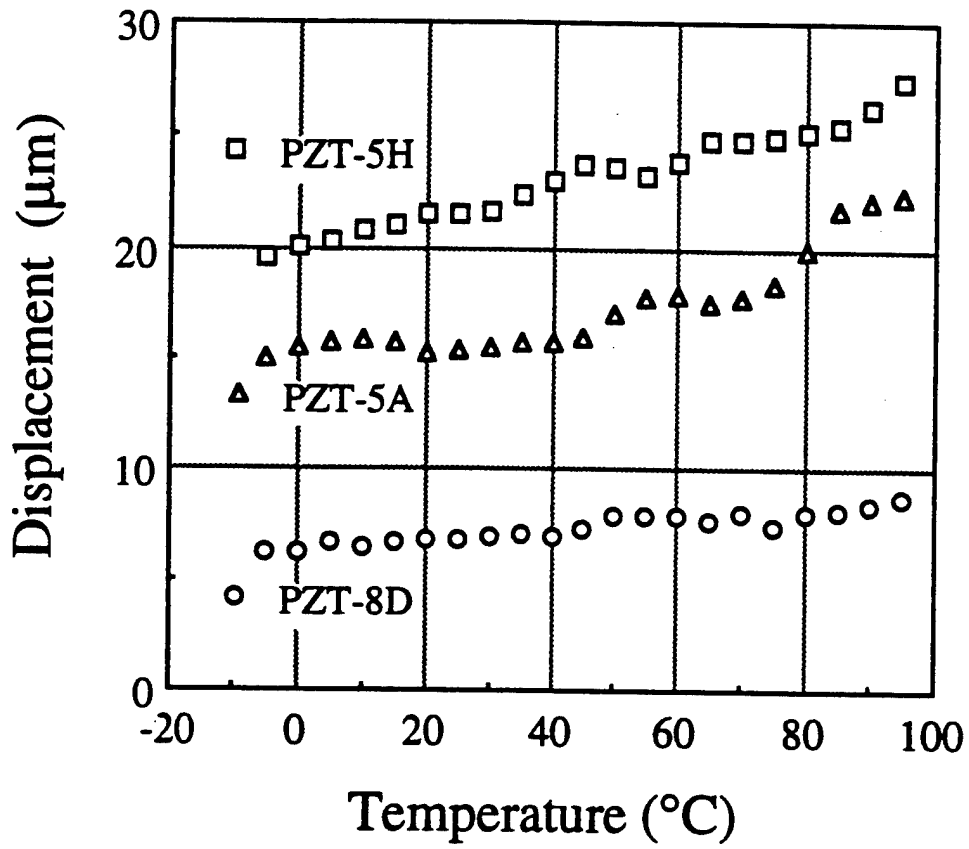


F14

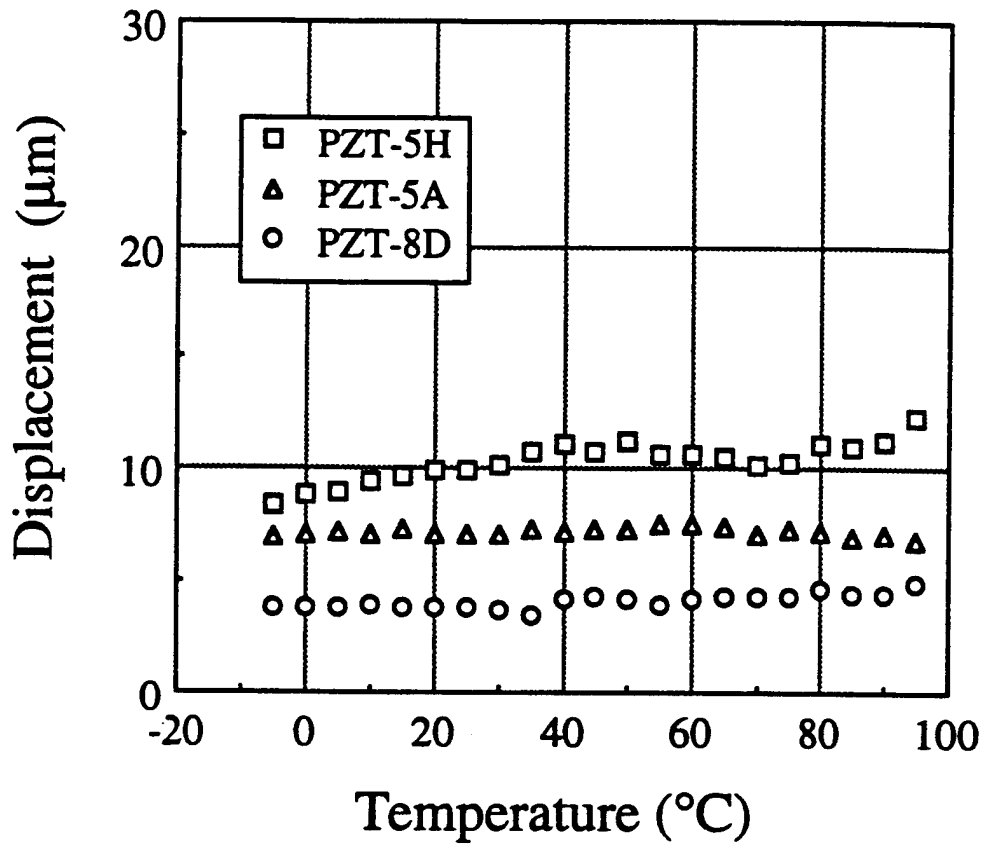
Brass Endcaps, Masterbond



Kovar Endcaps, Masterbond

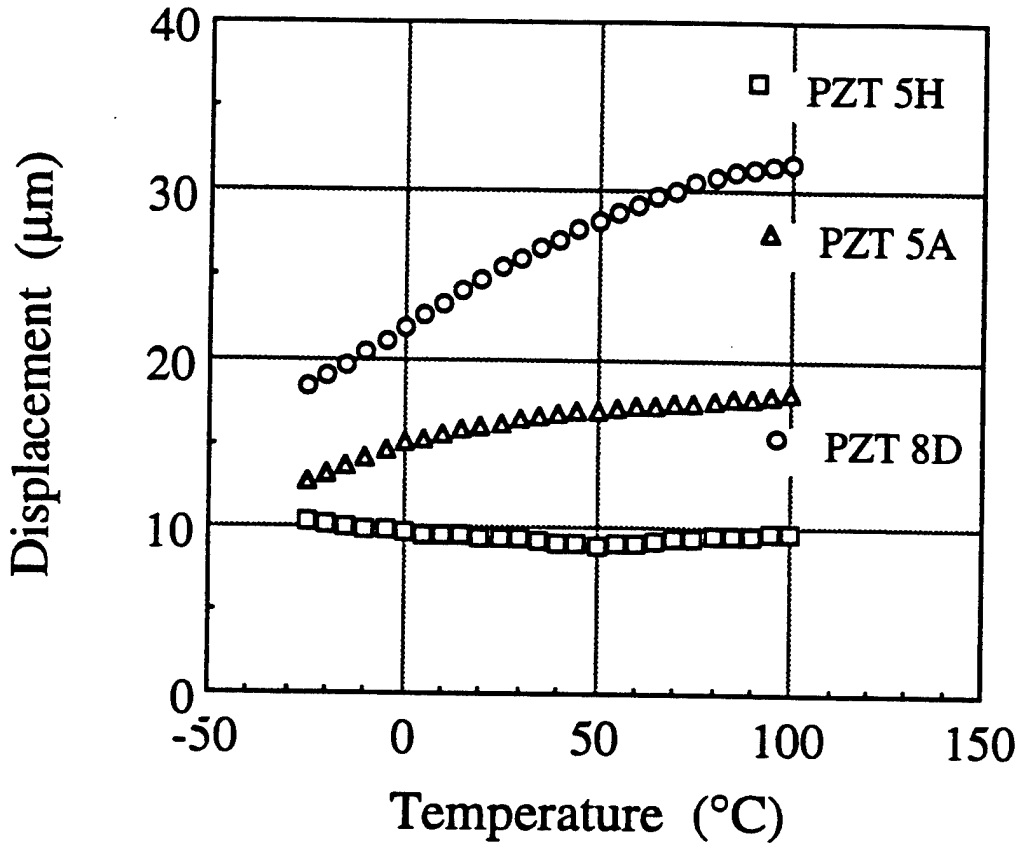


Tungsten Endcaps, Masterbond



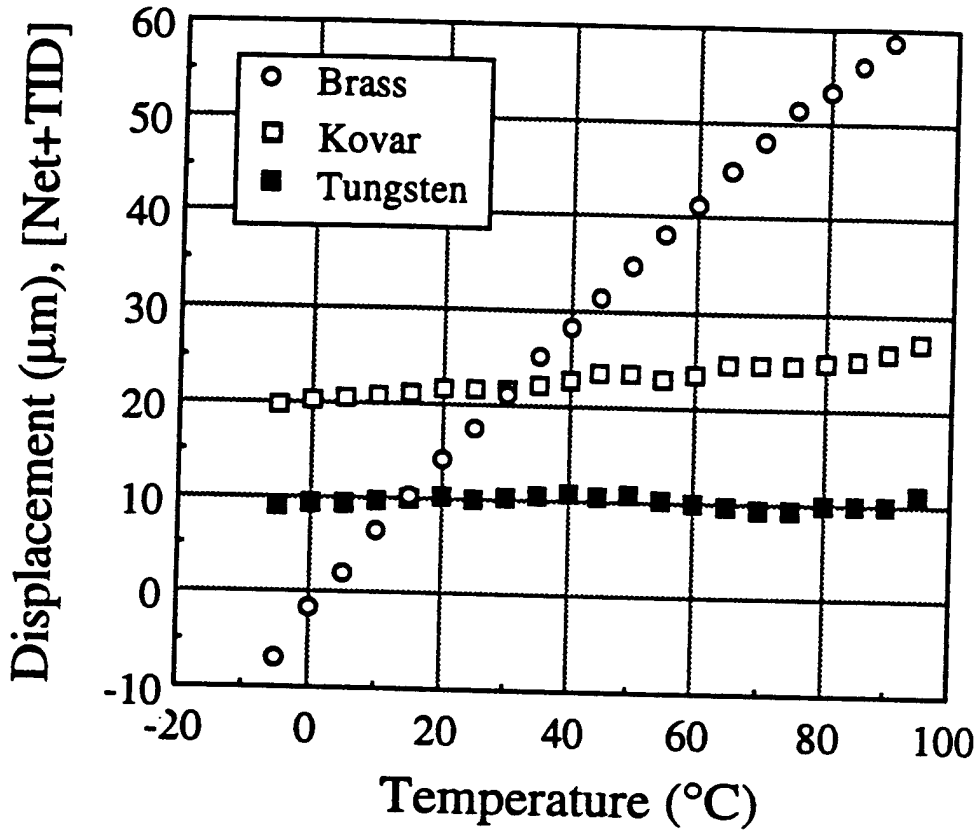
F 15 c

Calculated Data (Kovar Endcaps)



3.15.0

PZT 5H, Masterbond



APPENDIX 43

MEASURING METHODS FOR HIGH-POWER CHARACTERISTICS OF PIEZOELECTRIC MATERIALS

Seiji HIROSE^{***}, Sadayuki TAKAHASHI^{****}, Kenji UCHINO^{**}
Manabu AOYAGI^{*} and Yoshiro TOMIKAWA^{*}

^{*}Faculty of Engineering, Yamagata University, Yonezawa, 992 Japan

^{**}The Pennsylvania State University, MRL, University Park, PA 16802

^{***}R&D Group, NEC Corp., Miyazaki, Miyamae-ku, Kawasaki, 216 Japan

ABSTRACT Two kinds of measuring method of the high-power characteristics of piezoelectric transducers are described. One is the measurement method at the resonance frequency and another is the measurement method at the antiresonance frequency. The vibrational velocity dependences of the equivalent circuit constants and the temperature rise were measured by using each measurement method under the constant vibrational velocity control. These results are useful for designing the ultrasonic power devices such as the ultrasonic motor, and also useful for investigating the new advanced piezoelectric materials for high power use. Especially, by using the results obtained at the antiresonance frequency, a stable state driving method, named as antiresonance driving, with high-efficiency and low-temperature rise can be achieved.

1. Introduction

In a piezoelectric ceramic transducer operating under high-power excitation at the resonance frequency, the quality factor Q of the transducer becomes lower, and therefore, heat generation at and around the maximum-stress position increases markedly. In this situation, even if the applied electric power is increased, almost only heat generation will increase, but the vibrational energy will not. Under such a high-power operation, the equivalent electric circuit constants such as the mechanical quality factor Q can be no longer measured by the ordinary admittance circle method, because the admittance circle becomes unstable.

First, in the paper, a measuring method for obtaining the high-power characteristics of the equivalent electric constants at the resonance frequency is described. During the measurement, the constant vibrational velocity control is performed for avoiding the jump phenomenon in the resonance characteristics.

Next, the measuring method at the antiresonance frequency is described. When a high-power ultrasonic devices such as an ultrasonic motor is practically used, the maximum efficiency is obtained at the antiresonance frequency, not at the resonance frequency. This phenomenon is

caused by the increase of the dielectric loss related to the vibrational velocity; that is, dielectric loss increases as a function of the vibrational velocity. Dielectric loss can be obtained by using the equivalent constants measured both at the resonance and antiresonance frequencies.

Finally, the efficiency of conversion from electric input power to mechanical output power is shown. This result has been calculated by using the experimental values of the equivalent circuit constants and the dielectric loss. A stable state driving method, named as antiresonance driving, with high-efficiency and low-temperature rise is discussed.

2. Measurement method at the resonance frequency

As you know well, there are two resonances in the piezoelectric transducers. One is resonance and another is antiresonance. It is supposed that the piezoelectric transducer can not vibrate mechanically at the antiresonance frequency. However, even at the antiresonance frequency, transducers can vibrate mechanically up to the large vibrational level. In this paper, for making it clear that both of these resonances are the mechanical ones, the mechanical vibrations at the resonance and antiresonance frequencies are called *A*-type and *B*-type res

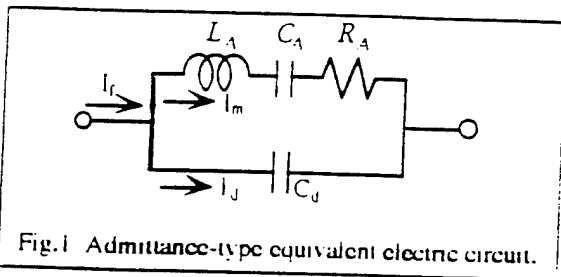


Fig.1 Admittance-type equivalent electric circuit.

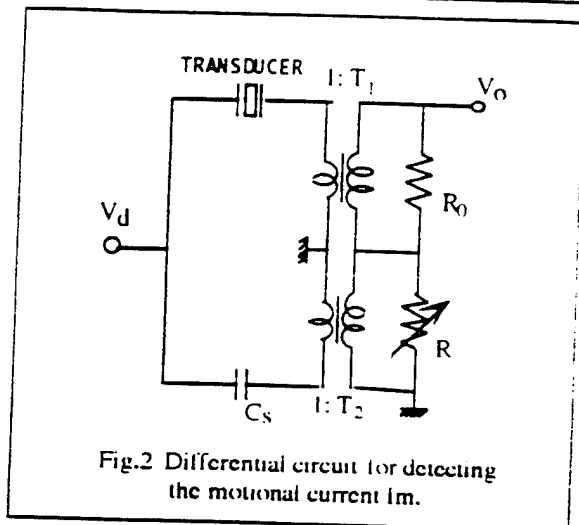


Fig.2 Differential circuit for detecting the motional current I_m .

onances. Therefore, the subscript "A" or "B" is attached to the equivalent constants.

Figure.1 shows the well-known, so-called, admittance type equivalent electric circuit. Here, L_A , C_A and R_A are the equivalent inductance, capacitance and resistance, respectively, and C_d is the damped capacitance. Currents I_f , I_m and I_d are the free current, motional current and damped current, respectively. The motional current I_m is proportional to the vibrational velocity v , and written as follows;

$$I_m = Av, \quad (1)$$

where A is the force factor.

Figure 2 shows a differential circuit for detecting the motional current. Here, C_s and R are a capacitance and a resistance, respectively, for cancelling the damped capacitance C_d .

The output voltage V_o of the differential circuit in Fig.2 is given by,

$$V_o = -(R_0/T_1)Y_m V_d - j\omega((R_0/T_1)C_d - (R/T_2)C_s)V_d, \quad (2)$$

where T_1 and T_2 are the transformation ratio of current detection transformer. When R is adjusted for the resonance curve to be symmetric, V_o becomes equal to $-(R_0/T_1)Y_m V_d$, that is, $-(R_0/T_1)I_m$. Hence, the motional current I_m can be obtained from the output voltage V_o . When V_o is controlled to be constant, the vibrational velocity v can be kept constant in the vicinity of the resonance frequency f_1 .

MEASURING PROCEDURE

(1) Damped capacitance C_d : In Fig.2, R is adjusted so that the output voltage V_o under constant velocity shows a symmetric resonance curve with respect to the A-type resonance frequency on a logarithmic scale. After this adjustment, the damped capacitance is given by,

$$C_d = (T_1/T_2)(R/R_0)C_s, \quad (3)$$

(2) A-type resonance frequency f_1 : When the constant vibrational velocity control (namely, constant I_m control) is employed, f_1 is given by the frequency where the driving voltage V_d indicates minimum value. This frequency can be obtained by the automatic measurement system using micro-computer control¹⁾.

(3) Quality factor Q_A : Using the frequency perturbation method²⁾, the quality factor Q_A can be obtained by,

$$Q_A = \frac{2f_A}{f_2 - f_1} \sqrt{K_p(1+K_p)}, \quad (4)$$

where f_1 and f_2 are frequencies very close to the resonance frequency f_1 , and are in the relation $f_1 < f_1 < f_2$. In addition, K_p is the perturbation ratio, which is given by the following equation under the constant vibrational velocity control,

$$K_p = (V_d - V_{d0})/V_{d0}, \quad (5)$$

where V_{d0} is the driving voltage at the resonance frequency f_1 , and V_d is that at the frequency f_1 or f_2 . These values are measured by the digital voltmeters and transferred to the micro-computer through GP-IB. In this study, the value of K_p was selected below several percent.

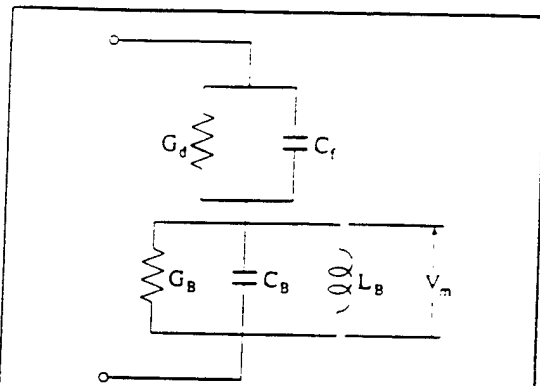


Fig.3 Impedance-type equivalent electric circuit.

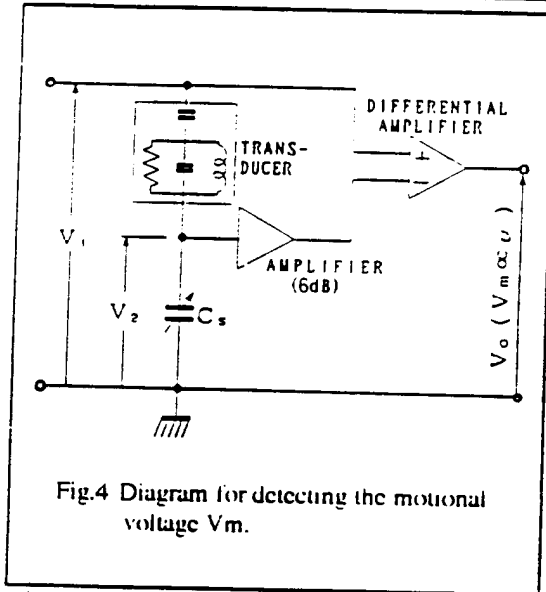


Fig.4 Diagram for detecting the motional voltage V_m .

(4)Equivalent resistance R_A : Using the motional current I_m and the driving voltage V_{d0} obtained at f_A , R_A is given by

$$R_A = |V_{d0}/I_m| (f=f_A). \quad (6)$$

(5)Equivalent inductance L_A and capacitance C_A : Since Q_A , R_A and f_A were given, equivalent inductance L_A and capacitance C_A are obtained by

$$L_A = \frac{Q_A R_A}{2\pi f_A}, \quad C_A = \frac{1}{(2\pi f_A)^2 L_A}. \quad (7)$$

3.3. Measurement method at the anti-resonance frequency

Fig.3 shows the improved, advanced equivalent circuit which is called the impedance-type equivalent circuit³⁾. Here, the conductance G_B means only me-

chanical loss. G_d is the conductance resulting from the dielectric loss angle $\delta^{(3)}$, and written as; $G_d = \omega C_d \tan \delta$. C_f is called the free capacitance and written by using the damped capacitance C_d and the coupling coefficient k as follows: $C_f = C_d / (1 - k^2)$.

The voltage V_m of the parallel resonance circuit indicated in Fig.3 is called the motional voltage, and written as follows:

$$V_m = j \omega_B / \omega \cdot A_B v, \quad (8)$$

where ω is the angular frequency, ω_B is the B -type resonance angular frequency, and A_B is the B -type force factor which is defined as follows:

$$A_B = A / \omega_B C_d, \quad (9)$$

where C_d is the damped capacitance and A is the A -type force factor. Therefore, V_m is proportional to the velocity v , providing $\omega \approx \omega_B$.

Figure 4 shows a diagram for detecting the motional voltage V_m ⁽⁴⁾. Here, C_s is a capacitance for cancelling the free capacitance C_f . In detecting V_m , G_d can be neglected because it is less than one fiftieth of ωC_f . When C_s is adjusted to be equal to C_f , V_o becomes equal to V_m . Hence, the motional voltage V_m can be obtained from the output voltage V_o . When V_m is controlled to be constant, the vibrational velocity v can be kept constant in the vicinity of f_B .

MEASURING PROCEDURE

(1)Free capacitance C_f : In Fig.4, C_s is adjusted so that the current I under constant velocity shows a symmetric resonance curve with respect to the B -type resonance frequency on a logarithmic scale. After this adjustment, the free capacitance is obtained by $C_f = C_s$.

(2) B -type resonance frequency f_B : When the constant vibrational velocity control (namely, constant V_m control) is employed, f_B is given by the frequency where the terminal current I indicates minimum value. This frequency can be obtained by the automatic measurement system using micro-computer control¹⁾.

(3) Quality factor Q_R : Using the frequency perturbation method⁴, the quality factor of B-type resonance Q_R can be obtained by

$$Q_R = \frac{2f_R}{f_2 - f_1} \cdot \frac{\sqrt{K_p(1-K)}}{(1-2K_p)} \quad (10)$$

where f_1 and f_2 are frequencies very close to the B-type resonance frequency f_R , and are in the relation $f_1 < f_R < f_2$. In addition, K_p is the perturbation ratio, which is given by the following equation under the constant velocity control,

$$K_p = (I - I_0)/I_0 \quad (11)$$

where I_0 is the terminal current at the resonance frequency f_R , and I is that at the frequency f_1 or f_2 . These values are measured by the digital voltmeters and transferred to the micro-computer through GP-IB.

(4) Equivalent conductance G_R : At the frequency f_R , susceptance ($\omega C_B - 1/\omega L_B$) of the parallel resonance circuit in Fig.3 becomes 0, hence only conductance G_R remains. By using the motional voltage $V_{m(t)}$ and the current I_0 obtained at f_R , G_R is given by

$$G_R = |I_0/V_{m(t)}| (f=f_R) \quad (12)$$

(5) Equivalent capacitance C_B and inductance L_B : Since Q_B , G_R and f_R were given, equivalent capacitance C_B and inductance L_B can be obtained by

$$C_B = \frac{Q_B G_R}{2\pi f_B}, \quad L_B = \frac{1}{(2\pi f_B)^2 C_B} \quad (13)$$

(6) Dielectric loss factor $\tan \delta$: By using ω_A and Q_A at the A-type resonance, and ω_B , Q_B and C_B/C_f at the B-type resonance, dielectric loss factor $\tan \delta$ can be given as follows;

$$\tan \delta = C_B/C_f \cdot (1/Q_A - \omega_B/\omega_A \cdot 1/Q_B) \quad (14)$$

4. Experiments

Quality factor Q_A and Q_B , temperature rises, capacitance ratio C_B/C_f and B-type

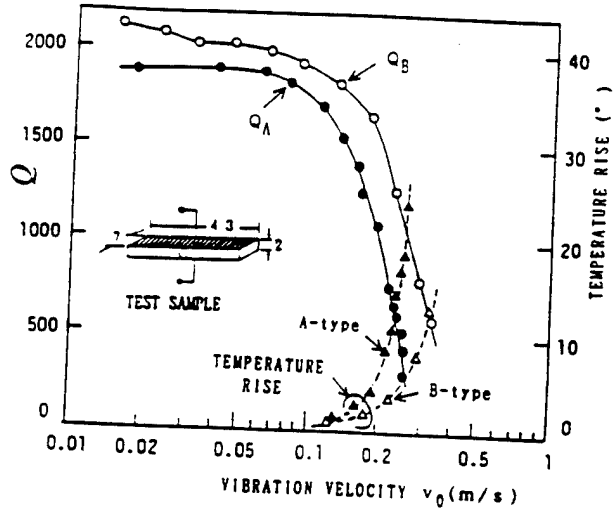


Fig.5 Vibrational velocity dependence of the quality factor and temperature rise for both A- and B-type resonances of a PZT ceramic longitudinally vibrating transducer.

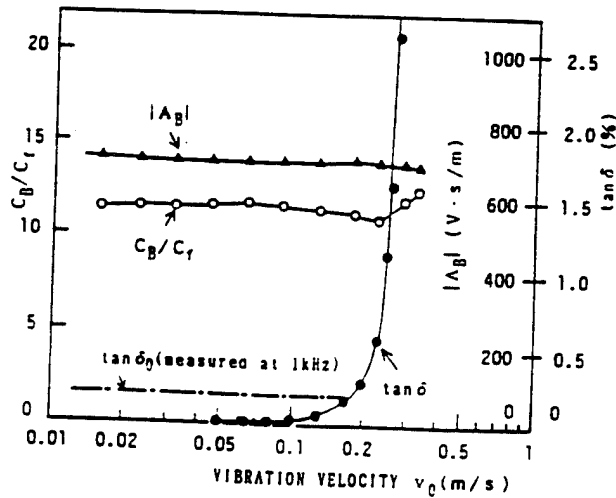


Fig.6 Vibrational velocity dependence of the capacitance ratio and force factor for B-type resonance and the dielectric loss factor $\tan \delta$.

force factor A_B have been investigated on a PZT ceramic rectangular bar. Vibrational mode considered here is the fundamental longitudinal mode. Experimental results of Q_A , Q_B and temperature rises are illustrated in Fig.5 as functions of vibrational velocity v_0 , which was measured at the end of the ceramic bar using the "Fotonic Sensor". Also, temperature rise was measured at the center of the ceramic rectangular bar using a thermocouple. In

Fig.5. the configuration and the dimensions of the test sample are illustrated.

From the figure, it can be recognized that Q_B is higher than Q_A over the whole vibrational velocity range investigated here; from $v_0 \approx 0.02$ to about 0.3 (m/s), and the difference between Q_A and Q_B becomes greater with increasing vibrational velocity. Temperature rise of B-type resonance is less than that of A-type resonance because $1/Q_B$ is smaller than $1/Q_A$. These facts are caused by the presence of dielectric loss and its nonlinearity.

In Fig.6, capacitance ratio C_B/C_f , B-type force factor A_B and the dielectric loss factor $\tan\delta$ are shown. $\tan\delta$ was obtained using the experimental results of Q_A , Q_B and C_B/C_f . For comparison, $\tan\delta_0$, which is directly measured at a sufficiently low frequency (1kHz) is also shown in the figure. $\tan\delta_0$ includes an elastic loss brought by a quasi-static strain⁵⁾, therefore it is larger than $\tan\delta$ in a small vibrational velocity. C_B/C_f and A_B can be viewed as almost constant over the whole velocity range considered here. However, $\tan\delta$ has become larger markedly in the large vibrational velocity above about 0.2 (m/s).

5.5. Driving frequency and efficiency

Equivalent circuit shown in Fig. 3 can be converted equivalently to the one shown in Fig.7. This figure shows an equivalent electric circuit including the two resistances R_d and R_m . Here, Resistance R_d indicating dielectric loss is given by

$$R_d = \tan\delta / (\omega_A C_d), \quad (15)$$

where ω_A is the A-type resonance angular

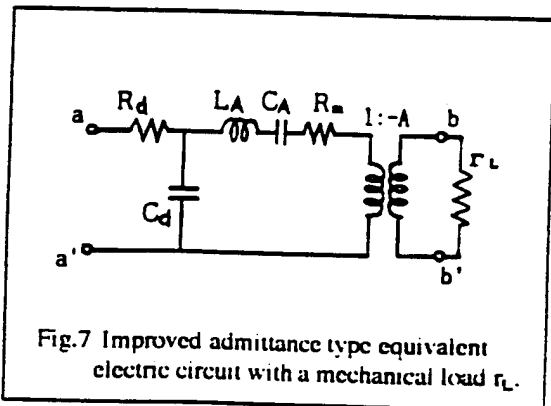


Fig.7 Improved admittance type equivalent electric circuit with a mechanical load r_L .

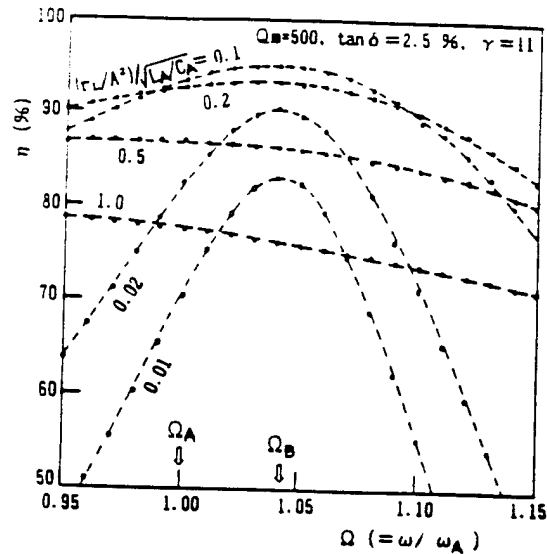


Fig.8 Frequency characteristics of the conversion efficiency η .

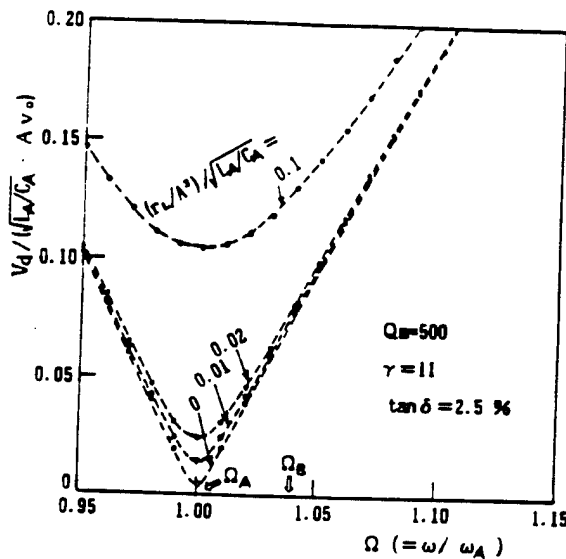


Fig.9 Driving voltage when the vibrational velocity is kept constant.

frequency. R_m is the equivalent resistance indicating mechanical vibration loss, which is given as

$$R_m = (\omega_A L_A) / Q_B, \quad (16)$$

where L_A is the A-type equivalent inductance.

A pair of the mechanical terminals indicated by b and b' in Fig.7 is placed to get mechanical power. For simulating the efficiency characteristics, mechanical load resistance r_L is connected to the mechanical terminals b and b' . Here, we as-

sume that the vibration mode of the transducer does not vary before or after connection of r_l . With the equivalent circuit shown in Fig.7, efficiency η (=mechanical output power/electric input power) can be calculated.

Figure 8 shows the calculated results of the frequency characteristics of η . Here, the horizontal axis is represented by a normalized angular frequency Ω (= ω/ω_0). In this calculation, the experimental results of $\tan \delta = 2.5\%$ and $Q_B = 500$ were utilized, and the parameter is the mechanical load resistance r_l normalized by the specific impedance $\sqrt{L_1 C_1}$ of the equivalent circuit. When r_l is small, η represents a sharp frequency characteristics, and the apparent maximum point of η can be recognized. The value of Ω yielding maximum η is 1.045 in case of capacitance ratio τ being 11, and this value of Ω coincides with the normalized electrical antiresonance angular frequency $\Omega_a (= \sqrt{1+1/\tau})$. When r_l becomes larger, the frequency characteristics curve of η becomes less sharp.

Maximum efficiency can be calculated only by using the equivalent circuit which separately represents dielectric loss and mechanical vibration loss as shown in Fig.7. These results account for the experimental phenomena occurring in the high power operating piezoelectric devices such as an ultrasonic motor. On the other hand, in case of an ordinary equivalent circuit which incorporates dielectric loss and mechanical loss together; that is, includes only one equivalent resonant resistance, the peak point of efficiency may not appear.

Figure 9 shows the calculated results of the driving voltage when the vibrational velocity is kept constant; in other words, the driving voltage necessary to obtain the same vibrational velocity at any frequency near the resonance and antiresonance frequencies. Driving voltage at the antiresonance frequency is about several times larger than at the resonance frequency. However, this disadvantage can be overcome by the thin PZT layers such as in the multilayer actuator.

56. Conclusions

Methods of measuring the vibrational level dependence have been described for two driving frequencies; that is, resonance and antiresonance frequencies. In this paper, electrical resonance coincides with the mechanical A-type resonance, and electrical antiresonance coincides with the mechanical B-type resonance. From the experimental results, it has been shown that the quality factor Q_A of A-type resonance is always smaller than that of B-type resonance Q_B and the difference between them becomes larger with increasing vibrational velocity, and the temperature rise of B-type resonance is less than that of A-type resonance. In addition, capacitance ratio C_B/C_A and force factor A_B of B-type resonance have been shown to be almost constant over the range from $v_0 \approx 0.02$ (m/s) to about 0.3 (m/s). However, $\tan \delta$ has become larger markedly in the large vibrational velocity above about 0.2 (m/s).

By using the experimental results of the equivalent constants including the dielectric loss, efficiency of the transducers under high-power use has been calculated. From this results, maximum efficiency has been obtained at the antiresonance frequency. In addition, at this frequency, temperature rise is very small. Then, it has been concluded that the stable state driving of the high-power piezoelectric devices such as an ultrasonic motor can be achieved at the antiresonance frequency.

References

- 1) S.Hirose and H.Shimizu: Proc.1990 Spring Meeting of Acoust. Soc.Jpn. 2-2-2[in Japanese].
- 2) S.Saito, R.Aoyagi and H.Shimizu: J.Acoust.Soc.Jpn.33-10(1977)p.540 [in Japanese].
- 3) H.Shimizu and S.Saito: J.Acoust.Soc.Jpn.(E)6-3(1985)p.225.
- 4) S.Hirose and H.Shimizu et.al.: Jpn.J.Appl.Phys.Suppl.30-1(1991)p.117.
- 5) S.Saito and H.Shimizu: Jpn.J.Appl.Phys.Suppl.24-3(1985)p.145.

APPENDIX 44

Electro-Mechanical Characteristics of Lead-Zirconate-Titanate Ceramics Under Vibration-Level Change

Sadayuki Takahashi*
 NEC Corporation, Miyazaki, Miyamae-Ku,
 Kawasaki-Shi 216, Japan
 and

Seiji Hirose*
 Yamagata University, Yonezawa-Shi, Yamagata 992, Japan
 and

Kenji Uchino and Ki-Young Oh
 The Pennsylvania State University, MRL,
 University Park, PA 16802

Abstract -- Electro-mechanical characteristics by changing the vibration-level were studied in lead-zirconate-titanate (PZT) based ceramics using the constant current/velocity driving method. The fractional changes of Young's modulus and mechanical dissipation factor are a function of the square of the effective vibration velocity. The increase of the dissipated-vibration-energy with the vibration-level change causes heat generation. Ferroelectric hysteresis loss is assumed to affect the dissipated-vibration-energy through the mechanical dissipation factor.

I. INTRODUCTION

High-power piezoelectric devices, such as ultrasonic motors and piezoelectric actuators, have been vigorously studied in recent years [1]. A very high level or a great amplitude of piezoelectric vibration is required for these applications, and lead-zirconate-titanate (PZT) based piezoelectric ceramics are usually used for these devices. It has been shown, however, that a lot of heat generation as well as a drastic change in piezoelectric properties occurs in these ceramics under a high vibration-level [2]-[6]. The magnitude of the vibration-level in the high-power usage has been limited by these phenomena.

We have studied the electro-mechanical characteristics under a high vibration-level, aiming to develop the high-power usage piezoelectric materials [7]-[9]. The new measurement method of electro-mechanical characteristics under a high vibration-level was established. According to the method, the vibration-level dependence of electro-mechanical characteristics in PZT based ceramics was measured.

This paper deals with the stability of the electro-mechanical characteristics and the heat generation phenomena under the vibration level change in PZT based ceramic materials. The cause of the heat generation is discussed from the view point of a dissipated-vibration-energy due to internal friction.

II. EXPERIMENTAL

The PZT ceramics with the basic composition of $\text{Pb}(\text{Zr}_{0.54}\text{Ti}_{0.46})\text{O}_3$ and the ceramics doped with 0.5wt% of Nb_2O_5 or Fe_2O_3 were used here. The dopant Nb and Fe are known as a typical donor and an acceptor, respectively. Specimens of the ceramics were prepared by the conventional powder metallurgy technology.

Electro-mechanical characteristics were measured on the fundamental length expansion mode excited by the constant current/velocity driving circuit. Rectangular plate vibrators with 43mm long, 7mm wide and 2mm thick were used for all measurements.

The vibration-level was represented by the effective vibration velocity V_o which was an universal parameter of the vibration-level. The V_o value was determined by the following relation:

$$V_o = \sqrt{2} \pi f_o \xi_m \quad (1)$$

where ξ_m and f_o are the maximum vibration-amplitude and resonant frequency, respectively. The ξ_m was observed using an optical displacement sensor.

The temperature of the piezoelectric ceramic vibrators was measured by a thin thermocouple which was forced to contact the vibrational nodal line. The temperature initially increased with a time t while the vibrator was driven, but it converged on the constant value after heat generation and radiation reached their equilibrium state. This equilibrium temperature was defined as the temperature of vibrators here.

III. RESULTS AND DISCUSSIONS

A. Vibration-Level Dependence of Electro-Mechanical Characteristics

In Figs. 1(a) and (b), 2(a) and (b) Young's modulus Y_o^E , permittivity ϵ_{ij}^T , electro-mechanical coupling factor k_{ij} , and mechanical dissipation factor Q_m^{-1} in PZT ceramics with various dopants are shown as a function of V_o , respectively. The Y_o^E value decreases with increasing V_o , whereas ϵ_{ij}^T , k_{ij} , and Q_m^{-1} increase. These behaviors are markedly affected by the dopant. All properties in the Nb-doped PZT begin to change from a relatively low vibration level in comparison with the case in the Fe-doped PZT. The undoped one is somewhere in between.

In Figs. 3 and 4 the fractional change of Young's modulus $\Delta Y_o^E / (Y_o^E)_o$ and mechanical dissipation factor $\Delta Q_m^{-1} / (Q_m^{-1})_o$ are plotted as a function of V_o . The relations can be expressed as the following empirical formulas:

$$\frac{\Delta Y_o^E}{(Y_o^E)_o} = \alpha_Y V_o^2 \quad (2)$$

$$\frac{\Delta Q_m^{-1}}{(Q_m^{-1})_o} = \alpha_{Q_m^{-1}} V_o^2 \quad (3)$$

where $(Y_o^E)_o$ and $(Q_m^{-1})_o$ are the values of Y_o^E and Q_m^{-1} in the case when $V_o \rightarrow 0$, respectively. The α_Y and $\alpha_{Q_m^{-1}}$ are the nonlinear constants of Y_o^E and Q_m^{-1} , respectively and the constants depend on the materials.

The nonlinear constants determined experimentally are summarized in Table I. The constant represents the stability of materials as the vibration-level changes, for instance, a lower constant means a more stable material. The constant for the Fe-doped PZT is smaller and the Nb-doped PZT is larger than the undoped one. In short, the Fe-doped PZT is the most stable material as the vibration-level changes among these three compositions.

*Present address: The Pennsylvania State University, MRL, University Park, PA 16802, USA

The $|\alpha_r|$ is plotted versus $\alpha_{Q_m^{-1}}$ in Fig. 5, and the proportional relationship can be seen between them. The value of $\alpha_{Q_m^{-1}}$ is larger than $|\alpha_r|$ by approximately two orders of magnitude.

B. Heat Generation and Dissipated-Vibration-Energy

Temperature rise of the vibrator ΔT is shown as a function of V_0 in Fig. 6(a). The ΔT increases with V_0 and sharply goes up when V_0 reaches a certain value. Presently, it is impossible to obtain a higher vibration-level, since the maximum vibration-level is limited by the heat generation phenomenon. The magnitude of the maximum vibration-level increases in the order of Nb-doped, undoped and Fe-doped PZT.

Figure 6(b) shows the dissipated-vibration-energy per one second $\omega_0 W$ as a function of V_0 . The $\omega_0 W$ was calculated by the following equations [10]:

$$\omega_0 W = U \omega_0 Q_m^{-1}, \quad (4)$$

$$U = \bar{u} V = \frac{1}{2} \kappa Y_0^\varepsilon S_m^2 V, \quad (5)$$

$$S_m = \frac{\pi \bar{\xi}_m^2}{l}, \quad (6)$$

$$Y_0^\varepsilon = \frac{l^2}{\pi^2} \rho \omega_0^2, \quad (7)$$

where U , \bar{u} , ω_0 , S_m , l , V , ρ and κ means stored mechanical energy, average energy density of U , resonant angular frequency, maximum strain, vibrator length, volume, density and shape factor, respectively. The shape factor depends on the vibrator shape and vibration mode. In this case $\kappa = 1/2$. The behavior of $\omega_0 W$ versus V_0 seems analogous to that of the temperature rise as shown in 6(a). In Fig. 7 the ΔT is confirmed to be approximately proportional to the $\omega_0 W$. This fact suggests that the temperature rise is caused by the dissipated-vibration-energy.

In Fig. 8 the ΔT determined both experimentally and theoretically are represented as a function of time t for Fe-doped PZT. The calculation was carried out according to the following equation:

$$\Delta T = \frac{\omega_0 W t}{Mc}, \quad (8)$$

where M ($\sim 4.7g$) was the mass and c ($\sim 0.42J / g \text{ } ^\circ C$) was the specific heat, respectively. The experimental value initially increases with t and then gradually converges on a constant value. Whereas the calculated one monotonously increases with t , since the effect of heat radiation is not taken into account. It is clear, however, that the experimental value initially increases along with the calculated one. This fact also suggests that the dissipated-vibration-energy causes the temperature rise as well as the results of Figs. 6 and 7.

C. Dissipated-Vibration-Energy and Mechanical Dissipation Factor

Equation (4) can be rewritten as follows using Eqs. (5), (6) and (7):

$$\omega_0 W = \frac{1}{2} M V_0^2 \omega_0 Q_m^{-1}, \quad (9)$$

where M is the mass. Thus the $\omega_0 W$ is determined by V_0 and $\omega_0 Q_m^{-1}$ which means the dissipated ratio of the vibration energy per one second. The relation among the above three parameters of $\omega_0 W$, V_0 and $\omega_0 Q_m^{-1}$ is shown in Fig. 9. The calculated value coincides with the experimental one. The lower the $\omega_0 Q_m^{-1}$ is, the higher the practical upper limit of the vibration-level becomes. The $\omega_0 Q_m^{-1}$ value depends on the materials.

In Fig. 10 the fractional change $\Delta \omega_0 Q_m^{-1} / (\omega_0 Q_m^{-1})_0$ is plotted as a function of V_0 , where $(\omega_0 Q_m^{-1})_0$ is the $\omega_0 Q_m^{-1}$ value for $V_0 \rightarrow 0$. The following same empirical formula as Eqs.(2) and (3) is derived:

$$\frac{\Delta(\omega_0 Q_m^{-1})}{\omega_0 Q_m^{-1}} = \alpha V_0^2, \quad (10.a)$$

or

$$\omega_0 Q_m^{-1} = (\omega_0 Q_m^{-1})_0 (1 + \alpha V_0^2). \quad (10.b)$$

The α values are also listed in Table I. At a high vibration level ($V_0 > 1$ m/s),

$$\alpha V_0^2 \gg 1, \quad (11)$$

$$\omega_0 Q_m^{-1} \equiv \alpha (\omega_0 Q_m^{-1})_0 V_0^2. \quad (12)$$

Thus the $\omega_0 Q_m^{-1}$ can be represented approximately as an explicit function of V_0 . In the case when V_0 is constant, the dissipated-vibration-energy, in the other words the heat generation quantity is in proportion to $\alpha (\omega_0 Q_m^{-1})_0$ which is the constant value depending on the vibration mode, shape and size of the vibrator and material. The smaller the $\alpha (\omega_0 Q_m^{-1})_0$ is, the higher the practical upper limit of the vibration-level becomes after all.

D. Effects of Ferroelectric Hysteresis

The sharp increase of $\omega_0 W$ in the case of V_0 exceeding a certain value is resulted from the drastic increase of Q_m^{-1} since $\alpha_{Q_m^{-1}} \gg \alpha_r$.

The Q_m^{-1} is described as functions of elastically-originated dissipation factor ψ , dielectrically-originated dissipation factor φ and k_{31} as follows [11]:

$$Q_m^{-1} = \frac{1}{1 - k_{31}^2} (\psi + k_{31}^2 \varphi). \quad (13)$$

Considering that the change of Q_m^{-1} with changing the vibration-level is mainly caused by the change of φ and the φ is a sum of the intrinsic dielectric loss and the ferroelectric hysteresis loss due to domain wall motion [12],[13], it is reasonable to consider that the heat generation under the high vibration-level is basically caused by the ferroelectric hysteresis loss.

Ferroelectric hysteresis loop measured by applying the field with 0.1 Hz parallel to the polarization direction is shown in Fig. 11. The magnitude of the hysteresis loop increases in the order of Fe-doped, undoped and Nb-doped PZT. This order of the magnitude coincides with the results of Figs.6 (a) and (b).

The effective driving electric field E_{eff} is shown as a function of V_0 in Fig. 12. The E_{eff} necessary to realize a certain V_0 value increases in the order of Fe-doped, undoped and Nb-doped PZT. This enhances the difference between the magnitude of the hysteresis loss at the same V_0 value in the three composition PZT ceramics.

IV. CONCLUSION

Electro-mechanical characteristics in various PZT ceramics were studied as the vibration-level was changed by using the constant current / velocity driving method. The changes in the Young's modulus and mechanical dissipation factor are a function of the square of effective vibration velocity. The drastic increase of temperature occurs above a certain vibration-level. This phenomenon gives the practical upper limit of the vibration-level.

The dissipated-vibration-energy due to internal friction was calculated. The result suggests that the abrupt temperature rise with the vibration-level increase is caused by the increase in the dissipated-vibration-energy. The energy is proportional to the mechanical dissipation factor which is very sensitive to the magnitude of ferroelectric hysteresis loop.

REFERENCES

[1] S. Takahashi, *Ferroelectric Ceramics*. (Eds. N. Setter and E. L. Colla), Basel: Birkhauser Verlag, 1993, pp. 349-362.
 [2] R. A. Gdula, "High-field losses of adulterated lead zirconate-titanate piezoelectric ceramics," *J. Am. Ceram. Soc.*, vol. 51, pp. 683-687, 1968.
 [3] J. H. Belding and M. G. McLaren, "Behavior of modified lead zirconate-titanate piezoelectric ceramics," *Ceram. Bull.*, vol. 49, pp. 1025-1029, 1970.
 [4] H. J. Hagemann, "Loss mechanisms and domain stabilization in doped BaTiO₃," *J. Phys. C: Solid State Phys.*, vol. 11, pp. 3333-3344, 1978.
 [5] K. Lubitz and W. Wersing, "Automatic performance testing of piezoelectric ceramics for power transducers," *Ferroelectrics*, vol. 40, pp. 237-244, 1982.
 [6] K. Uchino, H. Negishi and T. Hirose, "Drive voltage dependence of electromechanical resonance in PLZT piezoelectric ceramics," *Jpn. J. Appl. Phys.*, vol. 28, Suppl. 28-2, pp. 47-49, 1989.
 [7] S. Takahashi and S. Hirose, "Vibration level characteristics of lead - zirconate - titanate piezoelectric ceramics," *Jpn. J. Appl. Phys.*, vol. 31, Pt. 1, No. 9B, pp. 3055-3057, 1992.
 [8] S. Takahashi and S. Hirose, "Vibration level characteristics for iron doped lead-zirconate-titanate piezoelectric ceramics," *Jpn. J. Appl. Phys.*, vol. 32, Pt. 1, No. 5B, pp. 2422-2425, 1993.
 [9] S. Takahashi, S. Hirose and K. Uchino, "Stability of PZT piezoelectric ceramics under vibration level change," *J. Am. Ceram. Soc.* [to be published]
 [10] K. Nagai and M. Konno, *Electro-Mechanical Vibrators and Their Applications*, Tokyo: Corona-Sha, 1974, pp. 41-44. [in Japanese]
 [11] T. Ikeda, *Fundamentals of Piezoelectric Materials Science*, Tokyo: Ohm-Sha, 1984, pp. 85-87. [in Japanese]
 [12] S. Hirose, Y. Yamayoshi, M. Taga and H. Shimizu, "A method of measuring the vibration level dependence of impedance-type equivalent circuit constant," *Jpn. J. Appl. Phys.*, vol. 30, Suppl. 30-1, pp. 117-119, 1991.
 [13] B. Lewis, "Energy loss processes in ferroelectric ceramics," *Proc. Phys. Soc.*, vol. 73, pp. 17-24, 1959.

Table I. Nonlinear constants of Young's modulus, α_y , mechanical dissipation factor, $\alpha_{\sigma'}$, and $\omega_0 Q_m^{-1}$, α .

PZT specimen	α_y (s ² /m ²)	$\alpha_{\sigma'}$ (s ² /m ²)	α (s ² /m ²)
Nb-doped	-7.7 x 10	4.6 x 10 ³	4.5 x 10 ³
undoped	-5.8	8.5 x 10 ²	8.4 x 10 ²
Fe-doped	-1.3 x 10 ⁻¹	1.7 x 10	1.7 x 10

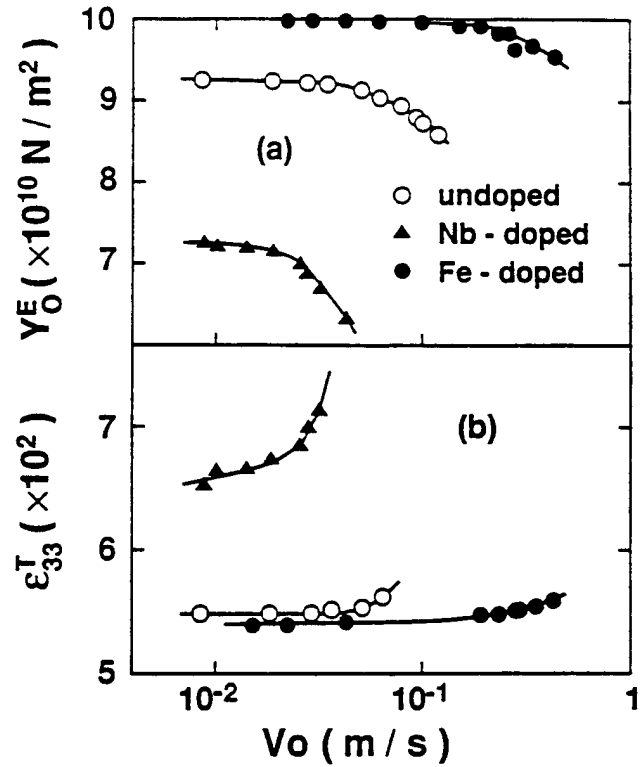


Fig. 1 Vibration-level characteristics of Young's modulus Y_0^E (a) and permittivity ϵ_{33}^T (b).

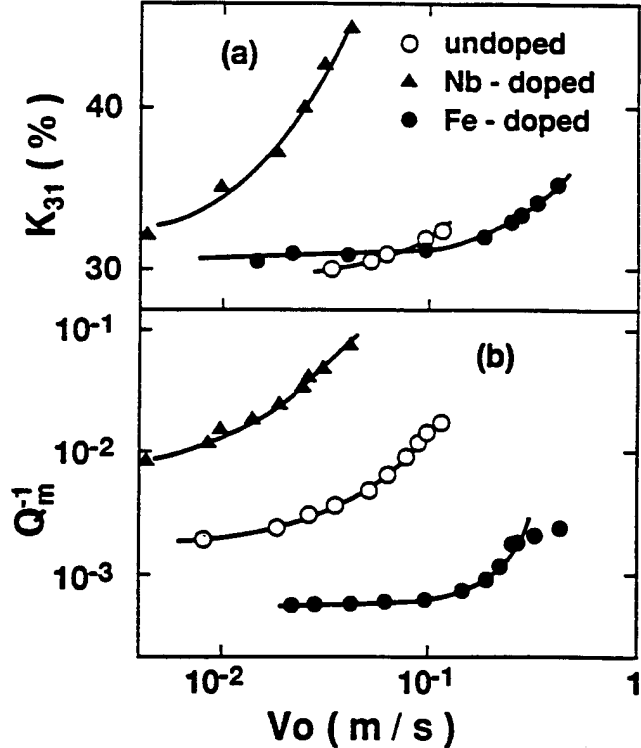


Fig. 2 Vibration-level characteristics of electro-mechanical coupling factor k_{31} (a) and mechanical dissipation factor Q_m^{-1} (b).

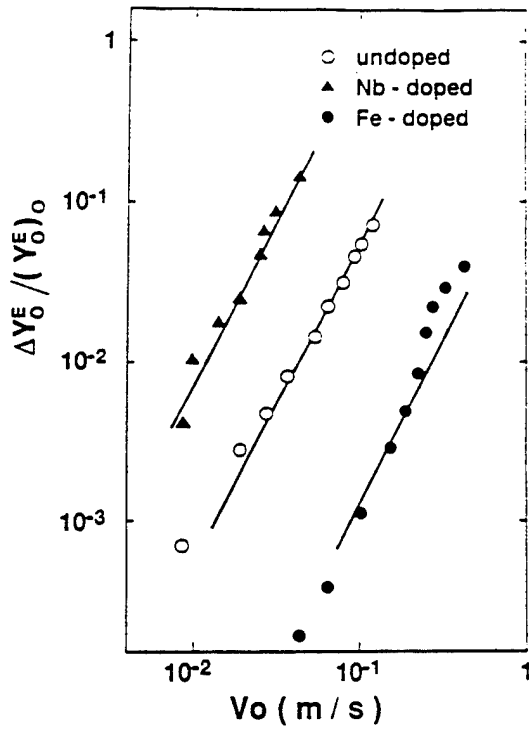


Fig. 3 Vibration-level characteristics of fractional change of Young's modulus $\Delta Y_0^E / (Y_0^E)_0$.

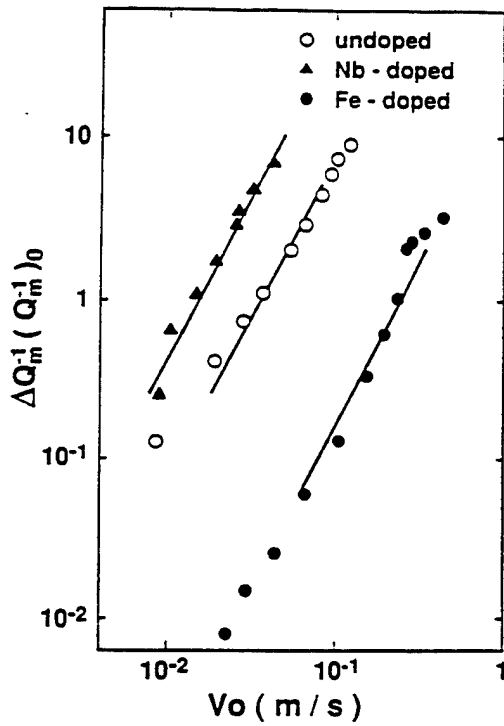


Fig. 4 Vibration-level characteristics of fractional change of mechanical dissipation factor $\Delta Q_m^{-1} / (Q_m^{-1})_0$.

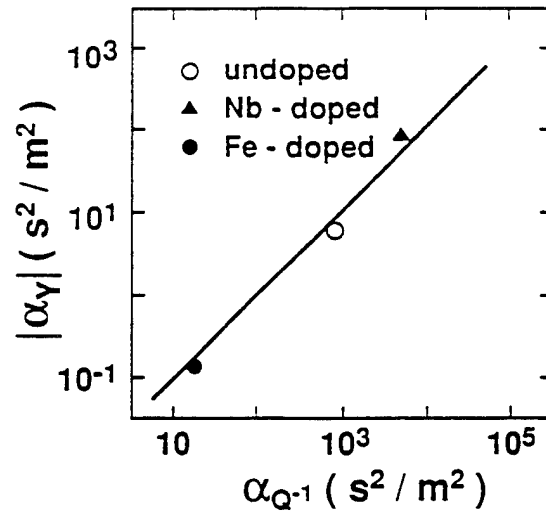


Fig. 5 Relation between the nonlinear constant of Young's modulus $|\alpha_Y|$ and that of mechanical dissipation factor $\alpha_{Q^{-1}}$.

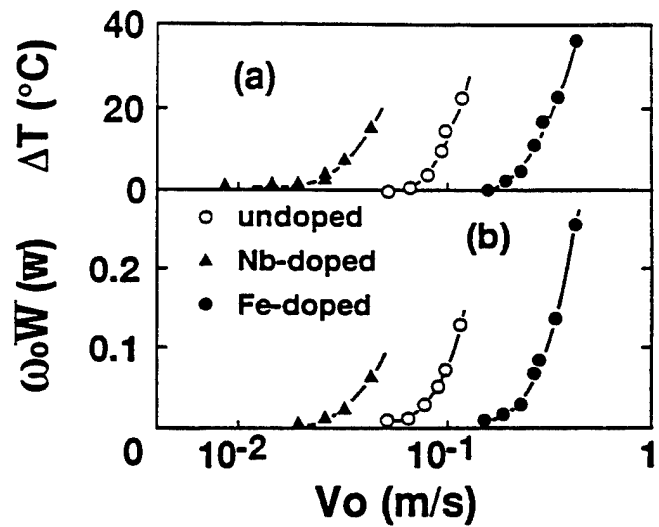


Fig. 6 Vibration-level characteristics of temperature rise ΔT (a) and dissipated-vibration-energy per one second $\omega_0 W$ (b).

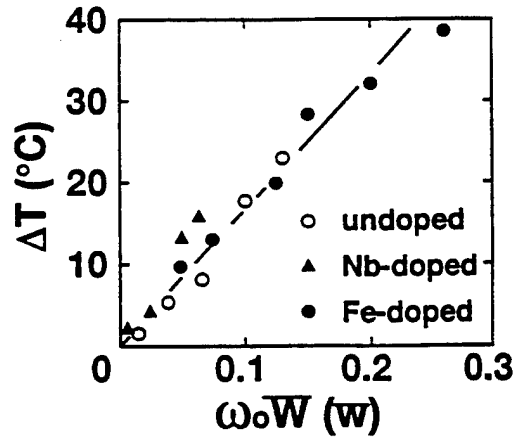


Fig. 7 Relation between temperature rise ΔT and dissipated-vibration-energy per one second $\omega_0 W$.

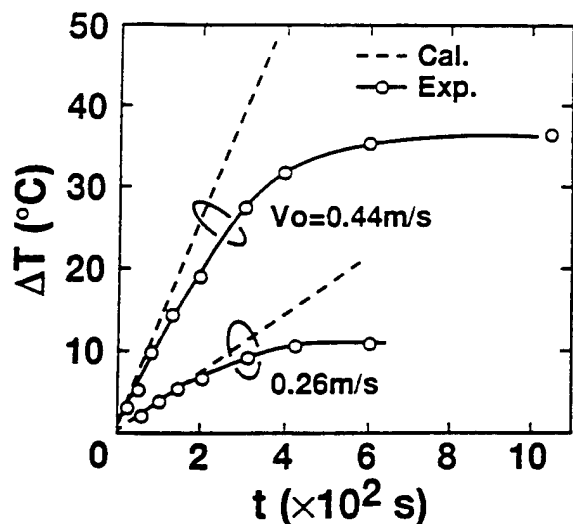


Fig. 8 Both experimental and calculated results for time dependence of temperature rise ΔT in Fe-doped PZT ceramics.

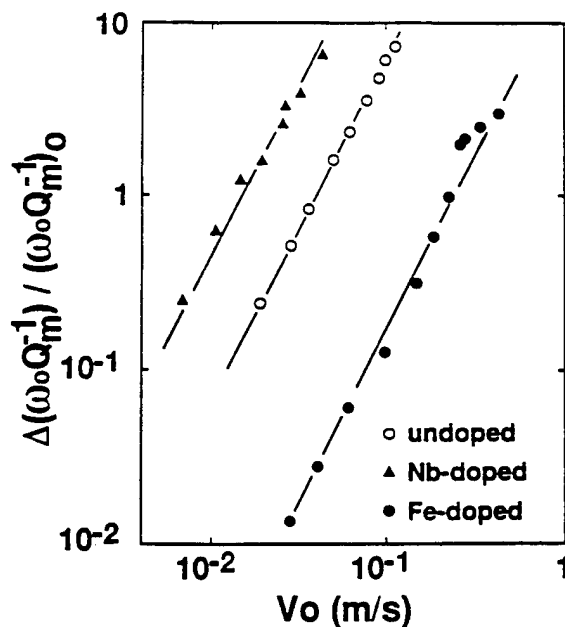


Fig. 10 Vibration-level characteristics of the fractional change $\Delta(\omega_0 Q_m^{-1}) / (\omega_0 Q_m^{-1})_0$.

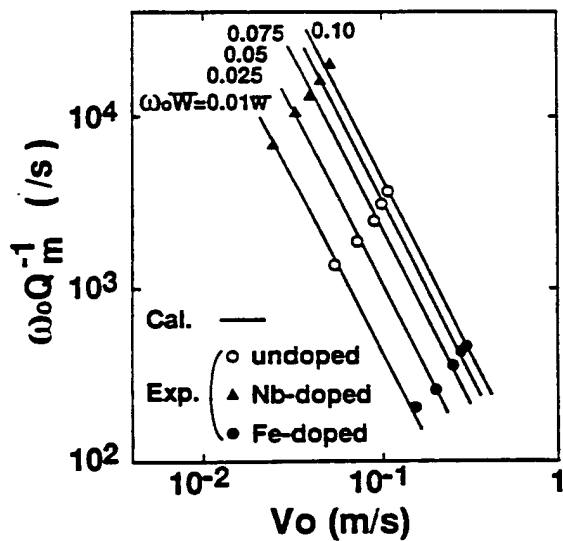


Fig. 9 Relation among three parameters of dissipated-vibration-energy per one second $\omega_0 W$, effective vibration velocity V_0 and dissipated ratio of the vibration energy per one second $\omega_0 Q_m^{-1}$.

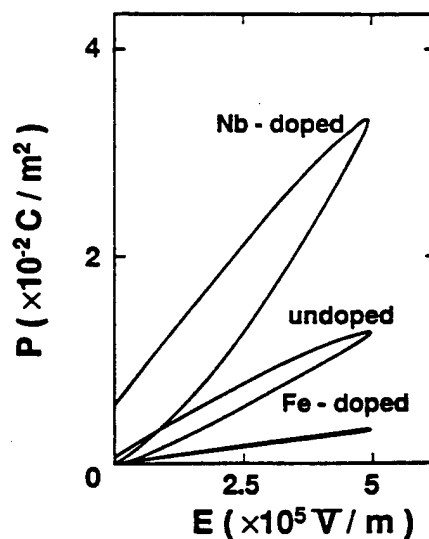


Fig. 11 Ferroelectric hysteresis loop measured by applying an electric field of 0.1Hz parallel to the polarization direction.

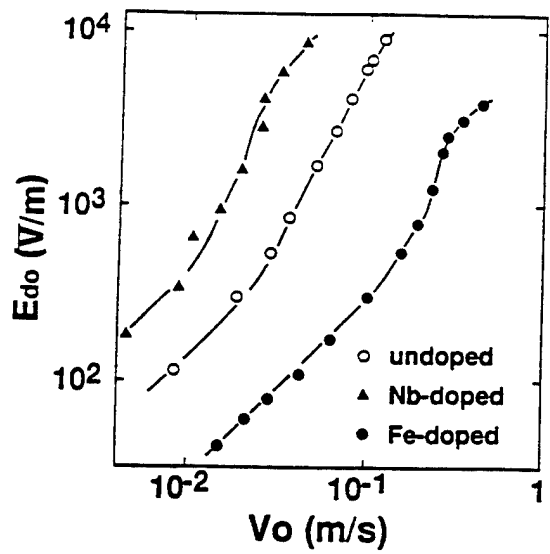


Fig. 12 Relation between effective driving electric field E_{do} and effective vibration velocity V_o .

APPENDIX 45

ELECTRO-MECHANICAL PROPERTIES OF PbZrO_3 - PbTiO_3 - $\text{Pb}(\text{Mn}_{1/3}\text{Sb}_{2/3})\text{O}_3$ CERAMICS UNDER VIBRATION-LEVEL CHANGE

SADAYUKI TAKAHASHI^{*,**}, YASUHIRO SASAKI^{*}, SEIJI HIROSE^{**,***}
AND KENJI UCHINO^{**}

^{*}NEC Corporation, 4-1-1, Miyazaki, Miyamae-ku, Kawasaki-shi 216, Japan

^{**}The Pennsylvania State University, MRL, University Park, PA16802

^{***}Yamagata University, Jyonan, Yonezawa-shi, Yamagata 992, Japan

ABSTRACT

Electro-mechanical properties in the pseudo-ternary solid solution system of PbZrO_3 - PbTiO_3 - $\text{Pb}(\text{Mn}_{1/3}\text{Sb}_{2/3})\text{O}_3$ piezoelectric ceramics were studied by changing the vibration-level using a constant current / velocity driving method. The vibration velocity is proportional to the driving electric field under a relatively low field. The velocity, however, deviates from a linear relationship as electric field increases and converges on a certain value.

The increase of the vibration-level is accompanied by a large amount of heat generation as well, and this heat generation sets a practical upper limit of the vibration-level. The heat generation is caused by a dissipated-vibration-energy which is represented as a function of vibration velocity and the constants depending on the materials and transducers.

In these pseudo-ternary solid solution ceramics, the compositional ratio which shows excellent electro-mechanical properties under a relatively low vibration-level does not necessarily coincide with the compositional ratio which is excellent under a relatively high vibration-level.

INTRODUCTION

High-power piezoelectric ceramic devices, such as ultrasonic motors¹ and piezoelectric actuators,² have been watched with keen interest in recent years. A finite-level (large amplitude) piezoelectric vibration is necessary for these devices, and lead-zirconate-titanate (PZT) based ceramic materials are conventionally used as electro-mechanical transducers. It has been shown, however, that a great amount of heat generation as well as a marked change in electro-mechanical properties occurs in these materials under a finite-level vibration.³⁻⁷ A practical upper limit of an available vibration-level has been restricted by these phenomena.

We have been studying the vibration-level characteristics of electro-mechanical properties in PZT based piezoelectric ceramics, aiming to develop the high-power usage piezoelectric ceramic materials.⁸⁻¹³ Primarily a new method to evaluate the electro-mechanical properties continuously changing a vibration-level from low to high was established. Then the effects of compositional ratio of Zr / Ti and the effects of dopants on the vibration-level characteristics of electro-mechanical properties in PZT were studied. The empirical formulas which represented the relations of both Young's modulus versus vibration velocity and mechanical dissipation factor versus vibration velocity were found. It was also found that the heat generation was caused by dissipated-vibration-energy.

Some kind of pseudo-ternary solid solution ceramics consisting of a compound of $\text{Pb}(\text{M}, \text{M}')\text{O}_3$ (M, M': metal ion) with PZT have been shown having high electro-mechanical coupling factor, high mechanical quality factor and high stability when they are driven under a relatively low vibration-level in comparison with the conventional binary solid solution PZT based ceramics. The ceramics with the composition of $x\text{PbZrO}_3$ - $y\text{PbTiO}_3$ - $z\text{Pb}(\text{Mn}_{1/3}\text{Sb}_{2/3})\text{O}_3$ (PZ-PT-PMS) have widely been used in a practical usage.¹⁴ These are regarded as one of the above pseudo-ternary solid solution ceramics in a sense, although the $\text{Pb}(\text{Mn}_{1/3}\text{Sb}_{2/3})\text{O}_3$ ceramics are not single phase perovskite. In this paper the effects of $\text{Pb}(\text{M}, \text{M}')\text{O}_3$ on the vibration-level characteristics of electro-mechanical properties in PZT are examined using the PZ-PT-PMS ceramics as a part of developing high power usage piezoelectric ceramic materials.

EXPERIMENTAL

Crystal structure and system of the pseudo-ternary solid solution PZ-PT-PMS ceramics are shown in Fig.1. The ceramics with a shaded compositional ratio were used as specimens here. These compositions are close to the morphotropic phase boundary (MPB) between the tetragonal ferroelectric phase (F_T) and the rhombohedral one (F_R). The ceramic specimens were prepared by the conventional powder metallurgy technology.

Electro-mechanical properties were measured on the fundamental length expansion vibration mode excited by a constant current / velocity driving method. Rectangular plate piezoelectric ceramic transducers with 43 mm long, 7 mm wide and 1 mm thick were used for all measurements.

The vibration-level was represented by the effective vibration velocity V_0 which was an universal parameter of the vibration-level. The V_0 value was determined by the following relation:

$$V_0 = \frac{1}{\sqrt{2}} \omega_0 \xi_m, \quad (1)$$

where ξ_m and ω_0 are a maximum vibration-amplitude and resonant angular frequency, respectively. The ξ_m was observed using an optical displacement sensor.

The temperature was measured by a thin thermocouple which was forced to contact the vibrational nodal line of the transducer. Initially, temperature increased with time and then gradually converged on its saturation value as heat generation and radiation approached their equilibrium state. This saturated temperature was defined as the transducer temperature here.

RESULTS AND DISCUSSIONS

Electro-Mechanical Properties under a Low Vibration-Level

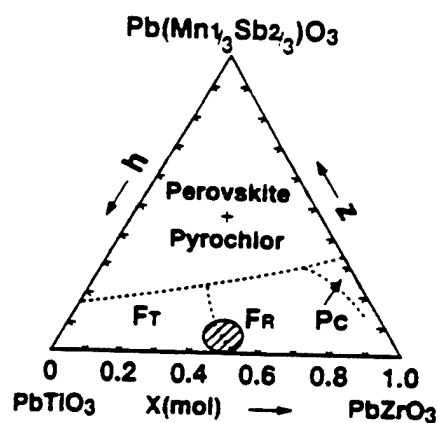


Fig.1 Crystal structure and symmetry of the pseudo-ternary solid solution PZ-PT-PMS ceramics.

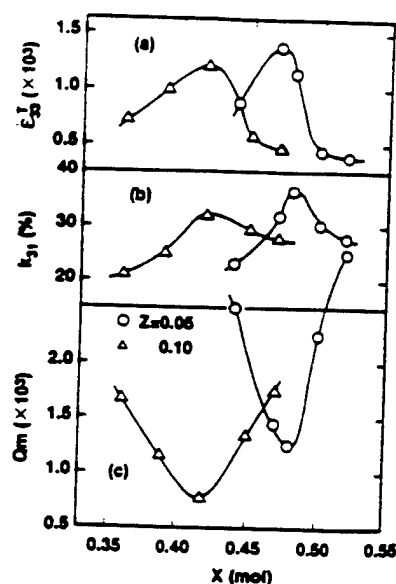


Fig.2 Dielectric constant ϵ'_{33} (a), electro-mechanical coupling factor k_{31} (b) and mechanical quality factor Q_m (c) in PZ-PT-PMS ceramics under a low vibration-level.

Dielectric constant ϵ_{33}^T , electro-mechanical coupling factor k_{31} , and mechanical quality factor Q_m under a relatively low vibration-level ($V_0 < 0.01$ m/s) are shown in Figs. 2(a),(b) and (c), respectively, where z is the fraction of $\text{Pb}(\text{Mn}_{1/3}\text{Sb}_{2/3})\text{O}_3$ content. The ϵ_{33}^T and k_{31} show maximum values close to the MPB, whereas the Q_m shows minimum. Each maximum or minimum value in the ceramics with the molar concentration of $z=0.05$ is larger than that in the ceramics with $z=0.10$.

Vibration-Level Dependence on the Driving Electric Field

The following relation is derived from the piezoelectric equations for the transducers vibrating in longitudinal expansion mode where both ends of the transducer are mechanically free:

$$-AtE_{do} + ZV_0 = 0, \quad (2)$$

where A , Z , E_{do} and t represent force factor, mechanical impedance at the transducer ends, effective driving electric field and the transducer thickness, respectively. Therefore V_0 is represented as a function of E_{do} as follows:

$$V_0 = \frac{At}{Z} E_{do} = \frac{4}{\pi} \sqrt{\frac{\epsilon_{33}^T}{\rho}} \frac{k_{31}}{Q_m^{-1}} E_{do}, \quad (3)$$

where ρ is density. Thus the V_0 should be proportional to E_{do} .

In Figs. 3 and 4, V_0 and mechanical dissipation factor Q_m^{-1} are shown as a function of E_{do} . It can be seen that the V_0 is actually proportional to E_{do} under a relatively low driving electric field. The V_0 , however, gradually deviates from the linear relationship as E_{do} increases and converges

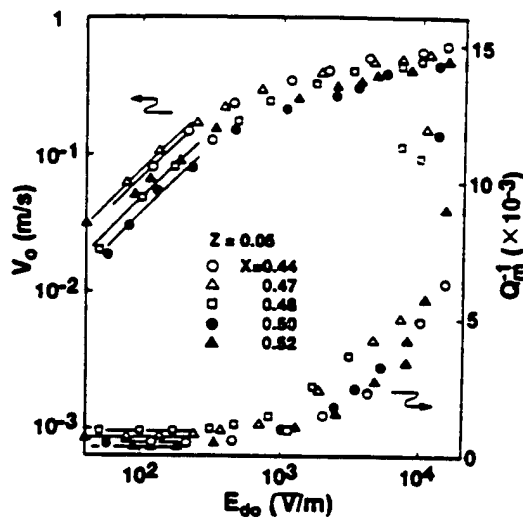


Fig.3 Effective vibration velocity V_0 and mechanical dissipation factor Q_m^{-1} in PZ-PT-PMS ceramics with $z=0.05$ as a function of effective driving electric field E_{do} .

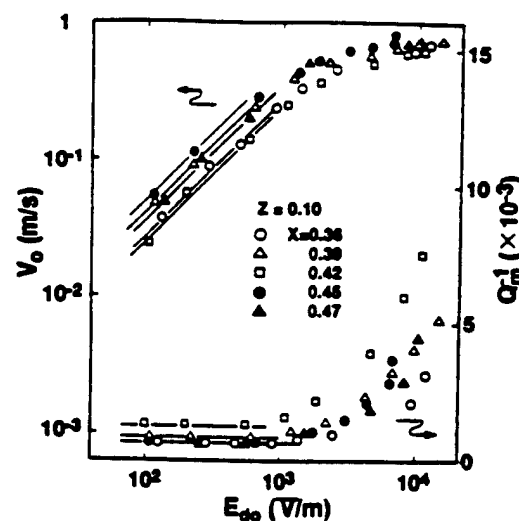


Fig.4 Effective vibration velocity V_0 and mechanical dissipation factor Q_m^{-1} in PZ-PT-PMS ceramics with $z=0.10$ as a function of effective driving electric field E_{do} .

on its saturation value after all. This phenomenon is considered to be caused by the increase of Q_m^{-1} with increasing E_{dc} , since both the ϵ_{33}^T and k_{31} tend to increase with increasing E_{dc} .¹¹ It is a fact that the Q_m^{-1} increases with increasing E_{dc} in accordance with the V_0 behavior.

Thus the available vibration-level does not necessarily increase with increasing driving electric field. The drastic increase of Q_m^{-1} which occurs when a driving electric field exceeds a certain value restricts a maximum of the available vibration-level magnitude.

Dissipated-Vibration-Energy Effect on Heat Generation.

In Figs. 5(a) and 6(a), the temperature rise of the transducers ΔT is represented as a function of V_0 . The ΔT markedly increases when V_0 exceeds a certain value depending on the ceramic compositions. This phenomenon essentially restricts a practically available magnitude of the vibration-level.

The dissipated-vibration-energy per one second $\omega_0 W$ is represented by the following equation:

$$\omega_0 W = U \omega_0 Q_m^{-1} = \frac{1}{4} Y_o^E S_m^2 V \omega_0 Q_m^{-1} = \frac{1}{2} M V_o^2 \omega_0 Q_m^{-1} \quad (4)$$

$$U = \int u dV = \bar{u} V, \quad \bar{u} = \frac{\kappa}{2} Y_o^E S_m^2,$$

$$Y_o^E = \frac{1}{\pi^2} l^2 \rho \omega_0^2, \quad S_m = \frac{\pi E_m}{l} \quad (5)$$

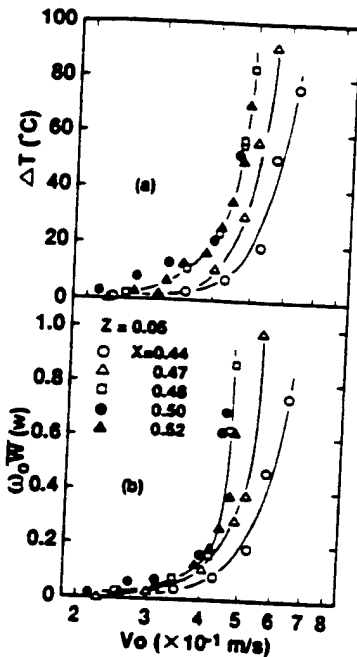


Fig.5 Temperature rise ΔT (a) and dissipated-vibration-energy per one second $\omega_0 W$ (b) in PZ-PT-PMS ceramics with $z=0.05$ as a function of effective vibration velocity V_0 .

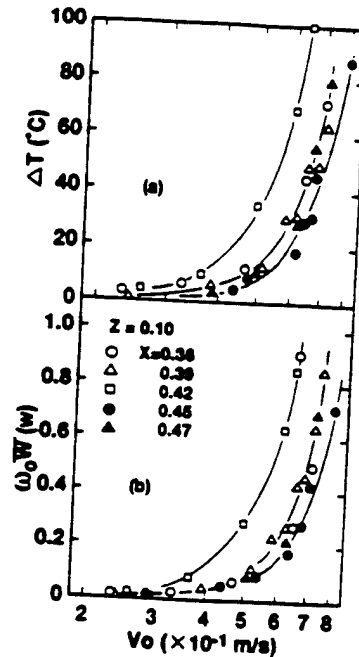


Fig.6 Temperature rise ΔT (a) and dissipated-vibration-energy per one second $\omega_0 W$ (b) in PZ-PT-PMS ceramics with $z=0.10$ as a function of effective vibration velocity V_0 .

where U , u , \bar{u} , Y_0^E and S_m are stored elastic energy, stored elastic energy density, average stored elastic energy density, Young's modulus and maximum strain, respectively. The κ is a constant depending on a shape and vibration mode of transducers, and here $\kappa = 1/2$.¹⁵ The M , V and l are mass, volume and length of the transducers, respectively.

Figures 5(b) and 6(b) show $\omega_0 W$ value as a function of V_0 . The behaviors are analogous to those of temperature rise (Figs. 5(a) and 6(a)). In Fig. 7 ΔT is plotted against $\omega_0 W$ and a linear relationship can be approximated between them. Therefore, as was discussed previously, the dissipated-vibration-energy is regarded as the dominant cause of the heat generation.¹²

Practical Vibration-Levels in PZ-PT-PMS

As mentioned above, the heat generation phenomenon essentially restricts the upper limit of the vibration-level in the practical usage. If, for instance, $\Delta T < 40^\circ\text{C}$ in a certain actual usage, the maximum available V_0 value in PZ-PT-PMS ceramics is represented in Fig. 8(a). In Fig. 8(b), V_0 under a very low driving field ($E_{dc} = 100\text{ V/m}$) is represented as well in comparison to (a). The results indicate that the available vibration-level of the ceramics with $z=0.05$ is higher than that of the ceramics with $z=0.10$ under a low driving field. It is seen, however, that the maximum of the practically available vibration-level is higher for the ceramics with $z=0.10$ than $z=0.05$. This fact suggests that the excellent piezoelectric materials under a low vibration-level are not necessarily excellent under a high vibration-level.

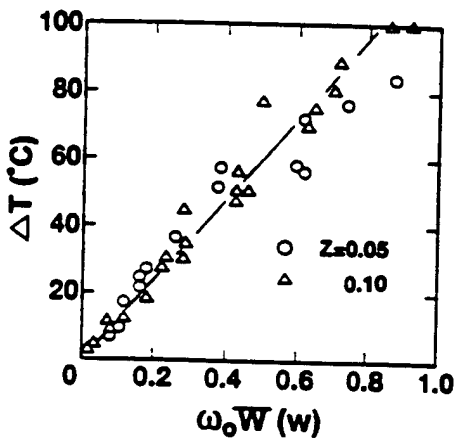


Fig.7 Relationship between temperature rise ΔT and dissipated-vibration-energy per one second $\omega_0 W$.

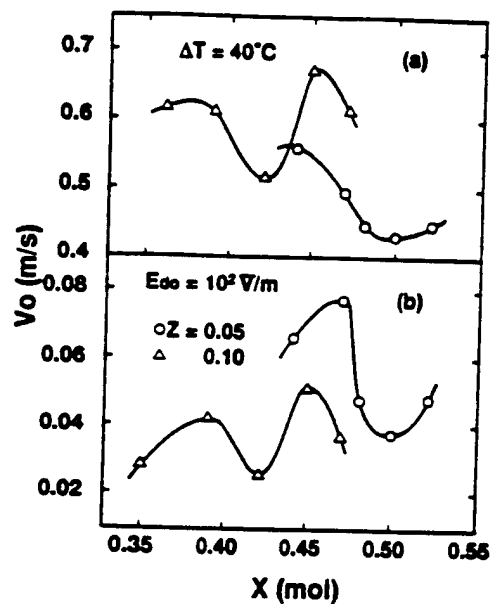


Fig.8 Maximum of the available effective vibration velocity when the temperature rise ΔT is below 40°C (a) and the effective vibration velocity under the relatively low driving electric field of 100 V/m (b).

CONCLUSION

Electro-mechanical properties in the pseudo-ternary solid solution system of $\text{PbZrO}_3\text{-PbTiO}_3\text{-Pb}(\text{Mn}_{1/3}\text{Sb}_{2/3})\text{O}_3$ (PZ-PT-PMS) ceramics were studied by changing the vibration-level using a constant current / velocity driving method as a part of developing high-power usage piezoelectric ceramics.

The vibration velocity linearly increases with a driving electric field under a relatively low level. However, the velocity gradually deviates from the linear relation as electric field increases and converges on its saturation value after all.

A high vibration-level generates a large amount of heat as well. This phenomenon sets a practical upper limit of the vibration-level. The heat generation is caused by a dissipated-vibration-energy which is represented as a function of vibration velocity and the constants depending both on the materials and transducers.

In PZ-PT-PMS ceramics, the compositional ratio which shows excellent electro-mechanical properties under a low vibration-level does not necessarily coincide with the compositional ratio which is excellent under a high vibration-level. The result suggests that there possibly exists excellent high power usage piezoelectric ceramics among the existing ceramics with multi-components, since the compositional ratio in the conventional multi-component piezoelectric ceramics has been determined to have excellent electro-mechanical properties just under a relatively low vibration-level.

REFERENCES

1. S. Ueha and Y. Tomikawa, *Ultrasonic Motors-Theory and Applications-* (Oxford, New York, 1993).
2. S. Takahashi, in *Ferroelectric Ceramics*, edited by N. Setter and E. L. Colla, (Birkhauser Verlag, Basel, 1993), p.249.
3. R. A. Gdula, *J. Am. Ceram. Soc.* **51**, 683(1968).
4. J. H. Belding and M. G. McLaren, *Ceram. Bull.* **49**, 1025 (1970).
5. H. J. Hageman, *J. Phys. C : Solid State Phys.* **11**, 3333 (1978).
6. K. Lubitz and W. Wersing, *Ferroelectrics*, **40**, 237, (1982).
7. K. Uchino, H. Negishi and T. Hirose, *Jpn. J. Appl. Phys.* **28**, Suppl.28-2, 47 (1989).
8. S. Takahashi and S. Hirose, *Jpn. J. Appl. Phys.* **31**, Pt.1, No. 9B, 3055 (1992).
9. S. Takahashi and S. Hirose, *Jpn. J. Appl. Phys.* **32**, Pt.1, No. 5B, 2422 (1993).
10. S. Hirose, Y. Yamayoshi, M. Taga and H. Shimizu, *Jpn. J. Appl. Phys.* **30**, Suppl.30-1, 117 (1991).
11. S. Takahashi, S. Hirose and K. Uchino, *J. Am. Ceram. Soc.* **77**, 2429 (1994).
12. S. Takahashi, S. Hirose, K. Uchino and K. Y. Oh, *Proceeding of the 9-th IEEE International Symposium on the Applications of Ferroelectrics*, (Penn. State, 1994). [to be published]
13. S. Hirose, S. Takahashi, M. Aoyagi and Y. Tomikawa, *Proceeding of the 9-th IEEE International Symposium on the Applications of Ferroelectrics*, (Penn. State, 1994). [to be published]
14. T. Ohno, N. Tsubouchi, M. Takahashi, Y. Matsuo and M. Akashi, *Technical Report of IEICE, Japan*, US71-37 (1972-02). [in Japanese]
15. K. Nagai and M. Konno, *Electromechanical Vibrations and Their Application* (Corona-Sha, Tokyo, 1974), p. 41. [in Japanese]